Leonardo Mendes e Silva

From pluripotency to early events leading to cardiogenesis

Faculdade de Medicina e Ciência Biomédicas

2022

Leonardo Mendes e Silva

From pluripotency to early events leading to cardiogenesis

PhD in Mechanism of Disease and Regenerative Medicine

Work under the supervision of:

Prof. Dr. José Bragança

Prof. Dr. Rui Martinho

Faculdade de Medicina e Ciência Biomédicas

2022

From pluripotency to early events leading to cardiogenesis

Declaration of authorship

I hereby declare to be the author of this work, which is original and unpublished. Authors and papers consulted are duly cited in the text and are listed in the included references.

Signature:_____

Date:____/____/____

Acknowledgments

Começando pelo início desta história de percurso académico…andava eu a brincar na escola primária quando fiz a minha primeira descoberta científica com o meu colega de recreio, e logo de seguida, esta foi submetida a avaliação-dos-pares, percebi que afinal o que parecia ser um ovo de dinossauro, era apenas uma pedra bem polida. Desde então, graças ao grande amor e suporte dos meus pais e do meu irmão, eu fui conseguindo explorar o mundo natural à minha volta (vantagens de quem cresce na aldeia, onde não há museus onde nada pode ser tocado).
O tempo foi passando, e, sempre com o apoio da minha grande família, amigos e dois ursos, fui tendo a possibilidade de continuar a aprender e a descobrir coisas novas. Portanto, como é de esperar numa distribuição pouco normal, só algumas pessoas contribuiram para as decisões que me levaram a estar a escrever isto, agora. Assim, gostava de lhes agradecer neste texto, salientando a prof. Ana Paula de biologia-geologia pelo ensino do conceito de "caderno de investigação", e juntamente com outros professores, pela organização de visitas ao Biocant; cada ida lá era: "wooow!" Por isso, sim, tive a sorte de aos 15 anos, antes de saber conduzir, já sabia pipetar; ainda hoje não sei trocar um pneu, mas sei trocar pontas. E agora as coisas ficam sérias. Na universidade, na cidade onde é bom viver para quem gosta de calor, agradeço ao prof. Eduardo Melo e ao prof. Jorge Martins, por direta ou indiretamente (já me falha a memória), me puxarem os limites e me manterem constantemente motivado para ir às suas aulas. Mais do que isso, o estágio de voluntariado no laboratório do prof. Eduardo certamente foi um ponto de viragem no meu currículo, onde tive a oportunidade de me preparar para o trabalho da tese de mestrado. Agora em inglês, já que fui ao estrangeiro fazer a tese de mestrado:
A special thanks to my previous supervisor, prof. Gert-Jan Euverink, for supporting me and giving me the opportunity to do research in his lab in Groningen. And to my Dutch and Indonesian friends that always told me to pursue this PhD. Depois do mestrado, tive a imensa sorte integrar o grupo de investigação do prof. Rui Guerra e da prof. Ana Cavaco, onde aprendi muito do que é e do como fazer investigação (dentro e fora de um laboratório); sem nunca esquecer que no fim do dia, somos todos humanos—muito obrigado por tudo. Foi assim, com o encorajamento de novas e antigas amizades, que cheguei ao ProRegeM; e foi com o grande apoio e paciência da minha namorada Dra. ACM que chego aqui. Neste programa de doutoramento, tive a oportunidade de ser orientado pelo prof. José Bragança, a quem gostaria de agradecer por me aceitar no seu laboratório e por me ter orientado durante estes últimos anos; juntamente com o prof. Rui Martinho. Sem a vossa orientação, este trabalho não seria possível. Para além dos supervisores, gostaria também de agradecer ao NM pelo seu papel de mentor durante o primeiro ano. Algo que foi fundamental para despertar espírito crítico, consolidar ideias e construir bases para os próximos anos. Fora/dentro da universidade/laboratório: um obrigado a todos os Bits pelos debates científicos, e por me alargarem os horizontes que me ajudaram a melhorar o meu método de trabalho. E a todos os meus colegas de que me ajudaram e dedicaram o seu tempo para me tornar num melhor investigador. Por fim, queria agradecer aos elementos da minha turma, que apesar de quase me terem liquidado (pun intended) com piadas #cufcuf. Sem eles estes quatro anos certamente teriam sido aborrecidos e de pouca #eficiencia. Ah, e as tartarugas ninja nunca teriam sido investigadas e apresentadas num poster científico.

A random thanks to the developers and makers of OnePlus, Obsidian, Mechvibes, Spotify, Todoist, Affinity Designer, Notion, GitHub, One Commander, Flow.Launcher, Zotero, Anet, Vivaldi and Telegram. And, to the musicians Jeremy Soule, Christian Löffler, Mounika, Monstercat and Liquicity for making songs with more than one hour.

Abstract

Heart diseases are the leading cause of death worldwide, which includes acquired cardiovascular diseases and congenital heart diseases. The Cited2 gene is important for proper heart development and cardiac cell differentiation from pluripotent stem cells. Previous studies suggested that the role of Cited2 in cardiac differentiation could begin during the early events that occur in pluripotent cells that undergo differentiation. In mouse embryonic stem cells, *Cited2* is important for self-renewal maintenance, as cells die or differentiate under *Cited2*-depleted conditions. In differentiation, embryonic stem cells depleted of Cited2 at the onset of differentiation show an impairment of cardiac cell differentiation. However, the mechanisms behind these observed phenotypes of *Cited2*-depletion are not well established. In this work, differentially expressed genes were identified in undifferentiated mouse embryonic stem cells and differentiated cells on day-4 of differentiation. Thus, using mouse embryonic stem cells that can be conditionally depleted of *Cited2*, after 16 hours of incubation it was observed that *Cited2*-depleted cells under undifferentiation conditions tend to show increased levels of the DNA damage marker γH2AX, concomitant with decreased expression of DNA repair genes (*Rad51c, Rad9b, and Mdc1*) and increased expression of pro-apoptotic genes (*p21, Ptges, Plk2*). In differentiation conditions using the hanging drop method, on day-4 of differentiation, epigenetic mark H3K27ac showed a decrease in the promoter region of cardiopoietic genes concordant with their downregulation (*Brachyury, Cdx2, Dkk1, Isl1, Kdr, Mesp1, Wnt5a*). However, the results of the H3K27me3 marks, showed higher variability and did not match the reciprocal marks of H3K27ac. Moreover, the increase in H3K27ac mark in undifferentiated *Cited2*-depleted cells corresponded, as expected, to an upregulation of the same genes. Lastly, histone acetyltransferase activity assay using the whole cell extract showed a tendency to increase acetylation in *Cited2*-depleted cells. In conclusion, the role of Cited2 in DNA repair and the cause of increased cell death remains to be established, while delayed expression of mesoderm/cardiac genes could be associated with misregulation of epigenetic H3K27(me3/ac) marks at the promoters of cardiopoietic genes.

Keywords: Cited2, DNA, differentiation, pluripotency, H3K27me3/ac, mouse

Resumo

As doenças cardíacas são responsáveis pela maioria das mortes a nível mundial de acordo com a Organização Mundial de Saúde. Este grupo de doenças inclui as doenças congénitas cardíacas e as doenças cardiovasculares. Embora as doenças cardiovasculares possam ser mitigadas pela adoção de estilos de vida saudáveis, as doenças congénitas cardíacas não podem ser tão facilmente evitadas. Isto, porque estas doenças têm uma componente genética que leva à malformação do coração, e apesar de em alguns casos ser possível operar os recém-nascidos, ainda não há terapias génicas que resolvam a totalidade destes casos. Portanto, é assim necessário perceber melhor o desenvolvimento cardíaco e o papel que alguns genes têm neste complexo processo. Esta complexidade reflete-se na coordenação de expressão de diferentes fatores de transcrição (*e.g.* Brachyury, Nkx2.5, Mesp1, Isl1), e ativação de diferentes vias de sinalização (*e.g.* FGF, TGF, BMP, NODAL, e a WNT). Estas vias atuam em sincronia tendo um efeito de ativação ou inibição de fatores de transcrição dependendo do tecido do embrião e do estádio de desenvolvimento (ou seja, também depende do tempo decorrido).

Este trabalho foca-se na compreensão dos diferentes papeis do gene Cited2 em condições de pluripotência e de diferenciação. Foi demonstrado que mutações neste gene em humanos estão associadas a doenças congénitas cardíacas. Em laboratório, a deleção deste gene em ratinho (*Mus musculus*) leva à sua morte *in utero,* principalmente por malformações do coração. Estudos em células estaminais embrionárias de ratinho mostraram que *Cited2* é também importante para a manutenção da pluripotência uma vez que *Cited2* promove a expressão de *Nanog*, que por sua vez leva à expressão de outros genes importantes para a manutenção da pluripotência. Contudo, quando *Cited2* é depletado (ou seja, a expressão é diminuída), verifica-se um aumento da morte celular e da diferenciação espontânea; mesmo em células mantidas em condições de pluripotência, usando meio suplementado com LIF. Em contexto de diferenciação verificou-se, usando também células estaminais de ratinho, que a depleção de *Cited2* no início do protocolo da gota suspensa levou a uma diminuição na capacidade de diferenciação cardíaca. Trabalhos anteriores do laboratório mostraram que existe um atraso na expressão de genes importantes para a especificação da mesoderme e de diferenciação cardíaca, nomeadamente: Brachyury, Mixl1 e Mesp1.

Este trabalho partiu da análise de dados de “microarrays” (Affymetrix) de um trabalho anterior no laboratório, que tinha como alvo identificar os genes diferencialmente expressos entre dois grupos de células: as células controlo (com expressão de *Cited2*) *vs* as células tratadas (sem

expressão de *Cited2*); e em duas condições experimentais: pluripotência e diferenciação. Deste modo, o trabalho foi separado em duas partes, uma dedicada ao papel do *Cited2* em pluripotência e outra em diferenciação. Para compreender o papel de *Cited2* na pluripotência, foram feitas experiências com células de ratinho que permitem a depleção condicional de *Cited2* quando se adiciona o composto 4HT ao meio de cultura (usando como controlo etanol). Assim, após análise dos "microarrays" verificou-se que existiam alguns genes de reparação do ADN que estavam regulados negativamente (*Rad51c*, *Rad9b* e *Mdc1*), enquanto alguns genes que promovem a morte celular por apoptose estavam regulados positivamente (*p21*, *Ptges*, *Plk2*). Portanto, estes resultados sugeriram que um possível mecanismo que leva ao aumento de morte celular quando *Cited2* é depletado que pode estar associado com dano do ADN. Deste modo, a quantidade de dano nas células foi avaliada por "Western Blot" e por microscopia de confocal, onde foi usado como marcador de dano no ADN a histona H2AX. Na presença de dano no ADN esta histona é fosforilada, e passa a denominar-se por γH2AX. Assim, verificou-se que apesar de existir um aumento dos níveis de γH2AX depois de 16 horas de tratamento, os resultados não foram estatisticamente significativos. Portanto, não foi possível estabelecer com certeza que a causa de morte celular devido à depleção de *Cited2* é causada pelo aumento de dano no ADN. Contudo, os resultados de "microarray" sugerem que genes associados ao p53 possam estar envolvidos (referidos acima). Como perspetivas futuras é proposto que se estude a possível modelação por CITED2 da atividade do p53 através da acetilação por p300/CBP.

Relativamente ao papel de *Cited2* na diferenciação, a análise dos "microarrays" sugeriu que alguns genes que estavam regulados negativamente são controlados por um complexo repressor de expressão (PRC2). Portanto levantou-se a hipótese de que o atraso na expressão dos genes marcadores da mesoderme e de diferenciação cardíaca possam estar bloqueados quando *Cited2* está pouco expresso. Deste modo, realizaram-se experiências de immunoprecipitação de cromatina tendo como alvo duas modificações pós-traducionais: H3K27me3 e H3K27ac. Estas modificações são recíprocas, onde a tri-metilação (me3) está associada a repressão dos genes, e a acetilação (ac) está associada a ativação de expressão dos genes. Os resultados mostraram que, de facto, embora não estatisticamente significativos, existe uma tendência para uma diminuição da marcação H3K27ac ao dia-4 de diferenciação nos promotores dos genes *Brachyury*, *Cdx2*, *Dkk1*, *Isl1*, *Kdr*, *Mesp1* e *Wtn5a*. Concordante com estes resultados, e como seria de esperar, estes genes encontraram-se negativamente regulados. O inverso foi observado para as condições de pluripotência, ou seja, a baixa expressão de *Cited2* levou a uma tendência

para aumento de acetilação, que foi seguida pelo também esperado aumento de expressão desses mesmos genes. Contudo, a marcação de metilação mostrou ter um erro maior, e não seguia a esperada reciprocidade com os resultados da acetilação. Por fim, de modo a perceber a influência de *Cited2* na capacidade de acetilação das células foi realizado um ensaio *in vitro* para comparar os níveis de acetilação de extratos proteicos totais de células expressando e não-expressando *Cited2*. Os resultados mostram que as células depletadas de Cited2 têm um aumento de acetilação. Contudo, não foi possível demonstrar que a acetilação de histonas por p300/CBP é diretamente modulado por CITED2.

Em suma, este trabalho não permitiu de forma clara demonstrar que o aumento da morte e diferenciação espontânea seja causado por dano no DNA aquando da depleção de Cited2. No entanto, este trabalho propõe que o atraso da expressão de genes importantes para a diferenciação cardíaca tenha uma componente associada à desregulação de mecanismos epigenéticos, nomeadamente regulação de H3K27me3/ac.

Palavras chave: Cited2, ADN, diferenciação, pluripotência, H3K27me3/ac, ratinho

Table of contents

ACKNOWLEDGMENTS ..... **VII**
ABSTRACT ..... **IX**
RESUMO ..... **XI**
TABLE OF CONTENTS ..... **XV**
LIST OF FIGURES ..... **XVII**
LIST OF TABLES ..... **XXI**
NON-STANDARD ABBREVIATIONS AND ACRONYMS ..... **XXIII**
1 INTRODUCTION **1**
1.1 Heart diseases **1**
1.2 Mammalian heart development **2**
1.3 Gene of interest: Cited2 ..... **5**
1.3.1 Cited2 in heart development 6
1.4 Pluripotency and stem cells **7**
1.4.1 Pluripotency network 9
1.4.2 Cited2 and pluripotency 11
1.4.3 Maintenance of stem cells 11
1.4.4 DNA integrity 12
1.4.5 A state of transition 15
1.5 Cardiac differentiation in vitro **16**
1.5.1 Cited2 in differentiation 18
1.5.2 Epigenetic regulation 20
1.6 Objectives **22**
2 METHODOLOGY **23**
2.1 Cell culture **23**
2.1.1 Cell lines 23
2.1.2 Cell maintenance 23
2.1.3 Treatments 24
2.1.4 *In vitro* differentiation 25
2.2 Immunoassays **26**
2.2.1 Immunoblotting (Western Blot) 26
2.2.2 Immunocytochemistry and immunofluorescence (ICC/IF) 27
2.2.3 Immunoprecipitation (IP) 28

2.2.4 Chromatin Immunoprecipitation (ChIP) 28
2.2.5 Antibodies used 30

2.3 Molecular biology 30
2.3.1 RNA isolation and cDNA synthesis 30
2.3.2 gDNA isolation 30
2.3.3 Real-time-PCR (qPCR): mRNA and gDNA 31
2.3.4 Microarrays 32
2.3.5 Whole protein extraction and quantification 36

2.4 Image analysis 36
2.4.1 Embryoid bodies 36
2.4.2 Western blot semi-quantification 37
2.4.3 γH2AX speckles 37

2.5 Histone acetylation assay 37

2.6 Data analysis and statistics 38
3 RESULTS 39

3.1 Cited2 affects pluripotency and differentiation 39

3.2 The suggested role of *Cited2* in DNA repair 42
3.2.1 DNA damage increase 46
3.2.2 DNA damage rescue with recombinant Cited2 54
3.2.3 DNA damage under differentiation conditions 58
3.2.4 Cited2-KO cells present downregulation of pro-apoptotic genes 62

3.3 Epigenetic regulation of differentiation (H3K27me3/ac) 64
3.3.1 Cited2 inhibits histone acetyltransferase activity 78
4 DISCUSSION 81

4.1 The proposed model and future perspectives 90
5 CONCLUSION 93
6 REFERENCES 95

List of Figures

FIGURE 1.1 SIMPLIFIED SCHEMATIC REPRESENTATION OF GASTRULATION. 4

FIGURE 1.2 SIMPLIFIED SCHEMATIC REPRESENTATION OF CITED2 PROTEIN AND ITS DOMAINS. 6

FIGURE 1.3 SIMPLIFIED SCHEMATIC REPRESENTATION OF SIGNALLING PATHWAYS REGULATING PLURIPOTENCY. 9

FIGURE 1.4 SIMPLIFIED SCHEMATIC REPRESENTATION OF DNA DAMAGE RESPONSE. 14

FIGURE 1.5 SIMPLIFIED SCHEMATIC REPRESENTATION OF THE DIFFERENTIATION STEPS FROM PLURIPOTENT CELLS TO CARDIOMYOCYTES. 19

FIGURE 3.1 EXPERIMENTAL DESIGN TO DETERMINE DIFFERENTIALLY EXPRESSED GENES. 40

FIGURE 3.2 *CITED2*-PARTIAL_KO GROUPS CLUSTER APART FROM THEIR CONTROL GROUP. 41

FIGURE 3.3 DIFFERENT REGULATION OF GENES BETWEEN CELLS EXPRESSING AND NOT EXPRESSING *CITED2* UNDER UNDIFFERENTIATED CONDITIONS. 43

FIGURE 3.4 *CITED2*-PARTIAL_KO AFFECTS PLURIPOTENCY FACTORS TERMS OF CHEA/ENCODE DATABASE. 44

FIGURE 3.5 *CITED2*-PARTIAL_KO AFFECTS DNA REPAIR BIOLOGICAL PROCESSES IN PLURIPOTENCY CONDITIONS. 45

FIGURE 3.6 EXPERIMENTAL DESIGN TO ASSESS DNA DAMAGE. 46

FIGURE 3.7 *CITED2* EXPRESSION IS DOWN-REGULATED UNDER UNDIFFERENTIATING CONDITIONS. 48

FIGURE 3.8 *CITED2*-PARTIAL_KO INCREASES SPONTANEOUS DIFFERENTIATION AND CELL DEATH. 49

FIGURE 3.9 *CITED2*-PARTIAL_KO DOES NOT CHANGE γH2AX SPECKLES NUMBER BUT INCREASES THEIR INTENSITY. 50

FIGURE 3.10 INCREASE IN γH2AX PROTEIN LEVELS IN *CITED2*-PARTIAL_KO CELLS AFTER 16 HOURS. 51

FIGURE 3.11 SUGGESTED DECREASED γH2AX PROTEIN LEVELS IN *CITED2*-PARTIAL_KO CELLS AFTER 48 HOURS 52

FIGURE 3.12 EXPERIMENTAL DESIGN OF THE VALIDATION OF DOWN-REGULATED AND UP-REGULATED GENES IN PLURIPOTENCY. 52

FIGURE 3.13 *CITED2*-PARTIAL_KO SUGGESTS AN ALTERATION OF THE DNA DAMAGE RESPONSE, INCREASED APOPTOSIS, AND UNBALANCED P53 RESPONSE GENES. 53

FIGURE 3.14 EXPERIMENTAL DESIGN TO ASSESS DNA DAMAGE, WITH THE RESCUE OF *CITED2*-PARTIAL_KO. 54

FIGURE 3.15 WIDE-FIELD FLUORESCENCE MICROSCOPY OF ΓH2AX RESCUE EXPERIMENT. 55

FIGURE 3.16 *CITED2*-PARTIAL_KO RESCUE WITH RECOMBINANT CITED2 APPEARS TO DECREASE THE NUMBER OF ΓH2AX SPECKLES. 56

FIGURE 3.17 *CITED2*-PARTIAL_KO RESCUE SHOWS UNCHANGED ΓH2AX PROTEIN LEVELS. 57

FIGURE 3.18 EXPERIMENTAL DESIGN TO ASSESS DNA DAMAGE IN MONOLAYER DIFFERENTIATION CONDITION 58

FIGURE 3.19 $C2^{FL/FL}$[CRE] CELLS CULTURED IN DIFFERENTIATION-INDUCING CONDITIONS (IN MEDIUM WITHOUT LIF). 59

FIGURE 3.20 *CITED2*-PARTIAL_KO DECREASES ΓH2AX FOCI NUMBER AND THEIR INTENSITY. 60

FIGURE 3.21 SUGGESTION THAT ΓH2AX LEVELS DECREASE OVER TIME UNDER *CITED2*-PARTIAL_KO IN DIFFERENTIATING CONDITIONS. 61

FIGURE 3.22 *CITED2* EXPRESSION IS UNCHANGED UNDER UNDIFFERENTIATING CONDITIONS AT TWO TIME POINTS. 61

FIGURE 3.23 EXPERIMENTAL DESIGN TO EVALUATE DNA DAMAGE AND P53-RESPONSE GENE IN *CITED2*-KNOCKOUT CELLS 62

FIGURE 3.24 DOWNREGULATION OF DNA DAMAGE RESPONSE, AND APOPTOTIC GENES IN *CITED2*-KO CELLS 63

FIGURE 3.25 DIFFERENT REGULATION OF GENES BETWEEN CELLS THAT EXPRESS AND DO NOT EXPRESS *CITED2* IN DIFFERENTIATION CONDITIONS ON DAY 4. 65

FIGURE 3.26 THE DEPLETION OF *CITED2* REDUCES AFFECTS PLURIPOTENCY TRANSCRIPTION FACTORS OF CHEA/ENCODE DATABASE. 66

FIGURE 3.27 *CITED2* DEPLETION AFFECTS HEART DEVELOPMENT. 67

FIGURE 3.28 VALIDATION OF DOWN-REGULATED GENES IN DIFFERENTIATION CONDITIONS OBTAINED FROM MICROARRAYS. 69

FIGURE 3.29 EXPERIMENTAL DESIGN TO ASSESS PROMOTER ENRICHMENT OF H3K27ME3/AC. 70

FIGURE 3.30 *CITED2*-PARTIAL_KO DECREASES THE SIZE AND FORM FACTOR OF EMBRYOID BODIES. 73

FIGURE 3.31 *CITED2*-PARTIAL_KO EMBRYOID BODIES SHOW IMPAIRED CARDIAC DIFFERENTIATION. 74

FIGURE 3.32 REPRESENTATIVE IMAGE OF THE SHEARED CHROMATIN SMEAR..... 74

FIGURE 3.33 SUGGESTION THAT *CITED2*-PARTIAL_KO CHANGES PROMOTER ENRICHMENT LEVELS OF H3K27ME3. 75

FIGURE 3.34 SUGGESTION THAT *CITED2*-PARTIAL_KO CHANGES PROMOTER ENRICHMENT LEVELS OF H3K27AC. 76

FIGURE 3.35 *CITED2*-PARTIAL_KO DOWNREGULATES CARDIAC DIFFERENTIATION GENES IN DIFFERENTIATION CONDITIONS BUT UPREGULATES IN UNDIFFERENTIATION CONDITIONS.. 77

FIGURE 3.36 EXPERIMENTAL DESIGN TO ASSESS THE ABILITY OF HISTONE ACETYLATION. 78

FIGURE 3.37 UNDIFFERENTIATED *CITED2*-PARTIAL_KO CELLS SUGGESTED INCREASED GLOBAL HISTONE ACETYLTRANSFERASE AND UNCHANGED ACETYLATION BY P300. 79

FIGURE 4.1 SIMPLIFIED SCHEMATIC REPRESENTATION OF THE PROPOSED MODEL OF THE ROLE OF CITED2 IN PLURIPOTENCY AND DIFFERENTIATION. 92

List of Tables

TABLE 2.1 LIST OF USE ANTIBODIES, THEIR APPLICATION AND ITS DILUTION OR QUANTITY USED. 30

TABLE 2.2 LIST OF PRIMERS USED IN QPCR TO ANALYSE THE EXPRESSION LEVEL OF TARGET GENES. 33

TABLE 2.3 LIST OF PRIMERS USED IN QPCR TO ANALYSE THE ENRICHED PROMOTER REGIONS FROM CHIP EXPERIMENTS. 35

Non-standard abbreviations and acronyms

In this work the standard nomenclature for chemicals and unit symbols proposed by IUPAC were used.

4HT	4-Hydroxytamoxifen
53BP1	Tumor Protein P53 Binding Protein 1
8R-CITED2	Recombinant Human Cited2 With Eight Arginines In The N-Terminal
aa	Amino Acid
ac	Acetylation, Post-Translation Modification
APS	Ammonium Persulfate
Asb4	Ankyrin Repeat And Socs Box Containing 4
ATAC-seq	Assay For Transposase-Accessible Chromatin Using Sequencing
ATM	ATM Serine/Threonine Kinase
ATR	ATR Serine/Threonine Kinase
AU	Arbitrary Units
BAX	Bcl2 Associated X, Apoptosis Regulator
BMP	Bone Morphogenetic Protein
BSA	Bovine Serum Albumin
$C2^{fl/fl}$[cre]	Mesc *Cited2*-Floxed $C2^{fl/Fl}$[Cre] *Cited2*
CBP	Creb-Binding Protein Or Crebbp
cDNA	Complementary Desoxyribonucleic Acid
CDX2	Caudal Type Homeobox 2
CER1	Cerberus 1
CH1	Cysteine/Histidine-Rich 1, P300/Cbp Domain
ChIP	Chromatin Immunoprecipitation
CITED2	Cbp/P300-Interacting Trans-Activators With Glutamic/Aspartic Acid Rich Carboxy-Terminal 2
c-Kit	Kit Proto-Oncogene, Receptor Tyrosine Kinase
Cq	Cycle quantification
CR1-3	Conserved Region, Cited2 Domains
cre	Cre Recombinase
$Cre\text{-}ER^{T2}$	Cre Recombinase Tamoxifen-Inducible Estrogen Receptor
Ct	Cycle threshold
CXCR4,7	C-X-C Motif Chemokine Receptor 4,7

DAPI	4',6-Diamidino-2-Phenylindole
DEG	Differentially Expressed Genes
DKK1	Dickkopf Wnt Signaling Pathway Inhibitor 1
DMSO	Dimethyl Sulfoxide
DNA	Desoxyribonucleic Acid
DPBS	Dulbecco's Phosphate Buffered Saline
E	Murine Embryonic Day
e.g	For Example
eb	Embryoid Body
Eb(s)	Embryoid Body(Ies)
ECL	Enhanced Chemiluminescence
EDTA	Ethylenediamine Tetraacetic Acid
EMT	Epithelial-To-Mesenchymal Transition
EOMES	Eomesodermin
EpiSC	Epiblast Stem Cells
ERK	Extracellular Signal-Regulated Kinase
ESC	Embryonic Stem Cell
EtOH	Ethanol
EZH2	Enhancer Of Zeste 2 Polycomb Repressive Complex 2 Subunit
FBS	Fetal Bovine Serum
FGF	Fibroblast Growth Factor
FGFR	Fgf Receptor
FHOD1	Formin Homology 2 Domain Containing 1
FLAG	FLAG-Tag (DYKDDDDK)
FOXA2	Forkhead Box A2
FOXC2	Forkhead Box C2
FOXF1	Forkhead Box F1
GATA4	Gata-Binding Factor 4
GDF15	Growth Differentiation Factor 15
GFP	Green Fluorescent Protein
GMEM	Glasgow Minimum Essential Medium Bhk-21
GMEM+	Supplemented GMEM0
GMEM++	LIF Supplemented GMEM+

GMEM0	Plain GMEM
GSC	Goosecoid Homeobox
Gsk3	Glycogen Synthase Kinase 3
H1,23,4	Histone 1,2,3,4
H2AX	H2A.X Variant Histone
HAND1-2	Heart And Neural Crest Derivatives Expressed 1-2
HIF1α	Hypoxia Inducible Factor 1 Subunit Alpha
i.e.	That Is
ICC	Immunocytochemistry
IF	Immunofluorescence
IgG	Immunoglobulin G
IP	Immunoprecipitation
iPSC	Induce Pluripotent Stem Cell
ISL1	Insulin Gene Enhancer Protein Isl-1
JAK-STAT	Janus Kinases
KDR	Kinase Insert Domain Receptor
KLF4	Krueppel-Like Factor 4
KO	Knockout
LEFTY	Left-Right Determination Factor
LIF	Leukemia Inhibitory Factor
LIM	LIM Domain
LIN28	Zinc Finger, Cchc Domain Containing 1
MAPK	Mitogen-Activated Protein Kinase
MDC1	Mediator Of Dna Damage Checkpoint 1
me	Methylation, Post-Translation Modification
me3	Tri Methylation, Post-Translation Modification
MEF2C	Myocyte-Specific Enhancer Factor 2c
MEM-NEAA	Minimum Essential Medium Non-Essential Amino Acids
mESC	Mouse Embryonic Stem Cells
MESP1	Mesoderm Posterior Bhlh Transcription Factor 1
MEX3b	Mex-3 Rna Binding Family Member B
MiliQ	Ultra Pure Water Trade Mark Of Merck
MIXL1	Mix Paired-Like Homeobox

mRNA	Messenger Ribonucleic Acid
N2B27	Cell Culture Medium N2B27
NANOG	Homeobox Transcription Factor Nanog
NFATC1-2	Nuclear Factor Of Activated T-Cells, Cytoplasmic
NHEJ	Non-Homologous End Joining
NODAL	Nodal Signalling Pathway
NOXA	Phorbol-12-Myristate-13-Acetate-Induced Protein 1
ns	Non-Significant
OCT4	Octamer-Binding Protein 4, Or POUF5
P/S	Penicillin-Streptomycin
P19	Mouse Embryonic Carcinoma Cell Line
p21	Cyclin Dependent Kinase Inhibitor 1a
p300	E1a Binding Protein P300
p53	Tumor Protein P53
PBS	Phosphate Buffered Saline
PC1,2	Principal Component 1,2
PCR	Polymerase Chain Reaction
Pcsk5	Proprotein Convertase Subtilisin/Kexin Type 5
PERP	P53 Apoptosis Effector Related To Pmp22
PFA	Paraformaldehyde
PI3K	Phosphatidylinositol-4,5-Bisphosphate 3-Kinase Catalytic Subunit Delta
PITX2	Paired-Like Homeodomain Transcription Factor 2
PLK2	Polo Like Kinase 2
PMSF	Phenylmethanesulfonyl Fluoride
PP2A	Protein Phosphatase 2
PRC2	Polycomb Repressive Complex 2
Prdm6	Pr/Set Domain 6
PUMA	Bcl2 Binding Component 3
PVDF	Polyvinylidene Fluoride
px	Pixel
qPCR	Real-Time PCR
RAD51	DNA Repair Protein Rad51 Homolog 3

RAD9b	Rad9 Checkpoint Clamp Component B
Rasgrp3	Ras Guanyl Releasing Protein 3
Rbm24	Rna Binding Motif Protein 24
rcf	Relative Centrifugal Force, same as *g* force
RNA	Ribonucleic Acid
RNA-seq	RNA-Sequencing
ROI	Region Of Interest
ROS	Reactive Oxygen Species
Rspo3	R-Spondin 3
SALL4	Spalt Like Transcription Factor 4
sd	Standard Deviation
SDS-PAGE	Sodium Sodecyl Sulphate-Polyacrylamide Gel Electrophoresis
SEM	Standard Error Of Mean
SOX17	SRY-Box Transcription Factor 17
SOX2	SRY-Box Transcription Factor 2
SRJ	Serine-Glycine Rich Junction, Cited2 Domain
STAT	Signal Transducer And Activator Of Transcription Proteins
SUZ12	Suz12 Polycomb Repressive Complex 2 Subunit
T	Brachyury
TAZ1	See CH1
TBS	Tris Buffer Saline
TBST	Tbs With 0.1 % Tween-20
TBX1,5,20	T-Box Transcription Factor 1,5,20
TCF3	Transcription Factor 3
TE	Tris EDTA
TEMED	Tetramethylethylenediamine
TGF-b,	Transforming Growth Factor Beta
TNNT2	Troponin T2, Cardiac Type
TRIS	2,4,6-Tris[(Dimethylamino)Methyl]Phenol
TUBB3	Tubulin Beta 3 Class Iii
UCP2	Uncoupling Protein 2
undiff	Undifferentiated Cells
UTX	Lysine Demethylase 6A, Or KDM6

WNT	Wnt Signalling Pathway
γH2AX	Phosphorylated H2A.X Variant Histone

1 Introduction

1.1 Heart diseases

Heart diseases are the leading cause of death worldwide, followed by cancer. Heart diseases can be split into two main groups: congenital heart diseases and cardiovascular acquired diseases (noncongenital heart diseases) (Wang et al., 2019). The origin of heart disease is associated with multiple variables, such as genetic factors, environmental factors, and lifestyle (Liu et al., 2009; Who, 2021). Some heart diseases appear later in life due to ageing, poor adoption of healthy habits, stress, and obesity (Kivimäki and Steptoe, 2018; Paneni et al., 2017; Ravera et al., 2016). In western countries, there is an increase in heart diseases that pose a burden on national health care systems (Hoffman, 2013). Although cardiovascular diseases can be mitigated with a healthy lifestyle, it is still necessary to develop new treatments and/or therapies (Fiuza-Luces et al., 2018).

The emergence of personalized medicine (Currie and Delles, 2018) exploiting the theoretical regenerative abilities of stem cells makes them good candidates for the development of new therapies (Kimbrel and Lanza, 2015). Therefore, some possible therapies can help with the treatment of ischemic heart failure and heart infraction (Bragança et al., 2019; Ng et al., 2010; Rikhtegar et al., 2019). At the present, 393 clinical trials to treat ‘heart diseases’ with ‘stem cells’ are registered on clinicaltrials.gov (ClinicalTrials.gov). Nonetheless, promising results using an injection of autologous bone marrow mononuclear cells were obtained to treat ischemic heart failure (Perin et al., 2011).

Congenital heart diseases showed an increase in neonates worldwide of approximately 10% from 2010 to 2017 (Liu et al., 2019). In Europe, an increase was also observed from 1997 to 2018 in adults with congenital heart disease (Vida et al., 2020). Yet, the global count could be a consequence of increased detection due to improvements in echocardiography (Liu et al., 2019). In Portugal, from data reporting back to 2015, the prevalence of congenital heart disease is 5:1000 (Melo et al., 2020), which is lower than the numbers observed in other European countries of approximately 8:1000 (Eurocat, 2022), which in turn is similar to the global average (Liu et al., 2019). Among the large list of congenital heart defects observed ventricular septal defect, atrial septal defect, coarctation of the aorta and Fallot’s tetralogy, are the most predominant. Hopefully, some heart malformations can be avoided or mitigated with folic acid, and micronutrient supplementation during pregnancy (Milne et al., 2010; Obeid et al., 2019;

Santander Ballestín et al., 2021), the same cannot be said for congenital heart diseases with a genetic source.

Genetic factors in congenital heart diseases account for 20 % of congenital heart diseases (Blue et al., 2012). Due to the complexity of genetics, it is difficult and requires extensive research to reach treatment. For example, single mutations associated with a specific cardiac congenital disease would be easier to find than diseases caused by different and multiple mutations in multiple genes (Fahed and Nemer, 2012). However, lives can be saved as cardiac defects can be surgically treated, which is the case for atrial septal defect closure and muscular ventricular septal defect closure (Menaissy et al., 2019; Pettitt, 2020). However, not all the time embryos and foetuses reach term, which results in abortions that account for 13 % of miscarriages (Chinn et al., 1989). Therefore, genetic studies with cellular models and cell therapy trials are being carried out worldwide (Brown et al., 2020; Oh, 2017), with the final goal of reducing the implications of embryo development caused by genetic factors, and improving the lives of those affected by congenital heart diseases.

1.2 Mammalian heart development

Heart development (or cardiogenesis) is a complex process that occurs in animals from worms to humans; thus, it is conserved in the animal kingdom. Although human gastrulation is not well studied since, in many countries, the allowed number of days to maintain a human embryo is fourteen (Ghimire et al., 2021; Noe, 2004). The fourteen days of development correspond to the beginning of gastrulation, then due to ethical reasons, there are no studies on human embryos. What is known derives from studies belonging to Carnegie collection (Noe, 2004). Therefore, most of the knowledge about gastrulation and cardiogenesis originates from animal models, *e.g.* xenopus, zebrafish, mouse, chick and macaque; which as models possess their limitations. Nonetheless, the heart development of mice and humans is similar in the development steps and genes involved (Krishnan et al., 2014).

As in most biological processes, cardiogenesis is controlled/organized by genes and signalling pathways (FGF, TGF, BMP, NODAL, WNT, etc.) to regulate the chain of events that lead to the adult heart. The genes that regulate heart development were preserved through evolution and are well conserved between species, for example, Nkx2.5 (Haun et al., 1998). The NKX2.5 was one of the first to appear in the tree of life and allowed organisms to develop a linear contractile tube (Bishopric, 2005). As the overall complexity of the organisms evolved, also did

the heart and the number of genes associated with heart development. Heart development begins early in embryo life when the initial pool of pluripotent cells begins to acquire different cell fates. The mechanisms involved are tightly regulated and follow a series of events that guides cells to differentiate in a step-wise manner to go from one developmental stage to another—until the whole organ is formed.

One of the first steps important for heart development and cardiac differentiation is gastrulation. During this stage of development, the three germ layers are formed: ectoderm, mesoderm, and endoderm (Muhr and Ackerman, 2022) (Figure 1.1**)**. Each of these three layers will give rise to different organs and tissues.

Human and mouse gastrulation share some similarities, yet there are some differences. One of these differences is the timing of second lineage segregation that leads to the formation of primitive endoderm and epiblast (Chazaud et al., 2006). While in mice during the migration of cells from the epiblast, cells have the FGF/Erk signalling pathway activated by the expression of FGF4, FGFR1, and FGFR2 that promote the expression of the endoderm marker *Gata6* (Morris et al., 2010), the mechanism in humans is unknown (Boroviak et al., 2018). Another difference is the shape of the embryo: human embryos acquire a bilaminar (flat) disk configuration, while the mouse embryo acquires a concave egg cylinder configuration (or U-shape) (Molè et al., 2020).

Having an egg shape form, the mouse embryo, extra-embryonic lineages, and the hypoblast from embryonic day (E) 5 began to induce the first symmetry breaking, creating the anterior-posterior axis. Extra-embryonic ectoderm secretes BMP4 ligands that lead to the expression of *Wnt3* and *Nodal* (Arnold and Robertson, 2009). Similar results were obtained with human ESC, cultured on substrates that allow the control of its growth and movement (Martyn et al., 2019). Later, in mouse development, the NODAL signal is suppressed by the anterior ventral endoderm by secreted LEFTY1 and CER1 (Belo et al., 2000; Belo et al., 1997), and DKK1 (Kemp et al., 2005). On the opposite side of the embryo NODAL (Brennan et al., 2001) as well as WTN3 (Liu et al., 1999b), activate *Brachyury*, which is a marker for the migrating epiblast cells (Viebahn et al.).

At this stage, the epiblast and the hypoblast are the two layers that exist, before gastrulation begins (Figure 1.1). Thus, gastrulation leads to a three-layer structure now named the ectoderm, mesoderm, and endoderm (Rivera-Pérez and Magnuson, 2005). The movement of *Brachyrury* positive cells, through ingression, refers to the migration of epiblast cells that are also stimulated by the prechordal plate, by the secretion of signalling molecules such as FGF (Schulte-Merker

and Smith, 1995). During these processes, cell movement is allowed through activation of epithelial-to-mesenchymal transition (EMT) (Williams et al., 2012). The EMT allows cells to break bonds (by inhibiting the E-cadherins and other adhesion molecules) with neighbouring cells and thus gain the freedom to migrate through the primitive streak groove (Ichikawa et al., 2013; Müller and O'Rahilly, 2004). Additionally, during gastrulation the polarity of the embryo is established, *i.e.* the left-right axis and anterior-posterior axis are formed. This is achieved by a number of signalling molecules, among which Activin/Nodal are central (Hyatt and Yost, 1998; Katsu et al., 2013). Hence, the three layers of endoderm, mesoderm, and ectoderm are formed (Muhr and Ackerman, 2022).

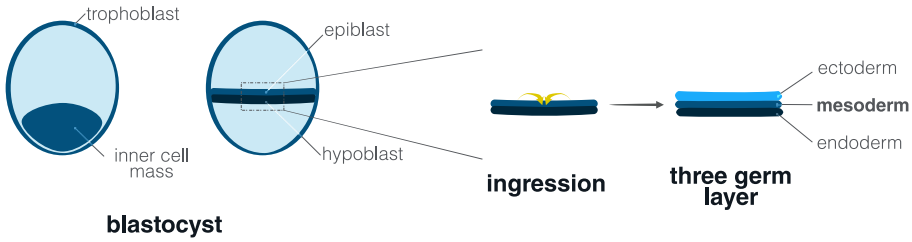

Figure 1.1 Simplified schematic representation of gastrulation. The pluripotent cells in the inner cell mass undergo differentiation and form two layers: epiblast and hypoblast. The epiblast ingresses through the migration of cells to form the three germ layers: endoderm, mesoderm, and ectoderm.

These three germ layers will be the basis for the embryo. However, more attention will be paid to the mesoderm, since the majority of cells in the heart derive from it (Abu-Issa and Kirby, 2007). Therefore, once the mesoderm is formed, specifically the splanchnic mesoderm, it further specifies into cardiac mesoderm (Muhr and Ackerman, 2022); which expresses *Brachyury* (*T*) (Stennard et al., 1997). Then the cardiac mesoderm originates two new pools of cells, called the first heart field and second heart field (Buckingham et al., 2005). The first heart field is positive for the makers *Nkx2*.5 and *Tbx5* (Bruneau et al., 2001; Lyons et al., 1995), while the second heart field is positive for *Isl1* (Cai et al., 2003). Next, in a simplified way, these layers differentiate and form two tubes that fuse to form the heart tube. Then this tube goes through a process called heart looping to originate a heart that resembles the adult heart. Therefore, from lineage tracing studies it was found that the first heart field will form the left ventricle and atria, while the second heart field will form outflow-tract and contribute to the right ventricle and atria (Buckingham et al., 2005). Thus, considering this knowledge and identifying the genes involved, one could predict what could be the clinical implication for patients.

1.3 Gene of interest: Cited2

The gene *CITED2* encodes the co-transcription factor protein CITED2 (CBP/p300-interacting trans-activators with glutamic/aspartic acid rich carboxy-terminal 2). This gene appeared in the tree of life around 473 million years ago in the node of the jawed vertebrates (*Gnathostomata*), and the last common ancestor between primates and rodents was around 82 million years ago in the node of (*Euarchontoglires*) (Encode, 2022). CITED2 lacks a DNA binding domain and thus acts as a co-transcription factor (Dunwoodie et al., 1998), and is expressed ubiquitously (De Guzman et al., 2004).

CITED2 belongs to the CITED family of genes, along with *CITED1*, *CITED4* and *Cited3* (only present in non-mammals) (Dunwoodie et al., 1998). The human protein (Uniprot:Q99967) and the mouse protein (Uniprot:O35470) proteins have similar sizes, respectively, 270 and 269 amino acids (aa), sharing a 94.8 % identity. This protein has four conserved regions: CR1-3 and serine-glycine rich junction (SRJ) unique to CITED2 (Figure 1.2). The CR2 (aa215-270) has a highly conserved region (aa234-255) that is necessary for the well-established physical interaction between p300/CBP at the cysteine-histidine-rich domain (CH1 or TAZ1) and is the domain characterizing CITED family members (Bhattacharya et al., 1999; De Guzman et al., 2004; Ruiz-Ortiz and De Sancho, 2020). The functions of CR3 (aa1-6) and the CR1 (aa110-123) have yet to be known. However, the SRJ region, is absent in one isoform of the *CITED2* gene (see transcript ENST00000618718.1), which could explain the observation that the whole excision of this region did not alter the normal development of mice (Chen et al., 2012).

The CR2 domain of CITED2 was associated with hypoxia regulation and is the central interaction domain identified with CITED-interactors (Bragança et al., 2019). Hypoxia regulation is achieved through a mechanism of negative regulation of HIF1-α, where both CITED2 and HIF1- α compete for the CH1 domain of p300/CBP (Bhattacharya et al., 1999; De Guzman et al., 2004). This binding is achieved by the disordered regions of the proteins that used the CH1 domain of p300/CBP as the scaffold. In this way, different transcription factors compete for CH1 binding to recruit p300/CBP to different promoter regions of different genes (Freedman et al., 2003).

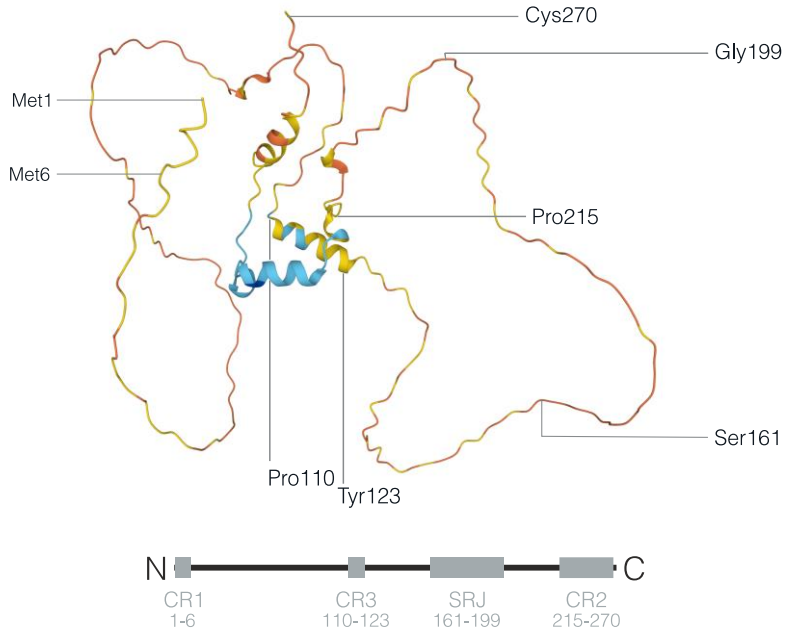

Figure 1.2 Simplified schematic representation of CITED2 protein and its domains. CITED2 has 270 amino acids and contains three domains: three conserved regions CR1 (1-6 aa), CR3 (110-123 aa), serine-glycine rich junction SRJ (161-199) and CR2 (215-270). Model of the 3D structure predicted by AlphaFold (Jumper et al., 2021; Varadi et al., 2022).

1.3.1 Cited2 in heart development

Various studies have shown that Cited2 is required for normal heart development. Indeed, *Cited2-knockout* mice embryos died *in utero* before the embryonic day (E) 17.5, with different combinations of cardiac defects. These embryos presented abnormal development of cardiac outflow tract, atrial and ventricular septal defects, double-outlet right ventricle, abnormal aortic arches, and abnormal left-right patterning (Bamforth et al., 2001; Bamforth et al., 2004; Yin et al., 2002). Additionally, these studies also showed other phenotypes, such as neural tube defects, and the absence of adrenal glands; this could be due to apoptosis in the midbrain region (Bamforth et al., 2001).

In humans, mutations in the *CITED2* gene were associated with congenital heart defects. The main heart defects were found to be mainly septal defects (Chen et al., 2012; Sperling et al., 2005; Yang et al., 2010), which is one of the most prevalent forms of congenital heart disease, as mentioned above. Most mutations seem to be located in the SRJ domain of the CITED2 protein. However, a study in mice recapitulating the human mutations failed to recapitulate the phenotype. In fact, deletion of the whole SRJ domain did not influence normal heart development in mice, suggesting that mutations in this region are not the only factor contributing to congenital heart disease (Chen et al., 2012).

Recently, a new mutation identified in humans (p.P101S), close to the CR1, was described with a gain of function of *Cited2* in mouse, possibly due to phosphorylation of the serine residue. This mutation led to a modest upregulation of CITED2-target genes *Gata4, Mef2c, Nfatc1&2, Nodal, Pitx2,* and *Tbx5* in P19 embryonic carcinoma cells (Yadav et al., 2021). Therefore, as discussed by others, it is possible that for a given mutation the phenotypes between mouse and human do not match (Chen et al., 2012); as observed for other diseases/mutations (Lombard et al., 2000).

Studies in mouse, focusing on the early stages prior to gastrulation, showed that *Cited2* is expressed in a restricted area of the embryo, the anterior visceral endoderm. Then *Cited2* showed increased expression in the mesoderm close to the anterior visceral endoderm and whole primitive streak. This increased expression was maintained through heart development and present in the myocardium and the septum transversum. Moreover, *Cited2* was also found to be in the antero-proximal endoderm and anterior mesoderm, at the neural-plate stage (Dunwoodie et al., 1998). Interestingly, *Cited2*$^{-/-}$ embryos showed reduced or abnormally distributed cardiac neural crest cells, which could be the cause of the identified cardiac developmental defects (Bamforth et al., 2001). Therefore, the role of Cited2 seems to be in the initial steps of embryo development.

1.4 Pluripotency and stem cells

Heart development and, in fact, the development of the whole organism is not possible without stem cells. The term stem cell was proposed by the German biologist Haeckel in 1887, who considered that the fertilized egg should be named stem cell (Ramalho-Santos and Willenbring, 2007). Only later in 1892, the term stem cell was applied to refer to the cells between the fertilized egg and the germ line. The term stem cell began to gain more traction in the early 1900s when it was used to refer to the precursor cells of the blood system (Ramalho-Santos and Willenbring, 2007). However, only about 80 years later the first mouse embryonic stem cells were isolated from the blastocyst and maintained *in vitro* (Evans and Kaufman, 1981). And, only in 1998 was reported the first isolation of human embryonic stem cells from a preimplantation blastocyst from fertilization facilities (Thomson et al., 1998).

Nowadays, stem cells are defined as cells that are unspecialized/undifferentiated and can maintain self-renewal, and thus can differentiate into any cell of the organism (Zakrzewski et al., 2019). Although there are different classifications for these cells depending on their potency

(or ability to differentiate in different somatic cells). In general, cells can be considered as totipotent, pluripotent, multipotent, oligopotent, and even unipotent. In a developing embryo, these cells are originated from the zygote (totipotent cell), which undergoes successive cleavages until the embryonic the structure known as blastocyst is formed (Gilbert, 2000). The blastocyst contains two layers of cells: the trophoblast and the inner cell mass (pluripotent cells). The inner cell mass is the source of pluripotent embryonic stem cells (Figure 1.1). This pool of cells will originate the whole organism once, which begins with the gastrulation process, as already elucidated (above). After this stage, the cells gain specification and the number of differentiated cell types that they can originate is smaller and smaller; therefore, the potency is being reduced as the embryo develops. For example, mouse embryonic stem cells isolated from implanted blastocysts, called epiblastic stem cells, are a differentiation step ahead of inner cell mass cells (Loh et al., 2015). And, interestingly, mouse epiblast stem cells are similar in potency to human embryonic stem cells (Loh et al., 2015).

Stem cells can also be characterized by their symmetric and asymmetric divisions. This characteristic allows their two abilities. Each stem cell can divide symmetrically and generate daughter cells that maintain self-renewal (preserving the same fate). When the division is asymmetric, the daughter cells differentiate and acquire a new fate (Morrison and Kimble, 2006). These two kinds of cellular divisions have implications not only during development, but also during the life of the organism. While during development this characteristic allows the creation of pools of cells due to the increase of the number of cells maintained by self-renewal, during adult life it is important for the maintenance of adult stem cells. The adult stem cells, which are multipotent cells, are maintained *in vivo* in stem cell niches that are characterized by providing the microenvironment that not only allows their maintenance, but also provides cues for their fate (Ferraro et al., 2010). Adult stem cells can be found in the adult organism, and evidence suggests that these cells can be isolated from different organs or tissues, where they play a critical role in the maintenance of homeostasis (Mannino et al., 2022). One of the well-known examples is the haematopoietic stem cell niche (Morrison and Scadden, 2014). Interestingly, a population of adult stem cells was identified in the heart (with positive markers for c-Kit) (Faucherre and Jopling, 2013).

Lastly, pluripotent stem cells can now be generated artificially in the laboratory, and are termed induced pluripotent stem cells (iPSC). This advance was possible after the discovery of the key pluripotency factors and signalling pathways responsible to maintain pluripotency in embryonic stem cells (Takahashi et al., 2007; Takahashi and Yamanaka, 2006). This new way of

generating pluripotent stem cells from somatic cells (terminally differentiated cells) opens the doors for new studies of disease, and to the development of new therapies. The use of iPSC has advantages compared to embryonic stem cells, for two main reasons: the ethical problems raised by using human embryonic stem cells are avoided, since the source of pluripotent stem cells is now the patient or a healthy patient after informed consent. And, in theory, any differentiated cell from an individual at any age or condition can be used to generate iPSC. These two points open the doors to personalized medicine (Braganca et al., 2019; Müller et al., 2018; Walsh et al., 2014).

However, there is concern that therapies that involve injecting pluripotent cells into injuries would result in the formation of teratomas, making these therapies less safe and appealing to the general public. On the contrary, some authors consider adult stem cells the golden standard of regeneration therapies (Prentice, 2019). This is because they are already predetermined to differentiate in the somatic cells of the injured tissue or organ. This seems to avoid the generation of teratomas or the rejection of grafts, which overall improves the quality of life of patients. Therefore, a better understanding of the biological processes underlying development and differentiation, are crucial for creating new advances in therapies for heart diseases (Noor et al., 2019; Zhao et al., 2020).

1.4.1 Pluripotency network

The maintenance of pluripotency by the cells is achieved through a vast and complex network of genes (Liu et al., 2018a). This network of genes is responsible for the regulation of numerous pathways that allow the cells to maintain their pluripotency characteristics (Figure 1.3). However, pluripotency regulation involves thousands of genes and is mainly regulated by a few numbers of core transcription factors (Liu et al., 2018b). The exploit of this feature is what allows the generation of iPSC, mentioned above.

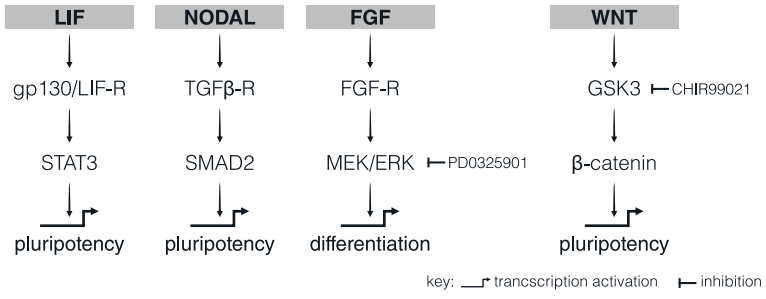

Figure 1.3 Simplified schematic representation of signalling pathways regulating pluripotency. In short, each pathway contributes to the maintenance of self-renewal and pluripotency as follows: in LIF pathway, LIF binds to the receptors (gp120/LIF-R) which activates STAT3; in NODAL pathway, ligands such as NODAL, ACTIVIN, TGFβ bind to the TGFβ receptor activates SMAD2; in the FGF pathway, ligands such as FGF4 activate MEK/ERK

which, inhibited by PD032590, prevents differentiation; lastly, in WNT pathway, by inhibiting GSK3 with CHIR99021, β-catenin does not translocate to the nucleus, which promotes pluripotency.

The three known core pluripotency transcription factors are Oct4, Sox2, and Nanog (Rodda et al., 2005). However, the classic known groups are the previously mentioned Yamanaka factors: Oct4, Sox2, Klf4, c-Myc (Liu et al., 2018b; Takahashi and Yamanaka, 2006), and the Thomson factors: Oct4, Sox2, Nanog, and Lin28 (Kashyap et al., 2009).

The three core pluripotency factors appear to contribute differently to the pluripotency network. Early studies demonstrated that the Oct4 knockout mice fail to develop a pluripotent inner cell mass in the blastocyst stage (Nichols et al., 1998). However, Sox2 knockdown experiments showed that murine embryos do not develop further than the morula stage, thus not reaching the inner cell mass (Keramari et al., 2010). Nonetheless, both Oct4 and Sox2 are necessary for the formation of the pluripotent cells, since the evidence shows that they form dimmers that target conserved regions in promoters of genes relevant for pluripotency promoting their expression, including Nanog (Rizzino and Wuebben, 2016; Rodda et al., 2005). Nanog has been referenced as the "gateway" to pluripotency, since its knockout mice leads to a halt in development at the blastocyst stage (Pan and Thomson, 2007). This block in development seems to be caused by the inability of cells to leave the pre-pluripotency state (Silva et al., 2009). Therefore, these three core transcription factors are necessary for the proper development of pluripotency in embryos.

The core pluripotency factors Oct4, Sox2 and Nanog were found to co-occupy 58 promoters of mouse embryonic stem cells, responsible for the maintenance of pluripotency (Liu et al., 2008). This resulted in the overlap of the signalling pathways (Figure 1.3), which are important to pluripotency, namely: Wnt, TGF-β, Notch, MAPK, JAK-STAT, p53, cell cycle, and apoptosis (Liu et al., 2008). Moreover, the same authors suggest that the roles of the two other Yamanaka factors Klf4 and c-Myc, are, respectively to regulate and enhance the function of the core factors, and to regulate the metabolism. Lastly, unlike, the previous gene that coded for transcription factors, Lin28a codes for an RNA binding protein, which is associated with the regulation of metabolism (Zhang et al., 2016b). These authors proposed that the role of Lin28a could be associated with the increased stability of mRNA for specific genes that favour pluripotency.

The intricate interaction of the different players in this network and the interplay between them suggests that the regulation of pluripotency requires a tight balance of their expression (Loh et al., 2015).

1.4.2 Cited2 and pluripotency

Cited2 was shown to be an important gene in maintaining pluripotency *in vitro*. The first clue was suggested from a screening study in which the authors demonstrated that *Cited2* overexpression sustained the pluripotency/undifferentiated state of mouse embryonic stem cells cultured in medium without LIF. This study also demonstrated that, compared to wild-type, *Cited2* could restore three characteristics of wild-type mouse embryonic stem cells: rapid growth, morphology, and positive result of alkaline phosphatase (Pritsker et al., 2006). However, the knockdown and knockout experiments showed conflicting results. On the one hand, established knockout cell lines did not show changes in self-renewal, but were accompanied by impairments in differentiation abilities (Kranc et al., 2009; Li et al., 2012b). On the other hand, the acute conditional knockout of *Cited2* lead to loss of pluripotency, reduced proliferation, spontaneous differentiation and cell death (Kranc et al., 2015). In the latter study, *Cited2* was shown to be present at the loci of the transcription factors *Nanog*, *Klf4* and *Tcf3*. Therefore, downregulation of *Cited2* was accompanied by downregulation of pluripotency factors. Indeed, the depletion of *Cited2* was rescued with the ectopic expression of *Nanog* (Kranc et al., 2015). Thus, it was established that the immediate response to an acute depletion of *Cietd2* was mESC death and spontaneous differentiation (Kranc et al., 2015), but over time a small fraction of mESC lacking *Cited2*-alleles may compensate for *Cited2* function and behave as pluripotent stem cells (Kranc et al., 2015; Li et al., 2012b). Consistent with these results is the overexpression of *Cited2* during mouse embryonic fibroblast reprogramming where it was observed the overexpression of *Nanog* (Saunders et al., 2017). Although *Cited2* overexpression was not sufficient to induce reprogramming, it increased the expression of *Nanog* and improved mouse-induced pluripotent stem cell generation (Charneca et al., 2017).

1.4.3 Maintenance of stem cells

Maintenance of mouse embryonic stem cells in culture was initially possible using a feeder layer of fibroblasts that secreted to the medium the necessary factors to maintain the undifferentiated cells (Evans and Kaufman, 1981). However, this limitation was solved when the extrinsic factor leukemia inhibitor factor (LIF) was identified. Thus, the use of LIF in combination with fetal bovine serum allowed the culture and pluripotency maintenance of mouse embryonic stem cells in a feeder-free manner (Nichols et al., 1998). This extrinsic factor (LIF) acts by activating the signal transducer and transcription activator STAT3, which then promotes the expression of self-renewal genes (Nichols et al., 1998). Subsequently, the

maintenance pluripotency was achieved in serum-free N2B27 medium with the supplementation of two inhibitors targeting the glycogen synthase kinase 3 (Gsk3) and the mitogen-activated protein kinase (MAPK/ERK)—these inhibitors are also known as 2i (Ying et al., 2008). Inhibition of Gsk3 by CHIR99021 leads to the activation of canonicals Wnt/β-catenin signalling, due to the stabilization of β-catenin and its translocation to the nucleus (Wray et al., 2010). While the inhibition of MAPK/ERK by PD0325901 enhances the expression of Nanog (Miyanari and Torres-Padilla, 2012). Therefore, instead of using external cues to promote undifferentiation, internal cues were used (Loh et al., 2015).

The different possible ways to achieve the maintenance of pluripotent cells *in vitro* led to the observation that there are different nuances of pluripotency. The term "naïve" and "primed" were proposed by Nichols and Smith in 2009 (Nichols et al., 2009). The cells that are not in a naïve state, or a ground state (Wray et al., 2010; Ying et al., 2008), are considered epiblast-like cells since they resemble the post-implantation cells of the epiblast. Therefore, mouse embryonic stem cells cultured in 2i medium are considered more naïve, compared to cells maintained in a medium with LIF, which are considered primed (Nichols and Smith, 2009).

When maintained in cell culture, human embryonic stem cells resemble mouse epiblastic stem cells (EpiSC), thus suggesting that isolated human embryonic stem cells are in a more primed state than mouse embryonic stem cells (Loh et al., 2015). These differences are supported by the fact that the two types of cells do not respond to the same factors when maintained in culture. For example, while mouse embryonic stem cells respond to LIF, BMP and WNT, the human embryonic stem cells respond to Nodal and FGF. Nonetheless, recent studies have shown that it is now possible to have naïve human embryonic stem cells using two different cocktails, for example: t2i/L/Gö (Takashima et al., 2014), and 5i/L/A (Fischer et al., 2022).

1.4.4 DNA integrity

The DNA is constantly exposed to damaging agents, either from outside or from inside the cells. The extrinsic factors can be split into two groups: the radiation agents (*e.g.* ionizing or ultraviolet radiation); or the chemical agents (*e.g.* alkylating, aromatic amines, etc). The intrinsic factors are: replication errors, DNA base mismatches, and oxidative DNA damage caused by reactive oxygen species (ROS) (Chatterjee and Walker, 2017). Interestingly, in mammals, pluripotent stem cells are in a relatively protected environment inside the uterus. To overcome DNA problems, cells present checkpoints during the cell cycle to assess DNA

damage, and if the damage exceeds a given threshold, the cells enter programmed cell death (or apoptosis) (Sherman et al., 2011; Wang, 2001).

Stem cells are characterized by their rapid proliferation in which cells show a shorter G1-phase of the cell cycle. However, this can increase DNA damage (Kapinas et al., 2013). However, stem cells can momentarily arrest the cell cycle in G2-phase in a p53-dependent manner upon activation of ATM to perform DNA repair (Stambrook and Tichy, 2010). During this arrest at G2-phase, the cells repair the DNA using a mechanism named homologous repair. The homologous repair of the DNA is considered a high-fidelity DNA repair, since it uses non-damaged DNA as the template (Sullivan and Bernstein, 2018). Conversely, for DNA repair during G1-phase the non-homologous end joining (NHEJ) is preferred, however, since it does not use a template to repair, micro insertions and deletions could occur (Rodgers and McVey, 2016; Symington and Gautier, 2011).

Upon DNA damage (*e.g.* caused by γ-radiation), the ATM protein becomes phosphorylated, which consequently phosphorylates H2AX, now γH2AX (Lowndes and Toh, 2005; Rogakou et al., 1998; Shiloh, 2001) (Figure 1.4). This signal is captured by cells and activates the DNA repair mechanism by other proteins. Among those proteins are ATM, MDC1, RAD51, and 53BP1 (Fernandez-Capetillo et al., 2004). Thus, γH2AX is considered a good indicator of DNA damage (Fernandez-Capetillo et al., 2004).

γH2AX is a variant histone from the H2A family that can be phosphorylated in serine-139 in the event of DNA damage (Rogakou et al., 1998). This phosphorylation occurs rapidly, and it peaks 60 minutes after DNA damage, and it can flank up to 100 kilobases (Shroff et al., 2004). This suggests that γH2AX might be necessary for the repair, but not at the DNA break (Lowndes and Toh, 2005). The distancing from the DNA break point seems to be involved in a mechanism where the two sister chromatids are in near proximity to avoid recombinational repair errors since one would be the template (Xie et al., 2004).

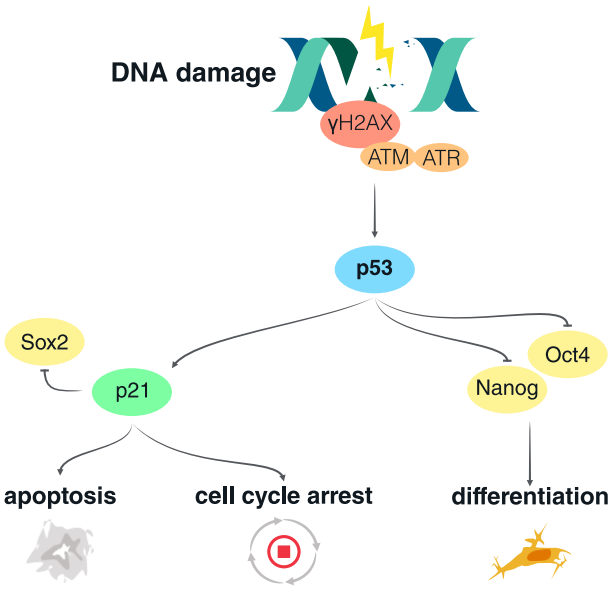

Figure 1.4 Simplified schematic representation of DNA damage response. Upon DNA damage H2AX is phosphorylated (γH2AX) by ATM/ATR at the damaged regions. The DNA damage signals p53, which in turn activates p21 that regulates apoptosis and cell cycle arrest. The inhibition of the pluripotency factors Nanog and Oct4 by p53, and Sox2 by p21, promotes the differentiation of undifferentiated cells.

Interestingly, stem cells have a relatively low rate of accumulated mutations, compared to differentiated cells, which can be attributed to the high basal levels of γH2AX or RAD51, which decreases with differentiation (Ahuja et al., 2016). And, to the increased mechanism of homologue repair over NHEJ (Tichy et al., 2010). Moreover, mouse embryonic stem cells showed relatively high levels of γH2AX that were associated with single-strand breaks that occurred in the S-phase, in which most cells are in (Chuykin et al., 2008). Not only that, but also high levels of γH2AX were associated with replicative stress of highly dividing cells *in vivo* when no DNA damage is induced (Ziegler-Birling et al., 2009).

Controlling the DNA integrity is crucial for cell survival. Thus, when the DNA damage goes beyond a reasonable point, it triggers cells to activate apoptosis. For example, apoptosis can be activated when pro-apoptotic BAX translocate to the mitochondria, and causes the release of cytochrome-c that further signals cells to die (Garrido et al., 2006; Vitale et al., 2017). Another possible mechanism is mediated by activating p53, which leads to the repression of pluripotency transcription factors, such as Nanog and Oct4 (Lin et al., 2005). Through p53, cells not only block the maintenance of pluripotency factors, but also activate differentiation-associated genes (Li et al., 2012a). Indeed, the last authors observed that DNA-damaged cells in a p53-dependent manner expressed earlier markers of endoderm (Gata4), mesoderm (Kdr), and ectoderm (Tubb3), compared to control pluripotent cells. Moreover, p53 also modulates pro-apoptotic genes, and according to the level of DNA damage, for example, p21 can lead to cell cycle arrest,

or if the damage is unbearable, BAX, PUMA, and NOXA induce apoptosis (Blanpain et al., 2011).

Embryonic stem cells have low levels of reactive oxygen species (ROS) when compared to somatic cells (Lyublinskaya et al., 2017). Reactive oxygen species can also induce cell genotoxicity, however, this is mostly controlled by the hypoxia-inducible factor 1 alpha subunit (HIF1α) and reversible uncoupling protein 2 (UCP2) (Xu et al., 2013). The DNA damage caused by hydrogen peroxide is similar to that of ionizing radiation, as demonstrated by (Dahm-Daphi et al., 2000). Other studies have demonstrated that about two-thirds of DNA damage in the DNA after irradiation results from the radiolysis of water (Ward et al., 1987). Interestingly, the increase of ROS was found to be concomitant with the overexpression of p53 in smooth muscle cells; therefore, the increase in ROS is dependent on p53; suggesting that increased p53-dependent ROS is what leads to apoptosis (Johnson et al., 1996).

With all this information, overall stem cells protect their population by inducing cells to differentiate, and therefore avoid the propagation of genomic errors in the pluripotent cell population. When there is no turnaround to the DNA damage, cells undergo apoptosis. In this way, stem cells protect the genomic integrity of the embryo by providing a mechanism to guarantee that the initial pool of cells is in the best condition.

1.4.5 A state of transition

The three pluripotency markers Oct4, Sox2, and Nanog, which maintain pluripotency, also guide the early differentiation events. These three factors are associated with the formation of the three germ layers during gastrulation. That is, Oct4 is related to mesoderm differentiation, while Sox2 is associated with ectoderm, and Nanog with endoderm. However, these three factors complement each other in the maintenance of pluripotency, by inhibiting transcription factors associated with differentiation (Thomson et al., 2011; Weidgang et al., 2016). This inhibition was evidenced by the presence of the core pluripotency factors in the promoter region of developmental genes, particularly a subset of developmental genes that are controlled by Polycomb Repressive Complex 2 (PRC2) with a repressive histone mark (Boyer et al., 2005; Lee et al., 2006). Therefore, pluripotency in a transition state in a constant dynamic equilibrium that quickly is disrupted to initiate development, which leads to terminally differentiated cells (Morgani et al., 2017).

1.5 Cardiac differentiation in vitro

Heart development occurs in the early stages of embryo development, starting from pluripotent cells in the inner cells. As stated above, pluripotent cells in the inner cells mass undergo gastrulation to form the mesoderm. The lineage specification that happens from the mesoderm to the differentiated cardiomyocyte requires the orchestration of various signalling pathways and transcription factors (Figure 1.5) (Batalov and Feinberg, 2015; Boettger et al., 2012; Zhang et al., 2021).

Cardiac differentiation begins when the mesoderm specifies from the mid-primitive streak, then into the lateral mesoderm, then into the cardiac mesoderm, and then it differentiates into cardiomyocytes (Loh et al., 2016). These authors used single-cell RNA-seq, and ATAC-seq to identify these minimal steps that lead to the different embryonic developmental stages.

The first specification is into the primitive streak, which then splits into two populations the mid primitive streak (expressing *MIXL1*$^{+}$), and the anterior primitive streak. This population of cells is induced by TGF-β, Wnt and FGF, and inhibited by PI3K signalling (Loh et al., 2016). In the presence of exogenous BMP, the mid primate streak forms, and the anterior primitive streak is inhibited (Loh et al., 2014). Next, occurs the formation of lateral plate mesoderm (expressing HAND1 and FOXF1), in the context of FGF activation and TGF-β inhibition, and induced with exogenous BMP and inhibition of WNT (using the GS3K inhibitor) (Loh et al., 2016). However, if the BMP and WNT signalling were inverted, the paraxial mesoderm (expressing CDX2) would form, which would lead to the formation of the early somites (expressing FOXC2) instead of the cardiac mesoderm.

The lateral plate mesoderm also expresses BRACHYURY, which is one of the markers of the mesoderm, along with the early marker EOMES (David et al., 2011). These two genes have peak expression on the fourth day of differentiation (Santos et al., 2019), which is followed by peak expression of Mesp1 one day later (Bondue et al., 2008). Tosic et al. (2019), purpose that Brachyury and Eomes, through ATAC-seq experiments, that these two transcription factors function together to control the chromatin landscape to promote the specification of mesendoderm by inhibiting neuroectoderm and pluripotency (Oct4, Sox2, Nanog) (Tosic et al., 2019).

Furthermore, it is suggested that Cdx2, a known marker of trophoblast (Huang et al., 2017), which is a structure that does not develop from mouse pluripotent cells (Beddington and Robertson, 1989), is likely to play a role in the specification of the mesoderm (Bernardo et al.,

2011). At the beginning of development, Cdx2 was shown to repress Oct4 in the trophoblast during the development of mouse blastocyst, but not in the inner cell mass (Wang et al., 2010). These authors suggested that this inhibition of Oct4 by Cdx2, which regulates the specification of the mesoderm specification (Zeineddine et al., 2006), is mediated by Brg1 chromatin remodulation, since Cdx2 knockdown leads to the increased expression of Oct4 in the trophectoderm. In more advanced stages, at the epiblast, Cdx2 appears to be downstream of Brachyury, and both regulate the expression of mesoderm markers in mouse and human iPSC (Bernardo et al., 2011). Furthermore, Cdx2 and Nanog appear to have a negative interaction loop at the promoter level that is required for the mesoderm specification (Mendjan et al., 2014). In particular, the knockdown of Nanog leads to the absence of beating colonies (clusters of spontaneous contracting cardiomyocytes), yet only if the cell originated from the anterior primitive streak mesoderm. Conversely, no alterations were observed if the Nanog knockout was performed in a late primitive streak (Mendjan et al., 2014). Interestingly, the same authors also reported that Cdx2 knockdown increased Nkx2.5 expression, suggesting that Cdx2 blocks cardiac differentiation, similar to what was observed *in vivo* (Chen et al., 2009).

The expression of Mesp1 precedes the expression of other transcription factors that regulate morphogenesis, which indicates that Mesp1 plays a role in early mesoderm specification (Kitajima et al., 2000). Mesp1 expression promotes the rapid activation of genes (Mef2c, Gata4, Nkx2.5, Hand2, and Myocardin), and the suppression of non-cardiopoietic genes (FoxA2, Sox17, Gsc). This seems to occur by Mesp1 binding directly to the promoter of these genes. In this way, Mesp1 seems to function as a switch that activates a unidirectional irreversible cascade of the transcriptional network necessary for cardiac development (Bondue et al., 2008).

The expression of $NKX2.5^{+}$ is an indicator that cardiac mesoderm specification was achieved. As demonstrated by Loh et al. (2016), this can be induced in the presence of BMP and FGF, with the inhibition of WNT. This pool of cells is also expressing Kdr as demonstrated by lineage tracing experiments (Ema et al., 2006; Moretti et al., 2006). From this cardiac mesoderm, it seems that two populations of cells arise, as mentioned above: the first heart field and the second heart field. The first heart field is positive for the expression of Nkx2.5, Hand1, Hand2 Tbx1, Tbx5, and Tbx20, and the second heart field is also positive for Nkx2.5, Fgf10, Fgf8, Tbx1, Fohd1, Mef2c, Hand2, Tbx20, and Isl1 (Buckingham et al., 2005).

Lastly, the first beating cardiomyocytes, generated from the first heart field, are expressing TNNT2 and can be induced by inhibiting WNT and exogenous BMP of the cardiac mesoderm (Loh et al., 2016). This demonstrates the importance of blocking WNT signalling to properly

induce cardiac cell differentiation. Therefore, this process is known as the “WNT blockade” (Lian et al., 2012; Schneider and Mercola, 2001).

1.5.1 Cited2 in differentiation

Different studies demonstrated that Cited2 plays a role in the regulation of differentiation through the modulation of pluripotency factors. On the one hand, *Cited2*-knockout cells showed an impairment to undergo differentiation, due to the delay in the downregulation of *Oct4* (Li et al., 2012b). On the other hand, *Cited2* seems to regulate *Nanog*, *Klf4*, and *Tbx3*, since *Cited2*-knockdown lead to the downregulation of those three pluripotency genes, and increased expression of differentiation genes such as *Brachyury*, *Foxa2* and *Sox17* (Kranc et al., 2015).

Following the last idea from the last topic, previous studies demonstrated that *Cited2*-depletion in mouse embryonic stem cells was rescued with supplementation of *Wnt5a* and *Wnt11* alone and or in combination, as evidenced by the increasing percentage of beating foci generated from the hanging drop method (Santos et al., 2019). Not only that, but an in vivo experiment with zebrafish morphants (*Danio rerio*), the supplementation of Wnts and recombinant *Cited2* also rescued the heart defects. Therefore, *Cited2*-depletion could be rescued with supplementation of signalling molecules, which open new therapeutic pathways to rescued cardiac defects (Santos et al., 2019).

Furthermore, the activation of Wnt signalling in the cardiac progenitor pool expressing *Isl1* (Loh et al., 2016) is concomitant with the expression of *Cited2* (Pacheco-Leyva et al., 2016). Therefore, the expression of *Cited2* and *Isl1* might support the increasing proliferation of cardiac progenitor cells that will give rise to the majority of the heart (Cai et al., 2003). This cooperation between *Cited2* and *Isl1* was shown to promote the positive regulation of cardiopoietic genes (Pacheco-Leyva et al., 2016). Interestingly, *Isl1* promotes the regulation of cardiopoietic genes, such as the expression of *Mef2c* by modulating the acetylation of H3 by p300, in a specific manner; since the H3 acetylation was unaltered for *Tbx5* and *Gata4* (Yu et al., 2013). Recent studies have demonstrated that CITED2 promotes *Isl1* expression of *Isl1*, by directly binding to its promoter in cardiac progenitor cells and by directly interacting with ISL1 through the LIM domain (Pacheco-Leyva et al., 2016).

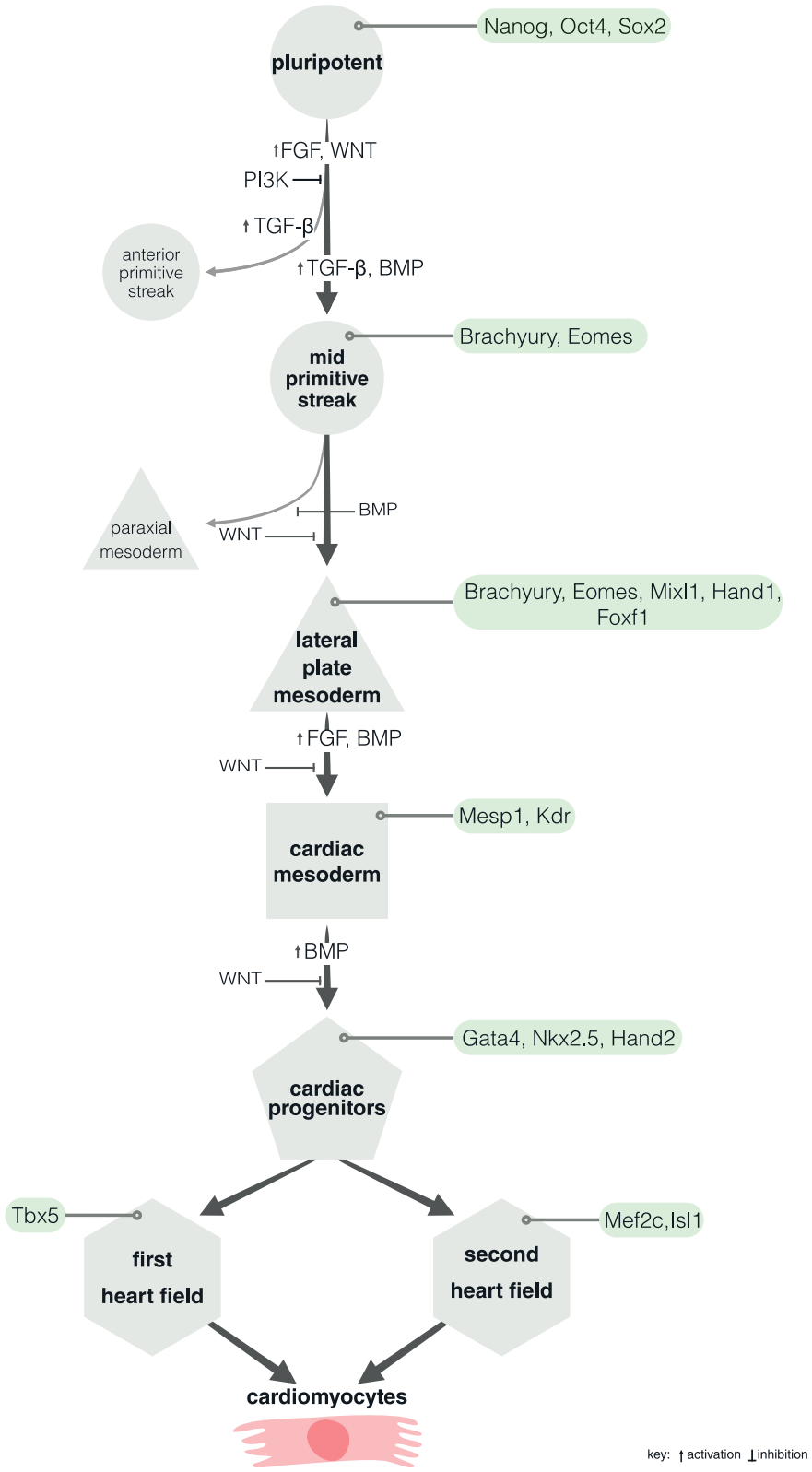

Figure 1.5 Simplified schematic representation of the differentiation steps from pluripotent cells to cardiomyocytes. The differentiation of cardiomyocyte begins from pluripotent cells that undergo a series of lineage specification steps, which include mid primitive streak, lateral plate mesoderm, cardiac mesoderm, cardiac progenitors, and first and second heart fields. Through each step activation or inhibition of signalling pathways FGF, TGFβ, WNT, BMP, PI3K. In the green callouts it is indicated the markers of each stage of differentiation.

Cited2 is also suggested to be associated with p300/CBP in differentiation processes, since, as described above, *Cited2* and p300 cooperate to promote the regulation of pluripotency (Chen et al., 2008; Zhong and Jin, 2009). Nonetheless, p300 is also associated to be an important player regulating differentiation, as discussed below.

1.5.2 Epigenetic regulation

During differentiation, specifically mesoderm specification, undifferentiated cells change their gene expression based on external queues (signalling molecules) that create a disequilibrium in favour of differentiation. The relatively quick response suggests that epigenetic mechanisms are involved (Barrero and Izpisua Belmonte, 2008). There are different mechanisms of epigenetic regulation, for example, DNA methylation, long-non-coding RNA, and histone modifications; the present study focuses on the latter.

In eucaryotes and somatic cells, the DNA is compacted in different structures going from the free DNA double-helix to the nucleosome and ending in the chromosome. When the DNA is less compacted in the nucleosome and in the "beads-on-a-string", the gene transcription is active. The nucleosome is a structure that contains the octamer with the four core histones (H2A, H2B, H3, and H4) and 146 base pairs of DNA wrapped around it. Longer chains of this unit are called "beads-on-a-string". The histones protein molecules have the N-terminal tail exposed to the outside of the nucleosome, which allows their post-translational modifications. Regulation of the chromatin landscape and gene expression can therefore be achieved by modifications such as acetylation, methylation, and ubiquitination (Dinant et al., 2008; Morgan and Shilatifard, 2020). Overall, modification of H3 lysine 27 (H3K27) with acetylation (H3K27ac) is associated with transcriptional activation, while the tri-methylation (H3K27me3) is associated with repression. However, H3K4me3 is recognized as an activation mark. This suggests that depending on the histone and the residue, the modification of methylation can sometimes indicate repression, but other times could also indicate activation (Voigt et al., 2013; Zentner et al., 2011).

The polycomb group of proteins is responsible for the methylation of bivalent domains, and developmental regulators (Boyer et al., 2006). The polycomb group is usually recruited to their target sites by transcription factors, and by highly conserved DNA methylated regions (CpG domains) in the regulatory regions of developmental genes (Tanay et al., 2007).

The concept of bivalency and poised genes proposes that gene expression can be controlled by different histone modifications. Therefore, this suggests that the activation mark and a

repression mark are present, or in equilibrium. This way, within a given signal threshold, the expression of a gene can be activated or repressed quickly (Voigt et al., 2013). For example, Mesp1 expression quickly raises and peaks at around day-3 of differentiation and is not expressed at day-4.

The regulation of enhancers and promoters by modifications to H3K27, showed that inactive enhancers presenting H3K27me3 also had occupancy of p300/CBP (Holmqvist et al., 2012; Zentner et al., 2011). This occupancy suggests a possible role as a switch to activate gene expression (Holmqvist and Mannervik, 2013). As proposed by Pasini et al. (2010) this can be attributed to external cues (e.g. differentiation, or oncogenes), and partner transcription factors that allow the acetylation. However, demethylation of H3K27me3 by UTX (or KDM6) is also required for the acetylation activity of p300 to obtain active enhancers (Wang et al., 2017). Thus, UTX and p300 function as antagonists of PRC2.

Interestingly, mouse p300 knockout embryonic stem cells can maintain pluripotency, yet they showed an impairment to undergo differentiation (Zhong and Jin, 2009). Although this could be due to the redundancy with CBP, it shows that p300 is necessary for differentiation (Zhong and Jin, 2009). This impairment of differentiation could be attributed to the inhibition of acetylation of core histones, which induce the activation of differentiation genes, in particular H3K27ac (Martire et al., 2019; Raisner et al., 2018). Recent studies with mouse embryonic stem cells with p300-knockdown showed that p300 is associated with promoter regions (instead of enhancer regions) and that there was a gain of acetylation in regions of genes regulated by p53—suggesting the possible link between p300 and *p53* in gene regulation (Martire et al., 2020). Furthermore, decreased levels of p300 appeared to also decrease the acetylation in the promoter region of the core pluripotency genes; which is concomitant with the downregulation of these genes in conditions of *Cited2*-depletion and spontaneous differentiation (Kranc et al., 2015).

Lastly, p300 acetyltransferase activity is not exclusive to histones (Holmqvist and Mannervik, 2013). Other proteins (seventy, according to Wang et al. (2018)) were also acetylated by p300, including *p53* in tumour cells (Gu and Roeder, 1997; Liu et al., 1999a).

1.6 Objectives

The role of Cited2, in cardiac differentiation, has not yet been completely elucidated. On the one hand, Cited2 contributes to the maintenance of pluripotency of mouse embryonic stem cells and improves the efficiency of human induced pluripotent stem cells. On the other hand, Cited2 is required for the proper development of the embryo, particularly for heart development.

In pluripotency, evidence supports that mouse embryonic stem cells that are conditionally depleted of Cited2 either die or differentiate, even when maintained in undifferentiated conditions (with medium supplemented with LIF). While, in differentiation, through the hanging-drop method, Cited2-depletion at the onset of differentiation (with medium without LIF) causes a delay in the expression of cardiac differentiation genes and a reduction of the percentage of embryoid bodies that show spontaneous contractile activity.

Nevertheless, the mechanisms behind the increased cell death and spontaneous differentiation under pluripotency conditions, and the impaired cardiac differentiation remain unsolved. In this work, starting from microarray analysis and its results validation, we explored the role of Cited2 in pluripotency through the lens of DNA damage (γH2AX) and apoptosis, and in differentiation through the lens of epigenetics (H3K27me3/ac) at the early stages of differentiation (fourth day of differentiation).

2 Methodology

2.1 Cell culture

Cell culture was conducted in sterile conditions using a laminar flow hood, and incubation was carried out in a humidified atmosphere kept at 37 ºC with 5 % CO_2. All cultures were carried out in flasks, plates, or glass cover slips coated with 0.1 % gelatine type-A prepared in distilled water (Sigma, G2500) for 15-30 minutes at room temperature before cell seeding (Kranc et al., 2015), unless otherwise stated. Washes were performed using DPBS (VWR, K813) or (Bioconcept, 3-05K00-I). The presence of mycoplasma was tested regularly by PCR and agarose gel electrophoresis (Uphoff and Drexler, 2002).

2.1.1 Cell lines

In this study, mouse embryonic stem cell lines previously established in the laboratory were used (Kranc et al., 2015; Pacheco-Leyva et al., 2016; Santos et al., 2019): $C2^{fl/fl}$[cre] (clone A), $Cited2^{fl/fl}$, and $Cited2^{-/-}$. Briefly, $Cited2^{fl/fl}$ isolated from blastocyst, harbour the exon-2 of *Cited2* floxed (between two loxP sites) that can be excised by Cre-recombinase. To achieve this, these cells were stably transfected with Cre-ER^{T2}, which is a modified Cre that becomes active in the presence of synthetic oestrogen antagonists, such as 4-hydroxytamoxifen (4HT) (Feil et al., 1997). From this transfection, one of the colonies was isolated, named $C2^{fl/fl}$[cre], allowing the conditional knockout of *Cited2* upon the addition of 4HT to the culture medium. Once established, this cell line was then transducted with lentiviral particles with *CITED2*-GFP or GFP, isolated by cell sorting, kept in culture with 4HT, and thus emerging colonies that overcome the knockout of *Cited2* originated a stable *Cited2* knockout line, termed $Cited2^{-/-}$ (Kranc et al., 2015).

2.1.2 Cell maintenance

Pluripotent cells were maintained in Glasgow Minimum Essential Medium (GMEM) BHK-21 (Gibco, 21710) supplemented with: 10 % Fetal bovine serum (FBS) (Sigma, F7524), 2 mM L-Glutamine (Gibco, 25030), 100 U/mL Penicillin-Streptomycin (P/S) (Gibco, 15140), 1 mM sodium pyruvate (Gibco, 11360), 1 % Minimum Essential Medium Non-Essential Amino Acids (MEM-NEAA) (Gibco, 11140) and 0.05 mM 2-Mercaptoethanol (Gibco, 31350), as previously described (Kranc et al., 2015). For the maintenance of pluripotency, the medium was further

supplemented with 10 ng/mL of recombinant murine leukaemia inhibitory factor (LIF) (Peprotech, 250-02). The medium without supplementation was named: GMEM0; then after supplementation: GMEM+; and after LIF was added: GMEM++.

For cell passaging, cells were dissociated with 0.05 % Trypsin-EDTA (Gibco, 25300-054) or (Sigma, T2610) or Accutase (Gibco, A1110501), then pelleted (at 138 *rcf* at room temperature), resuspended in GMEM+, before counting and their viability accessed with Trypan-Blue (Gibco, 15250-061). For cell culture maintenance between 10000-15000 viable cells/cm^2 were plated in a T25 (Thermo Fisher, 156367 or SPL, 70025). The medium was changed every two days, and the cells were split every two to three days. For the cells plated for experiments, the medium was changed one the day before, *i.e.* approximately 16 hours before the beginning of the experiment. Different cell density (cells/cm^2) was used according to the experiment being conducted.

Cell long-term storage was performed at -150 ºC in freezing medium (% v/v): 45 % GMEM+, 40 % FBS and 15 % DMSO (Sigma, 8418). Once the cell pellet was obtained, it was resuspended in 1 mL of freezing medium and transferred to a freezing vial (VWR, 479-1262). The vial was immediately placed in a "Mr. Frosty" freezing container (Thermo Fisher, 5100-0001) and kept at -80 ºC during 1-2 days before being carried over to long-term storage at -150 °C.

2.1.3 Treatments

Before an experiment, C2$^{fl/fl}$[cre] cell cultures were treated with 1 µg/mL of puromycin (Invitrogen, ant-pr) to ensure the harbouring of Cre-construct. Incubation with this antibiotic was conducted overnight before the experiment started, or applied also overnight to the cells in the passage before the experiment, *i.e.,* in passage *n-1*.

To deplete *Cited2* both in pluripotent and differentiation conditions using C2$^{fl/fl}$[cre] cells, 1 µM of 4HT (4-Hydroxytamoxifen) (Sigma, H6278) was added to the culture medium. The stock solution was prepared according to the manufacturer's instructions in absolute ethanol (Panreac, 121086.1212), aliquoted and stored protected from light at -20 ºC. An aliquot of the same ethanol was kept for the posterior used in the control condition.

To induce DNA damage, cells were treated with 50-100 µM of hydrogen peroxide H_2O_2 (Alfa Aesar, L13235) from a freshly prepared solution of 0.01 M solution prepared in GMEM0 (Maynard et al., 2019), which was diluted in culture medium. For the positive control wells, 30

min before harvesting or fixation the medium was replaced with GMEM0 with H_2O_2 at 100 µM.

To rescue Cited2 depletion, a human recombinant protein (previously produced in-house) was used, which contains a modification of eight arginines at the N-terminal (8R-CITED2), which increases cellular uptake (Nakase et al., 2004; Nascimento, 2015; Pacheco-Leyva et al., 2016). This protein is stored in elution buffer (50 mM Tris-HCl, 10 mM reduced glutathione (GSH)), pH 8.0 at -80 ºC.

2.1.4 *In vitro* differentiation

To induce mESC to differentiate, the hanging drop protocol was used (Potter and Morris, 1985; Santos et al., 2019). This protocol consists in inducing pluripotent cells to spontaneously differentiate in the three germ layers through a series of steps over a span of time that can last up to twelve/fourteen days.

It starts at day-0 with embryoid body (eb) formation (or spheres) with the preparation of differentiation medium (GMEM+ with 20% FBS) with 50 000 cells/mL—that is 1000 cells per 20 µL drops—therefore, 50 drops were placed in low adhesion plates (bacterial grade Petri dishes (VWR, 391-0599)). The plate was then turned upside-down to form a hanging-drop, and 1 mL of PBS is added to the lid to maintain humidity. Then, on day-2 with the embryoid bodies formed and growing, the PBS is removed to allow the plate to be turned down, and fresh 5 mL of GMEM+ was added, and ebs are allowed to continue to grow for three days, unless otherwise stated. Additionally, on this day-2 and day-4 ebs were observed and images acquired (OnePlus6 smartphone camera). The embryoid bodies were pelleted on day-5, and transferred to fresh GMEM+ already added to a previously 0.1 % gelatine coated P60 plate (TPP, 93060) to allow for their adhesion and growth. From day-6 to day-8 they are observed to assess the first day, *i.e.* at least one embryoid body showed one beating foci. Additionally, on day-8 the number of embryoid bodies beating was counted, as well as the number of foci in each one of them. On day-12 the embryoid bodies were discarded.

Cited2-depletion experiment in this protocol was applied at the onset of differentiation, that is at day-0.

2.2 Immunoassays

In this work, different immunoassays were used, and some share the same reagents, but were used in the different buffers used: the TRIS buffers were prepared with: TRIS (Thermo Fisher, 17926), NaCl (NZYtech, MB15901), Glycine (Applichem, A1067), SDS (VWR, 444462R) and HCl (Scharlau, AC07362500). For the in-house casting of the polyacrylamide gels, they were prepared with 40 % Protogel (National Diagnostics, EC-891), APS (Sigma, A3678), TEMED (National Diagnostics, EC-503). A table of antibodies is provided at the end of this topic (Table 2.1)

2.2.1 Immunoblotting (Western Blot)

To determine the expression level of a given protein, the Western blot technique was used (Santos et al., 2019; Towbin and Gordon, 1984). The 1.5 mm thick sodium dodecyl sulphate-polyacrylamide gels were hand cast for a final polyacrylamide gel content ranging from 10 %, 12 % or 6-12 % gradient (Miller et al., 2016), according to the target protein(s), in the resolving buffer (375 mM TRIS pH 8.8, 2.5 %(w/v) SDS). The stacking gel had 4 % polyacrylamide and was prepared in stacking buffer (125 mM TRIS pH 6.8, 2.5 %(w/v) SDS). SDS-PAGE electrophoresis was carried out in running buffer (25 mM TRIS, 192 mM Glycine and 0.1 %(w/v) SDS pH 8.3) for 20 min at 80 V, which was then increased to 120 V until the lightest marker reached the bottom of the gel. Once finished, the gel was placed in a box with transfer buffer (25 mM TRIS, 192 mM Glycine, 0.005 %(w/v) SDS and 20-10 % Methanol (Merck, 1.06009.2500), pH 8.3.) and allowed to equilibrate for 10-15 minutes. Protein wet transfer was performed to 0.45 µm PVDF membranes (GE, 10-6000-23) in transfer buffer from 60 to 180 minutes at a constant 0.2-0.350 A in the MiniProtean tank (Biorad, 1658004EDU) using Powerpack-HC power supply (Biorad, 1645052). The membrane was then probed for total protein quantification with No-Stain whole protein labelling (Thermo Fisher, A44717) according to the manufacturer's; or immediately blocked with 5 % (w/v) skim milk (Nestlé, Molico) in TBS (50 mM TRIS, 150 mM NaCl, pH 7.5)- 0.1% Tween20 (Sigma, P1379) (TBST) for 1 hour at room temperature with agitation; or with 5 % BSA in TBST, according to the antibody data sheet. Once blocked, the membrane was incubated with agitation in a solution of the relevant primary antibody diluted in blocking solution overnight at 4 ºC. After primary incubation, the membrane was washed for a total of 30 minutes with agitation in TBST, with changes in TBST every 10 minutes. The probe against the primary antibody was done with the respective secondary antibody for 1 hour at room temperature with agitation; also prepared in

blocking solution for antibody information (Table 2.1). To develop and reveal the signal the membrane was again washed three times and then rinsed with TBS, and then incubated with chemiluminescent reagent ECL (GE, RPN2232) for 5 minutes protected from light. Images were acquired immediately using an imaging system (Biorad, Chemidoc-XRS+) controlled by the software ImageLab v5.2.1 build 11 (Biorad). The acquired images were then used for quantification; see section 2.4.2 below.

2.2.2 Immunocytochemistry and immunofluorescence (ICC/IF)

To prepare samples for immunofluorescence observations cells were cultivated in 12-well plates (VWR, 734-2324) with 18 mm cover glasses (VWR, 631-0153) previously coated with 0.2% gelatine type-A. At the time point of interest, culture cells were washed with PBS two times and then fixed with 2 % paraformaldehyde (PFA) (Sigma, P6148) and prepared in PBS for 15 minutes at room temperature. The cells were then permeabilized with PBS 0.5 % Triton X-100 (Sigma, T9284) with gentle agitation on ice for 15 minutes. Once permeabilized, blocking buffer 5 % (w/v) BSA in PBS was added, and samples were incubated for 1 hour at room temperature. This was followed by incubation with relevant primary antibody in humidified chamber overnight at 4 °C (or at room temperature for 1 hour), followed by 30 minutes of washing with an abundant change of PBS every 10 minutes. The samples were then incubated with relevant secondary antibody for 1 hour at room temperature and washed as previously. See Table 2.1 for antibody information. The mounting of the samples was done on microscopy slides (Thermo Fisher, CB00130RA020MNT0) with mounting media containing nuclear staining Fluromount-G-DAPI (Invitrogen, 00-4959-52). The slides were stored at 4 ºC and protected from light before being scoped within the next days.

The samples were scoped on a widefield fluorescence microscope (Zeiss, Imager Z2) remotely controlled by AxioImager v 4.8 (Zeiss). Or in confocal microscopy (Zeiss, LSM710-Airsyscan) remotely controlled by ZenBlack v2.3 SP1 FP3 (Zeiss). Other image processing was performed in Zen Blue lite v3.2 (Zeiss).

When acquiring images of γH2Ax speckles in each session, the same confocal Airyscan settings were used, using the 63x objective. For the nuclei channel, the wavelengths (nm) of 405excitation/450emission were used and for the γH2AX channel 488excitation/523emission. The laser intensity was set to a maximum of 4 %, and the detector gain was set to a level that did not saturate the signal in the positive control sample. Random colonies were selected to acquire four 0.15 µm slice Z-stacks in a 512x512 frame in unidirectional directions. Next, the

original Airsyscan data set was pre-processed in Zen Black using the default settings, from which the resulting images were the maximum projected orthogonally (XY) in Zen Blue. Lastly, this image was submitted to the analysis pipeline, described in section 2.4.3 below.

2.2.3 Immunoprecipitation (IP)

To immunoprecipitate the relevant protein from mESC, cells were grown in 0.1% gelatine coated 100 mm dishes (VWR, 734-2321), and the cell pellet was harvested in 1.5 mL tube which was stored at -80 ºC until further processing. Cells were lysed with lysis buffer (as section 2.3.5 below), and once the lysate was clarified by centrifugation it was pre-cleared with 50 % unblocked slurry of Protein-G sepharose beads (Cytiva, 17-0618-01) in IP-buffer (50 mM TRIS pH 8.0, 0.5 % NP-40 and 150 mM NaCl, with protease inhibitor cocktail (Roche, cOmplete tablets 04293159001) and 1 mM PMSF (Sigma, P7626)) for 30 min with agitation at 4 ºC. Then, 1/10 of the volume of the lysate was saved as 'input', and the remaining volume was divided into two equal parts and transferred to two new tubes; the remaining volume was raised to 500 µL with IP-buffer. In one of the tubes, 5 µg of relevant antibody (anti-p300) was added, and in the other, the same amount of a nonspecific antibody (anti-FLAG) was added—thus, named target-IP and mock-IP; incubation proceeded overnight with agitation at 4 ºC. Then, 1/10 of the volume of 50 % slurry of blocked beads (with 5 %(w/v) BSA in IP-buffer) was added and incubated with agitation at 4 ºC for 45 minutes. Next, beads were washed three times with abundant IP-buffer, and spun down. The purified target protein was eluted with elution buffer (0.1 M glycine-HCl pH 3.5) for 5 minutes with gentle shaking and then 1/10 of the volume of neutralizing buffer (0.5 M TRIS-HCl pH 7.4 1.5 M NaCl) was added. The immunoprecipitated product was stored at -80 ºC until further use; see section 2.5 below).

2.2.4 Chromatin Immunoprecipitation (ChIP)

To immunoprecipitate the chromatin complexes of histones H3K27me3 and H3K27ac samples of mESC either undifferentiated or differentiated (as embryoid bodies at day-4) were fixed with 1 % formaldehyde (Fisher, BP531-25) for 20 minutes at room temperature, after washes with PBS. Unlike undifferentiated cells, the embryoid bodies were harvested in 1.5 mL tubes and fixation occurred with gentle agitation. Formaldehyde was quenched with 125 mM glycine and next the cells were washed five times with abundant PBS and TE (10 mM TRIS-HCl, 1 mM EDTA, pH 8.0), for undifferentiated cells and embryoid bodies, respectively. The cells were disrupted with cell lysis buffer (50 mM TRIS-HCl pH 8.0, 2 mM EDTA pH 8.0, 0.1 % (v/v)

NP-40 (Calbiochem, 492016) and 10 % (v/v) glycerol, with protease inhibitor cocktail and 1 mM PMSF) for 15 minutes on ice with occasional shaking. Next, the pellet was obtained by centrifugation at 5000 *rcf* at 4 ºC. To the pellet containing the nuclei, nuclei lysis buffer (50 mM TRIS-HCl pH 8.0, 10 mM EDTA pH 8.0 and 1 %(w/v) SDS) with protease inhibitor cocktail and 1 mM PMSF was added. Next, a volume of 300 µL of samples was transferred to a sonication tube (Diagenode, C30010016), and the sample was sonicated (Diagenode, Bioruptor Pico) with the following settings for undifferentiated cells and embryoid bodies, respectively: 3 cycles 30 s ON 30 s OFF, and 4 cycles 30 s ON 30 s OFF. The sonicates stayed on ice for 10 minutes. Sheared chromatin diluted in ChIP-buffer (20 mM TRIS-HCl pH 8.0, 2 mM EDTA pH 8.0, 150 mM NaCl and 1 %(v/v) Triton-X100, with protease inhibitor cocktail and 1 mM PMSF), and then precleared with 50 % protein-G sepharose blocked beads at 4 ºC with agitation for 60 minutes; beads were previously blocked for 1 hour with agitation in 100 µg/mL of BSA and 100 µg/mL of sonicated salmon sperm DNA in ChIP-buffer. After the sample is pre-cleared beads were eliminated by centrifugation at 2000 *rcf* and 1/10 of the supernatant was saved as 'input'' (or 'total dna'), and the remaining volume was split into two equal parts into two tubes for 'target-IP' and 'mock-IP'. The volume of each sample was increased to 800 µL with ChIP -buffer and 5 µg of relevant antibody were added. The incubation was carried out overnight at 4 ºC with agitation. The solution was then cleared with centrifugation at 12000 *rcf* for 10 minutes at 4 ºC. Then 40 µL of 50 % blocked bead slurry was added and incubated for 1 hour with agitation at 4 ºC. The beads were spun 3000 *rcf* for 1 minute at 4 ºC and washed seven times for 10 minutes with washing buffer (TE with 150 mM NaCl and 0.5 % (v/v) NP-40) with agitation at 4 ºC. The beads were then resuspended in 50 µg/mL RNaseA diluted in TE and incubated with agitation at 37 ºC on ThermoMixer at 1000 rpm (Eppendorf). Next, proteinase-K (Applichem, A4392) was added for the final concentration of 1 mg/mL as well as SDS for the final 0.5 % (w/v) and digestion occurred overnight at 65 ºC. Proteinase-K was inactivated by increasing the temperature to 85 ºC for 10 minutes. Then DNA was isolated as in (2.3.2 below) and analysed as in (2.3.3 below). DNA isolated from a sample of sonicated chromatin prior to antibody incubation was evaluated with 1.5 % agarose gel (Sigma, A9539) gel run at 90 V for 30 to 45 minutes in TAE buffer (NZYtech, MB11401); the DNA was stained with GreenSafe (NZYtech, MB13201), and revealed with Chemidoc (Biorad).

2.2.5 Antibodies used

In Table 2.1 the list of antibodies used in the different techniques mentioned above is presented.

Table 2.1 List of use antibodies, their application and its dilution or quantity used. Applications: WB (western blot), IP (Immunoprecipitation), (ICC/IF immune cytochemistry/immunofluorescence) or ChIP (Chromatin Immunoprecipitation). Hosts: d-donkey, m-mouse, r-rabbit, s-sheep.

Antibody	Target	Host	Conjugate	Application	Application dilution or µg
Millipore, 05-636	γH2AX	m	-	WB, ICC/IF	dil. 1000x,500x
Millipore, 05-257	p300	m	-	IP	5 µg
Cell Signaling, 2840	OCT4	r	-	ICC/IF	dil. 500x
ThermoFisher, A21202	m-IgG	d	Alexa488	ICC/IF	dil. 5000x
ThermoFisher, A21207	r-IgG	d	Alexa594	ICC/IF	dil. 5000x
Abcam, ab6002	H3K27me3	m	-	ChIP	5 µg
Abcam, ab4729	H3K27ac	r	-	ChIP	5 µg
Sigma, F1804	FLAG	m		ChIP	5 µg
Abcam, ab46540	r-IgG		-	ChIP	5 µg
GE, NA931V	m-IgG	s	HRP	WB	dil. 5000x
GE, NA934V	r-IgG	d	HRP	WB	dil. 5000x

2.3 Molecular biology

2.3.1 RNA isolation and cDNA synthesis

Total RNA was isolated from mESC using a commercial spin column kit (NZYtech, MB13402), and its quantification was achieved with a Nanodrop spectrophotometer (Thermo Fisher, Nanodrop 2000c) controlled by the Nanodrop2000/2000c v1.6.198. From here complementary DNA was synthesised from 1 µg of RNA using a reverse transcriptase kit (NZYtech, MB13405). The samples were stored at -20 ºC until analysis was performed by real-time PCR (qPCR).

2.3.2 gDNA isolation

To extract genomic DNA from ChIP samples, the volume was raised to 500 µL with ultra pure water (MiliQ), and an equal volume of phenol:chloroform:isoamly alcohol (25:24:1) (Acros, 327111000) or (VWR, K169) was added. Next, vigorous vortexing was applied for 30 s followed by centrifugation at maximum speed (27 000 *rcf*) at 4 ºC. The top aqueous phase was transferred to a new tube, and an equal volume of chloroform (Merck, 8.22265) was added, and

again vigorously vortexed as before, also followed by centrifugation. Next, the aqueous phase was transferred to a new tube, and it was added: 1/10 of the volume of 3 M sodium acetate pH 5.0 (Sigma, S7670), 1 µg of glycogen (Acros, 225900050), and two volumes of absolute ethanol. Next, for DNA precipitation, the tubes were incubated overnight at -20 ºC, and then centrifuged at 27 000 *rcf* for 45 minutes at 4 ºC. The supernatant was discarded, and the pellet was washed with 70 % (v/v) ethanol and pelleted down again at maximum speed for 15 minutes at 4 ºC. Again, the supernatant was discarded and the pelleted was allowed to dry at room temperature between 30-45 minutes. Finally, the purified DNA was reconstituted in 40 µL of MiliQ and incubated at 37 ºC with agitation in ThermoMixer. The DNA solution was stored at -80 ºC until it was subjected to real-time PCR (qPCR).

2.3.3 Real-time-PCR (qPCR): mRNA and gDNA

The analysis of transcripts (mRNA) and enriched genomic regions (gDNA) was performed using real-time PCR (or qPCR) (Heid et al., 1996). PCR was carried out in a clear white 96-well (Thermo Fisher, AB-0700) or opaque white 384-well plate (Biorad, MSB1001) in the CFX-96 or CFX-384 (both from Biorad), and both controlled by the software CFX Manager v3.1 (Biorad). The 20 µL reactions were prepared using the supermix SsoFast EvaGreen (Biorad, 172-5201) to which the final 400 nM final concentration of forward and reverse primers (Table 2.2 and Table 2.3). As a template, mRNA or gDNA samples were added, by adding 2 µL of the sample (*i.e.*, 50 ng of mRNA, and unknown quantity of gDNA); the remaining volume was filled with MiliQ. Two technical replicates (two wells) per sample were used. Cycling conditions followed the manufacturer's instructions and were for mRNA: enzyme activation 95 ºC 30 s, denaturation and annealing/extension [95 ºC 5 s, 60 ºC 30 s]x40, melt curve from 65-95 ºC with 0.5 ºC increments; and for gDNA: enzyme activation 98 ºC 120 s, denaturation and annealing/extension [95 ºC 5 s , 60 ºC 5 s]x45, melt curve from 40-95 ºC with 0.5 ºC increments. The cycle threshold (Ct) was automatically calculated for each primer pair using the default settings and the resulting quantification cycle (Cq) was exported to a comma-separated file. The fold-change or relative expression was calculated following the ddCt method (Livak and Schmittgen, 2001) considering the expression of *Gapdh* as the reference target. The enrichment of genomic regions from the Chromatin Immunoprecipitation experiments was calculated as a percentage of the ‘input’ (Asp, 2020). For both methods, the Cqs were processed using the R package *pcr* (Ahmed and Kim, 2018).

The primers used to detect transcript expression were already described elsewhere, and/or present in the Primer Bank database (Spandidos et al., 2008; Spandidos et al., 2010) (Table 2.2**)**. Although primers for promoter/enhancer regions were only described elsewhere (Table 2.3); the ChIP primers database (Kurtenbach et al., 2019) was tried but revealed to be unsuccessful.

2.3.4 Microarrays

To better understand the big picture of the differentially expressed genes between cells expressing and not expressing *Cited2*, an experiment with microarrays was previously conducted in the laboratory (Santos, 2019; Santos et al., 2019). In this work, part of that experiment is further explored, with the authors' approval. In short, $C2^{fl/fl}$[cre] cells were treated with 4HT to deplete *Cited2* and with EtOH for control cells in two condition groups: undifferentiated and differentiated; undifferentiated cells were harvested after 48 hours of incubation, while the differentiated cells (using the above protocol) where harvested at day-4 of differentiation. Next, the RNA was isolated and sent to microarray analysis (Affymetrix, Mouse Genome 430 version 2.0 arrays), and then data was processed using R: the relative expression calculated using *limma* package (Ritchie et al., 2015) after probe intensity was normalized with *oligo* package (Carvalho and Irizarry, 2010), as described in (Acharya et al., 2018; Santos et al., 2019). The enrichment gene set analysis was conducted with EnrichR either using the R package (*EnrichR*) or on the web (Chen et al., 2013; Kuleshov et al., 2016).

Table 2.2 List of primers used in qPCR to analyse the expression level of target genes. The sequence of nucleotides is written from 5' to 3'.

Target gene	Forward	Reverse	NCBI ID	PrimerBank-ID	Reference
Asb4	GGCATCACTGCCCCTATCAG	TCCACATCTATTTGCCTCTCGAT	NM_023048.5	17505202a1	(Shuai et al., 2013)
Bmp5	TTACTTAGGGGTATTGTGGGCT	CCGTCTCTCATGGTTCCGTAG	NM_007555.3	6671642a1	(Buikema et al., 2013)
Bmper	GCCTGGGATTACCTGCTGC	ACACATTATGCAAGGGTTGTCTG	NM_028472.2	24371216a1	(Buikema et al., 2013)
Brachyury	CTCTAATGTCCTCCCTTGTTGCC	TGCAGATTGTCTTTGGCTACTTTG	NM_009309	-	(Wilson et al., 1995)
Casq2	TGCTCATGGTGGGGGTTTATC	AGGTTCGTGGTAATAGAGACAGA	NM_009814.4	6753292a1	(Rivera-Torres et al., 2016)
Cdx2	CAAGGACGTGAGCATGTATCC	GTAACCACCGTAGTCCGGGTA	NM_007673.3	31560722a1	(Koga et al., 2014)
Cited2	CGCATCATCACCAGCAGCAG	CGCTCGTGGCATTCATGTTG	NM_010828	-	(Chen et al., 2007)
Cxcr4	GACTGGCATAGTCGGCAATG	AGAAGGGGAGTGTGATGACAAA	NM_009911.3	116268122c1	(Chen et al., 2015)
Cxcr7	AGCCTGGCAACTACTCTGACA	GAAGCACGTTCTTGTTAGGCA	NM_007722.4	31560715a1	(Rey et al., 2009)
Dkk1	CTGAAGATGAGGAGTGCGGCTC	GGCTGTGGTCAGAGGGCATC	NM_010051	-	(Kemp et al., 2005)
Fgf10	CAGCGGGACCAAGAATGAAG	TGACGGCAACAACTCCGATTT	NM_008002	-	(Sultana et al., 2009)
Foxf1	ACGCCGTTTACTCCAGCTC	CGTTGTGACTGTTTTGGTGAAG	NM_010426.2	6753902a1	(Cha et al., 2015)
Gapdh	TCCCACTCTTCCACCTTCGATGC	GGGTCTGGGATGGAAATTGTGAGG	NM_001001303	-	(Ivanova et al., 2006)
Isl1	CTTAAGCATGCCCTGTAGCTGG	CAGACAGGAGTCAAACACAATCCC	NM_021459	-	(Ivanova et al., 2006)
Kdr	ACTGCAGTGATTGCCATGTTCT	TCATTGGCCCGCTTAACG	NM_010612	-	(Fujimori et al., 2008)
Lin28a	GGTCTGGAATCCATCCGTGTCA	TCCTTGGCATGATGGTCTAGCC	NM_145833.1	-	(Edupuganti et al., 2017)
Mdc1	CAGGACTGCCTAGCTGGTAGT	TGTGGTTGGGACTTGACCTCT	NM_001010833.2	132626692c2	-
Mesp1	TGTACGCAGAAACAGCATCC	TTGTCCCCTCCACTCTTCAG	NM_008588	-	(Bondue et al., 2008)
Mex3b	ACCCAGTTCCGAACACGTCG	TGTTCTTGTTACGAGAGGCT	NM_175366.3	-	(Yan et al., 2016)

p21	CCTGGTGATGTCCGACCTG	CCATGAGCGCATCGCAATC	NM_007669.5	162287332c1	(D'Angelo et al., 2018)
p53	CTCTCCCCCGCAAAAGAAAAA	CGGAACATCTCGAAGCGTTTA	NM_011640.3	200203a1	(Zhu et al., 2021)
Pcsk5	CCATGCCCAGTCAACCTACTT	CAGGCTCCTTCGATATTCATGTC	NM_001190483.1	253314508c2	(Wei et al., 2012)
Perp	ATCGCCTTCGACATCATCGC	CCCCATGCGTACTCCATGAG	NM_022032.4	158508502c1	(Granier et al., 2014)
Plk2	GACTACTGCACCATAAGCATG	CTTCTGGCTCTGTCAACACCT	NM_152804.2	165932299c1	(Lee and Pelletier, 2017)
Prdm6	GGAGCCTAGTAAGTCGAGCTG	GGACGTTCAAGTTTTCATCCTGG	NM_001033281.3	146198827c3	(Fei et al., 2015)
Ptges	GGATGCGCTGAAACGTGGA	CAGGAATGAGTACACGAAGCC	NM_022415.3	11967941a1	(Cao et al., 2019)
Rad51c	CGGGAGTTGGTGGGTTATCC	CCGGCACATCTTGGTTTATTTGT	NM_053269.3	16716605a1	(Boege et al., 2017)
Rad9b	CCCAAAAGACTATTTCCCAAG	TGTTCACAAGATACAGCTCCAA	NM_144912.3	-	(Hu et al., 2008)
Rasgrp3	GGGAAAGCGGCAACACTAGAT	GGGCAAGTAACTGTCGTTCAG	NM_001166493.1	262072985c1	(Songqing et al., 2014)
Rbm24	GGGGCTACGGATTTGTCACC	TGGCTGCATGATTCTTGGTTT	NM_001081425.1	124487276c1	(Xie et al., 2017)
Rspo3	ATGCACTTGCGACTGATTTCT	GCAGCCTTGACTGACATTAGGAT	NM_028351.3	16605378a1	(Cai et al., 2014)
Tbx20	AAACCCCTGGAACAATTTGTGG	CATCTCTTCGCTGGGGATGAT	NM_194263.2	12082750a1	(Sampaio-Pinto et al., 2018)
Wnt5a	CAAATAGGCAGCCGAGAGAC	TCTAGCGTCCACGAACTCCT	NM_009524	-	(Chen et al., 2007)

Table 2.3 List of primers used in qPCR to analyse the enriched promoter regions from ChIP experiments. The sequence of nucleotides is written from 5' to 3', and the genomic range is relative to the mouse genome version UCSC.mm9.

Target	Forward	Reverse	Range	Reference
Cdx2	GTCTCCAGCCATTGGTGTCT	TTCTTTCCTCCCACCTCCTT	chr5:148118706-148118957	(Morey et al., 2013)
Dkk1	GTTCTTGATCGCGTTGGAAT	GAAGTTGAGGTTCCGCAGTC	chr19:30623685-30624012	(Wang et al., 2017)
Isl1	TTTTGGGTCTAACCGTCCTACTC	CCGCTTTCCTTCACTGACTC	chr13:117100331-117100486	(Kranc et al., 2015)
Kdr	GAGTCTGTGCCTGAGAACTG	CAGAACCACAGAGCGACA	chr5:76374121-76374350	(Bomsztyk et al., 2015)
Mesp1	GCGTCTCGATCTTGGTCAGGTT	AGCGGGAGAAGCTACGTATGC	chr7:86938006-86938216	(Liu et al., 2015a)
T	CGGCCAGTCTGATATGGCCGCGCA	CCCGCAAGGCGCGACAAGAGTAA	chr17:8626954-8627221	(Dahle et al., 2010)

2.3.5 Whole protein extraction and quantification

To obtain whole protein lysates, cultured cells were washed three times with PBS, lysis buffer was applied, cells were scrapped and pelleted down by centrifugation in 1.5 mL tube; in alternative cells were dissociated with trypsin and the pellet stored at -80 ºC until further processing. Cells were then resuspended into 4-5 volumes of lysis buffer (50 mM TRIS pH 8.0, 0.5 % NP-40 and 150 mM NaCl, which was supplemented right before the use with protease inhibitor cocktail, 1 mM PMSF, 0.2 µM sodium orthovanadate and 1 mM DTT (Sigma, D9799), unless otherwise stated. This mixture was placed on ice with occasional shaking for 20 minutes, and cleared by centrifugation at 14 000 *rcf* for 10 minutes at 4 ºC. The supernatant was transferred to a new tube and stored at -80 ºC until further use. Total protein was quantified using the Bradford method (Bradford, 1976) in 96-well plates: Bradford reagent (Alfar Aesar, J61522) was diluted two times and allowed to reach room temperature, 250 µL were loaded into each well, and then 5 µL of sample or calibration solution was added; for a total volume per well of 255 µL. The plate was then incubated at room temperature for 10 minutes and then the absorbance at 590 nm was read in a plate reader (Progema, Glomax) or (Molecular Devices, Spectramax iD3). The calibration curves were prepared with fresh BSA solutions (NZYtech, MB04602) ranging from 100-2000 µg/mL.

2.4 Image analysis

The image analysis in this work was performed with Fiji v1.53q (Schindelin et al., 2012) or with Cell Profiler v4.1.3 (McQuin et al., 2018; Stirling et al., 2021) running on Windows 10 v21H2 (Microsoft).

2.4.1 Embryoid bodies

Images of the embryoid bodies (4608 x 3456 px) were acquired on day-2 and day-4 of differentiation (see above) and converted to 8-bit grayscale using Cell Profiler in a batch process. Then, the images were analysed using a pipeline. Briefly, the following steps were applied: (1) a smooth was applied, to reduce the number of small objects detected (mainly debris); (2) enhance edges, to make more evident the embryoid body; (3) Gaussian filter, to reduce the sharpness of the edges and compensate for the out of focus edge of the embryoid body; (4) threshold with Otsu two-classes with correction factor 0.7 and size of adaptative

window 800 px; (5) erode 30 px to reduce the number of artefacts; (6) measure segmented objects Feret diameter, area, and form factor (7) filter for objects with Feret diameter higher than 700 px and form factor > 0.3, objects within these parameters are more likely to be debris or more than one embryoid body per drop. The results of the segmentation and quantification were exported as images and tables, respectively.

2.4.2 Western blot semi-quantification

A semi-quantification of the bands obtained from Immunoblotting (Western Blot) was achieved using a densitometric approach through Fiji built-in function *Gels*. Briefly, a region of interest was drawn on top of the lanes ranging from the first to the last lane of the blot matching the largest lane, then the pixel density was plotted and the area under the curve was quantified. Similarly, this quantification was performed for the total protein or the loading control band (with one ROI per lane) (Taylor et al., 2013). Next, the value of the relevant band was divided by the value of the loading control, thus expressed relative to the control.

2.4.3 γH2AX speckles

This pipeline is an adapted version of the pipeline provided on the official website for Cell Profiler examples speckle counting (www.cellprofiler.org). Briefly, the following steps were applied: (1) enhance feature, where the size of the speckles was considered to be 5 px; (2) an Otsu threshold with three classes using 65 px adaptative windows was applied to segment the nuclei using a declumping method based on shape; (3) next the nuclei were measured (area and shape) and the; (4) filtered were the accepted maximum Feret diameter was between 58.5-97.5 px, and the form factor between 0.5 and 1. Next, the speckles were segmented using (5) Otsu threshold with three classes using adaptative windows of 10 px, and the minimum size expected of 5 and maximum size of 20 px, declumping based on intensity. Next segmented results were (6) measured (area and shape), and (7) filtered by size, where speckles size was accepted if above 1 px and below 66 px. Next, (8) intensity measurements were performed and lastly, (9) parent-child relationship was established between nuclei and speckles. As before, the resulting segmentation images and quantification tables were also exported.

2.5 Histone acetylation assay

Using the immunoprecipitated samples from undifferentiated cells expression and depleted of *Cited2* (see above), the histone acetyltransferase activity was tested using a commercially

available kit (Abcam, ab204709) following the manufacturer's instructions. For this assay, 5 µL of the IP-p300 eluted was used, and 2 µL of the IP-input sample. The plate was incubated at 25 ºC and the fluorescence wavelength (nm) 535excitation/587emission was read for 60 minutes every 2 minutes.

2.6 Data analysis and statistics

The acquired data were analyzed in Excel (Microsoft) or RStudio v.2022.02.1+461 (RStudio) using the R programming language version 4.0.5 (Team, 2021). Summary statistics and hypothesis testing were performed using r-base functions or with the packages *rstatix* (Kassambara, 2021) or *ggpubr* (Kassambara, 2020). For all experiments, the null hypothesis was tested against the control group considering the difference between the two groups equal to zero. The arbitrary threshold of the P-value for statistical significance was 0.05 and significance levels represented as follows: 'ns': > 0.05; '*': ≤ 0.05; '**': ≤ 0.01; '***': 0.001; '****' ≤ 0.0001. The plots were generated using the R package *ggplot2* (Wickham, 2016), and the final figures were assembled in the vector graphics software Affinity Designer v1.10.5 (Serif).

3 Results

3.1 Cited2 affects pluripotency and differentiation

To further investigate the apparent dual role of *Cited2* in mouse embryonic stem cells, both in pluripotency (or undifferentiating conditions) and in differentiation conditions, differentially expressed genes (DEG) were examined. Previous studies showed evidence that, in the context of pluripotency, *Cited2* plays a role in maintaining cell self-renewal (Li et al., 2012b). In particular, *Cited2* enhanced the promoter activity *Nanog*, *Tcf3* and *Klf4* (observed by luciferase assays), yet no changes were observed for *Oct4* and *Sox2* (Kranc et al., 2015). While *Cited2*-depletion increased apoptosis markers and spontaneous differentiation, which from the *Cited2*-knockdown experiment showed increased upregulation of genes such as *Brachyury*, *Fox2a*, and *Sox15* (Kranc et al., 2015). The increased loss of self-renewal as evidenced by increased cell death and differentiation suggests that *Cited2* is also associated with differentiation mechanisms. Indeed, *Cited2* appears to be involved in the transition from pluripotency to differentiation by regulating *Oct4* to guide differentiation (Li et al., 2012b). During differentiation events, specifically cardiac differentiation, there is evidence that CITED2 interacts with the LIM domain of proteins, such as *Lhx2* (Glenn and Maurer, 1999) and ISL1 (Pacheco-Leyva et al., 2016). The interaction with ISL1 demonstrated that CITED2 co-operates with ISL1 for proper cardiac differentiation in cardiac progenitor cells.

Therefore, to elucidate the possible mechanism(s) where *Cited2* could play a role, our group performed a functional assay through a gene expression screening (microarray) using mESC. The cell line used in this study allows the conditional knockout of *Cited2* (although only partially) to be compared with the wild type. Thus, the differentially expressed genes were obtained from two culturing conditions: undifferentiated and differentiated (Figure 3.1), and the results were used as starting point for the present work.

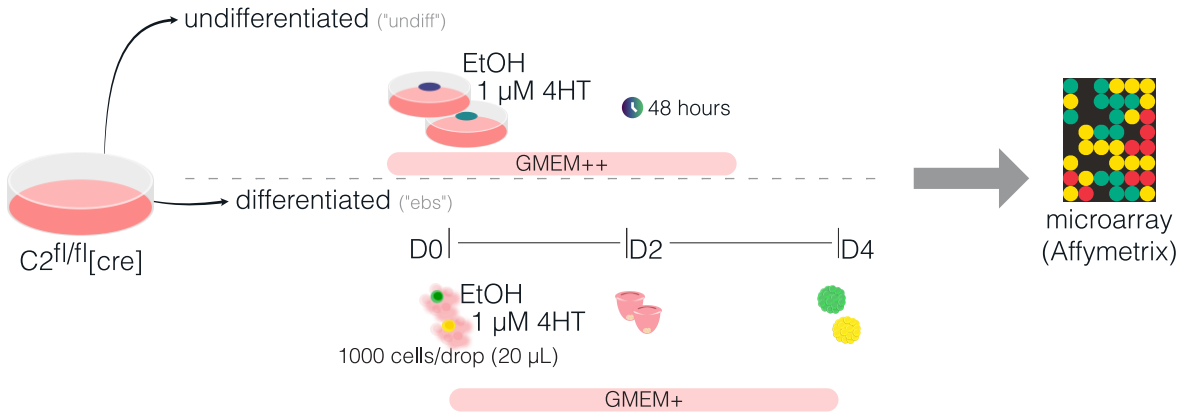

Figure 3.1 Experimental design to determine differentially expressed genes. $C2^{fl/fl}$[cre] cells were cultured in conditions sustaining pluripotency ("undifferentiated"), and in conditions triggering differentiation ("differentiated") (cells were induced to differentiate using the hanging drop protocol). In both conditions, cells were treated at the onset of the experiment (D0) with EtOH (control) or with 1 µM 4HT (*Cited2*). For the hanging drop protocol, 20 µL drops were prepared with 1000 cells. Cells were harvested at 48 hours and day-4 (D4), for undifferentiated and differentiated conditions, respectively. The RNA was isolated and sent for microarray screening (Affymetrix) (outsourced) and analysis performed in R using Bioconductor packages. "GMEM++" refers to the culture medium supplemented and containing LIF, while "GMEM+" refers only to supplemented medium. "D" stands for day.

To obtain an overview of gene expression under the four conditions a principal component analysis (PCA) was performed (Figure 3.2). The results showed that the four experimental groups have different gene expression patterns, as they clustered separately. Undifferentiated control cells clusters closer to differentiated *Cited2*-partial_KO cells; they are closer in both PC1 and PC2. Undifferentiated control cells are separated from undifferentiated *Cited2*-partial_KO cells; this separation is mainly explained by PC2. Lastly, differentiated control is separated from undifferentiated control, and differentiated *Cited2*-partial_KO in PC1, while being closer to undifferentiated *Cited2*-partial_KO in PC2. These results suggest that *Cited2*-depletion causes cells to spontaneously differentiate as previously reported (Kranc et al., 2015), yet through a path different from that observed in the differentiating conditions, where cells were induced to differentiate using the hanging drop method. Additionally, when cells were induced to differentiate but were depleted of *Cited2*, the expression pattern is closer to undifferentiated cells, suggesting a delay in the expression of differentiation genes as previously reported (Santos et al., 2019).

To better understand the role of *Cited2* in the maintenance of undifferentiated cells, self-renewal, and differentiation (focusing on cardiac differentiation), the microarray results were further analysed using gene set enrichment analysis. From the obtained results, new experiments were performed to further investigate the possible roles of *Cited2*. Therefore, the results of this work are presented according to the experimental context: one dedicated to the

role of *Cited2* in pluripotency conditions, and the other dedicated to the role of *Cited2* in differentiation conditions; respectively topics 3.2 and 3.3.

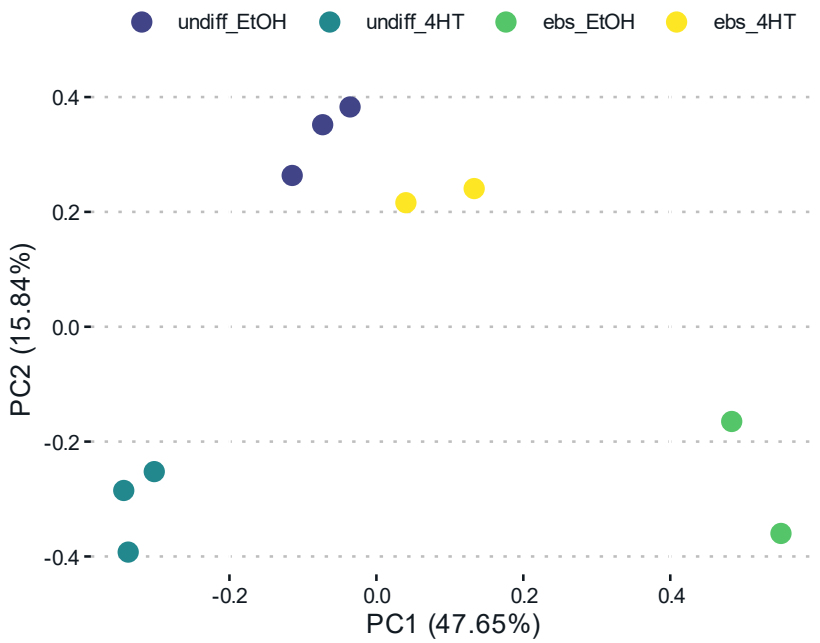

Figure 3.2 *Cited2*-partial_KO groups cluster apart from their control group. Differentially expressed genes was analysed using microarray (Affymetrix) from four experimental groups: undifferentiated cell culture in pluripotency condition treated with EtOH (● undiff_EtOH, control) and treated with 1 µM of 4HT (● undiff_4HT, *Cited2*-partial_KO) for 48 hours; differentiated embryoid bodies with hanging drop treated with EtOH (● ebs_EtOH, control) and 1 µM 4HT (● ebs_4HT, *Cited2*-partial_KO) harvested on day-4. The microarray results were processed with R, where the data were normalized and dimensions reduced using principal component analysis (PCA). Each point represents a sample. "PC" stands for principal component.

3.2 The suggested role of *Cited2* in DNA repair

Cited2 is associated with the pluripotency gene regulatory network; consequently, mouse embryonic stem cells depleted of *Cited2* die or differentiate spontaneously (Kranc et al., 2015). To better understand the role of *Cited2* in undifferentiated mESC, gene expression was compared between undifferentiated control and *Cited2-partial_KO* cells using microarray analysis (Figure 3.1). Then, from the list of genes, the DEGs that were down-regulated and up-regulated genes were obtained considering the thresholds of $|log(fold\ change)| > 1.2$ and P-value < 0.05. The analysis of DEGs indicated that there are more down-regulated genes than up-regulated genes, respectively, 126 vs 104 (Figure 3.3a).

Cited2-depletion under undifferentiation conditions led to a decrease in the expression of genes related to DNA-repair and an increase in genes related to apoptosis. When considering the top ten down-regulated genes (Figure 3.3b), it can be seen that *Rad51c* is present, which is a gene associated with DNA repair (Suwaki et al., 2011). Moreover, two genes are involved in DNA damage response and cell cycle arrest: *Itgb4* and *Gadd45g*. Interestingly, the *Lefty1* and *Lefty2* genes are also present. These two genes are associated with the maintenance of self-renewal and with embryo development, since they participate in the establishment of the left-right axis (Kim et al., 2014; Meno et al., 1999).

Next, to have a broader understanding of the transcription factors and biological processes implicated by the downregulation of *Cited2*, a gene set enrichment analysis was performed for the ChEA/ENCODE consensus and Gene Ontology biological processes were conducted using EnrichR (Chen et al., 2013; Kuleshov et al., 2016). The results of the ChEA/ENCODE consensus database showed terms associated with pluripotency transcription factors (NANOG, OCT4, SOX2, and TCF3), which are statistically significant, considering the adjusted P-value (Figure 3.4). On the contrary, no statistically significant terms were found for the up-regulated list of genes. However, the results showed terms such as SUZ12, SMAD4, GATA2 and P63 suggesting that the differentiation processes are affected by *Cited2* depletion. Indeed, the results obtained from the GO:biological processes on the up-regulated list showed “muscle contraction”, as the most statistically significant; followed by terms that are related to angiogenesis (Figure 3.5). No statistically significant hits were found for the down-regulated genes list considering the adjusted P-value.

However, among the obtained GO:biological processes terms obtained “strand invasion” and ‘DNA recombinase assembly’ were observed. These results suggested that *Cited2*-depleted

cells could have an impairment in DNA repair, specifically double-strand/single-strand DNA breaks since *Rad51c* is associated with the repair of dsDNA breaks (Godin et al., 2016; Suwaki et al., 2011). Therefore, these results suggest that the downregulation of genes associated with the repair of DNA damage, could ultimately lead to cell death, and/or differentiation, even when cells are kept in undifferentiating culture conditions (with LIF).

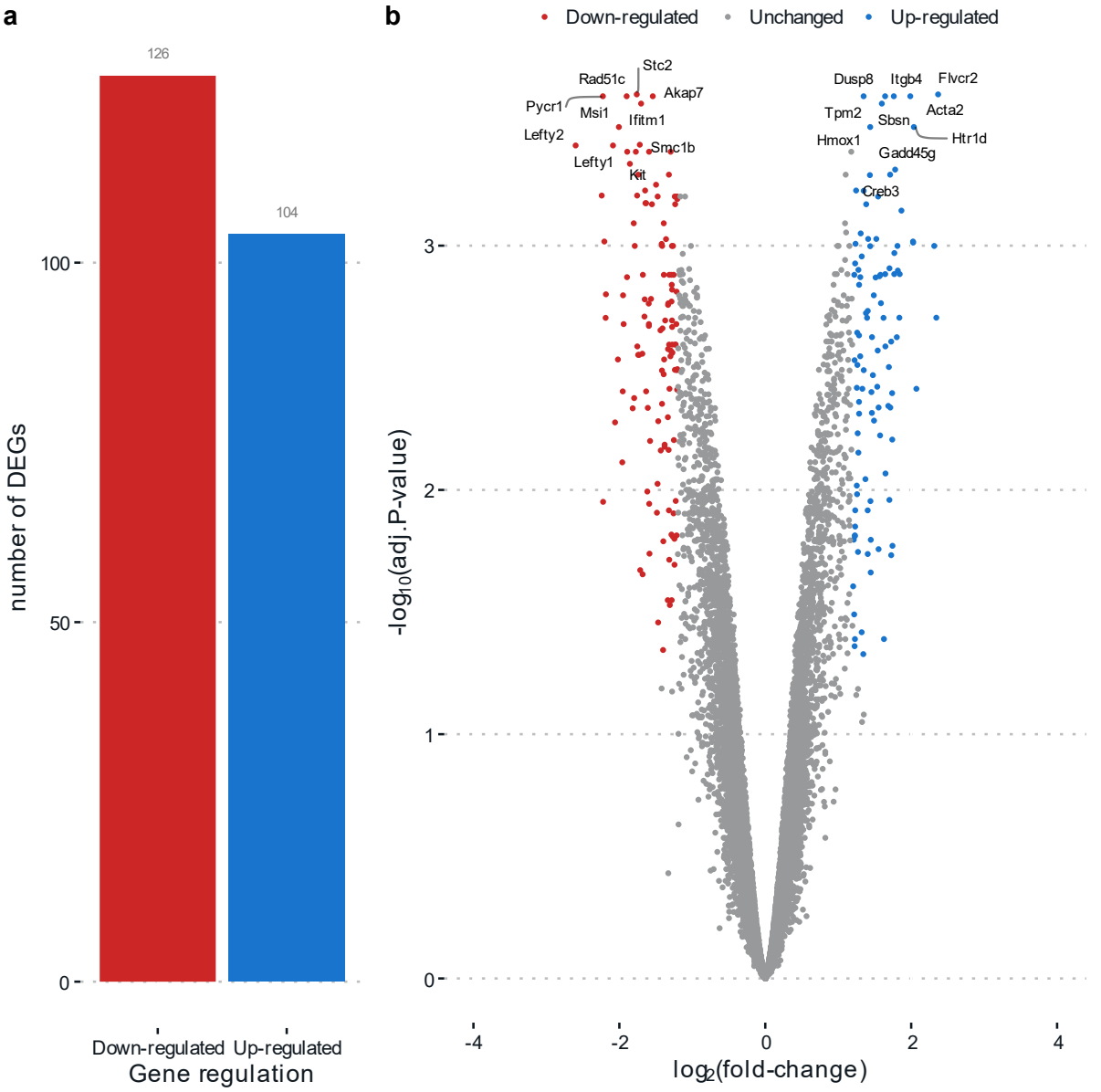

Figure 3.3 Different regulation of genes between cells expressing and not expressing *Cited2* under undifferentiated conditions. $C2^{fl/fl}$[cre] cells were cultured under undifferentiating conditions and treated with EtOH (control) or 4HT (*Cited2*-partial_KO) for 48 hours, and by microarray (Affymetrix) analysis the differentially expressed genes (DEGs) were obtained between the two conditions. **(a)** represents the total number of genes down-regulated and up-regulated between the two groups, represented as red (■) and blue (■), respectively. While **(b)** represents the total number of genes (20291) where in grey (●) are the genes with unchanged expression, while in red (●) and blue (●) are, respectively represented, the down-regulated and up-regulated that crossed the log_2(fold-change) threshold of 1.2 and the adjusted P-value of 0.05. The top ten most down-regulated are labelled. The top down-regulated genes arranged by adjusted P-value are: *Stc2, Pycr1, Rad51c, Akap7, Ifitm, Mis1, Smc1b, Lefty2, Lefty1, Kit*; and top up-regulated are: *Flvcr2, Acta2, Itgb4, Dusp8, Tpm2, Sbsn, Htr1d, Hmox1, Gadd45g, Creb3*.

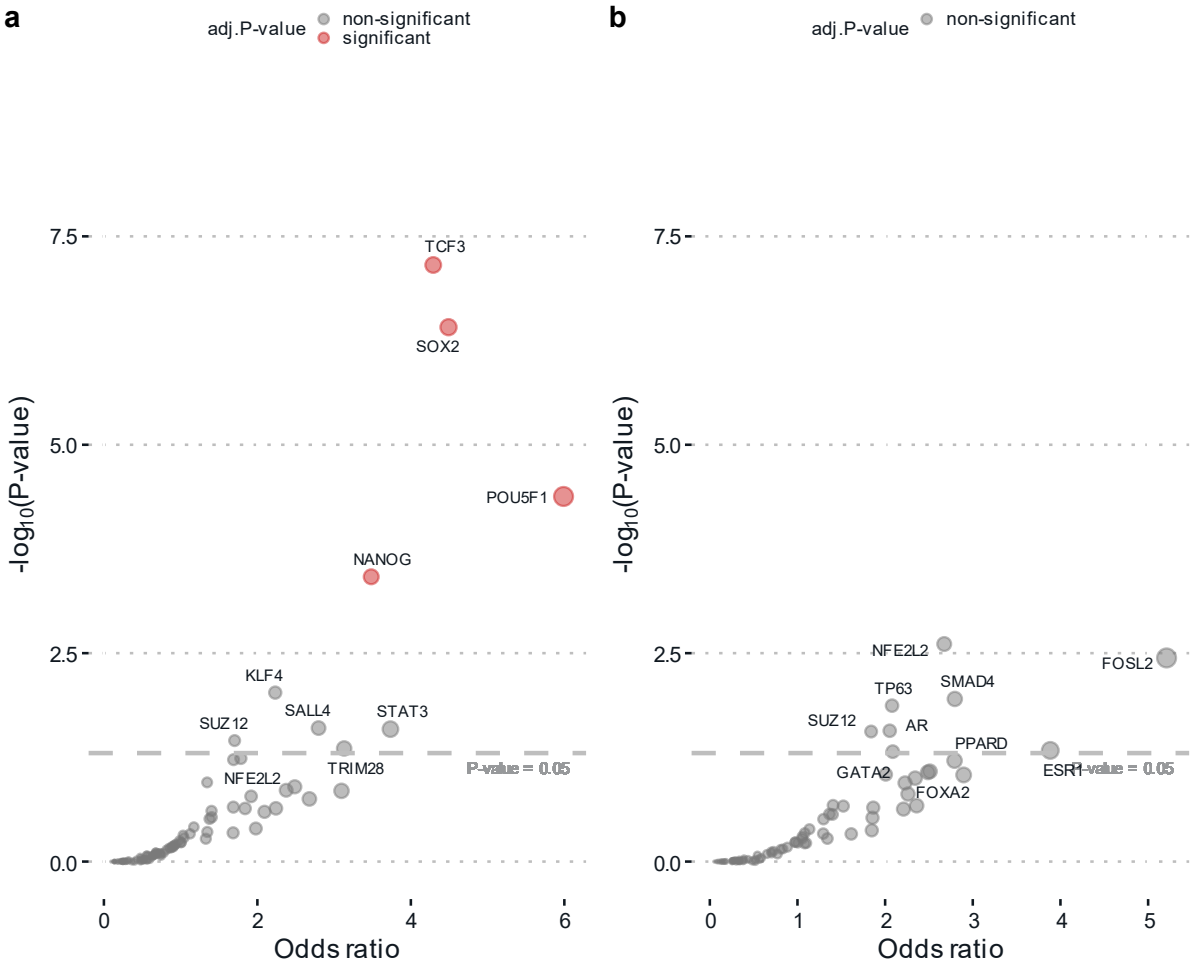

Figure 3.4 *Cited2*-partial_KO affects pluripotency factors terms of ChEA/ENCODE database. The two lists of differentially expressed genes (126 down-regulated and 104 up-regulated) in undifferentiating conditions were used to perform a gene set enrichment analysis for ChEA/ENCODE transcription factors consensus; using the tool EnrichR. The size of each point represents the overlap ratio, *i.e.* the number of genes in the list that are contributing to a term over the number of genes annotated for the transcription factor term. In **(a)** are represented the results of ChEA/ENCODE consensus terms from the down-regulated list, and in **(b)** the results of the up-regulated list. The grey points (●) represent nonsignificant while the accent colour respective to their regulation (down-regulated as red (●), and up-regulated as blue (●)) represent a smaller adjusted P-value than the threshold of 0.05. The dashed line (– –) represents the P-value threshold of 0.05. The top ten terms are labelled: top down-regulated are all ChEA: TCF3, SOX2, POU5F1, NANOG, KLF4, SALL4, STAT3, SUZ12, TRIM28, NFE2L2; and top up-regulated are: NFE2L2 CHEA, FOSL2 ENCODE, SMAD4 CHEA, TP63 CHEA, AR CHEA, SUZ12 CHEA, ESR1 CHEA, GATA2 CHEA, PPARD CHEA, FOX2A ENCODE.

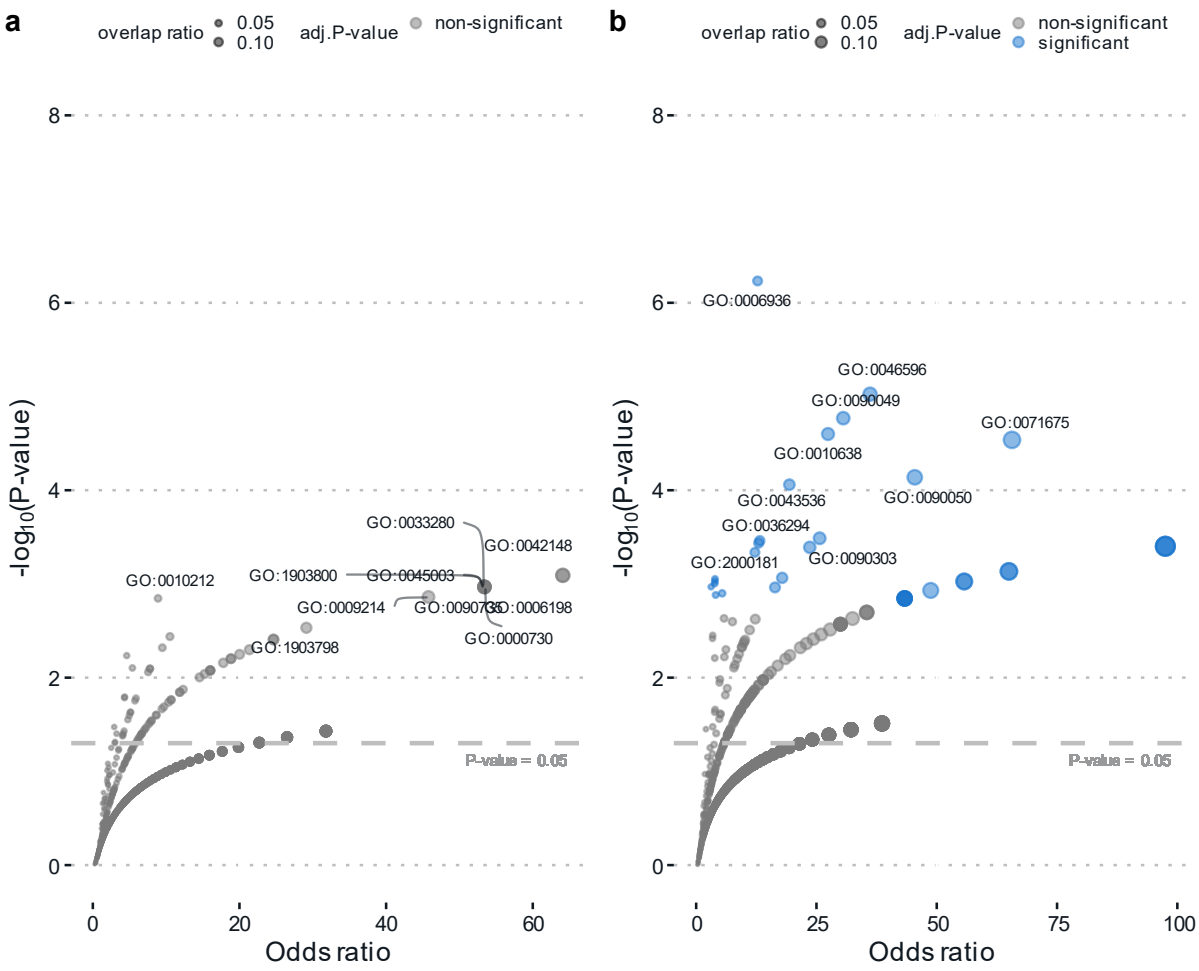

Figure 3.5 *Cited2*-partial_KO affects DNA repair biological processes in pluripotency conditions. The two lists of differentially expressed genes (126 down-regulated and 104 up-regulated) in pluripotency conditions were used to perform a gene set enrichment analysis for Gene Ontology (GO): biological processes; using the tool EnrichR. The size of each point represents the overlap ratio, *i.e.*, the number of genes in the list that are contributing to a term over the number of genes annotated for that gene ontology term. In **(a)** are represented the results of GO terms from the down-regulated list, and in **(b)** from the up-regulated list. The grey points (●) represent nonsignificant while the accent colour respective to their regulation (down-regulated as red (●), and up-regulated as blue (●)) represent a smaller adjusted P-value than the threshold of 0.05. The dashed line (– –) represents the P-value threshold of 0.05. The top ten terms are labelled. The top down-regulated are: strand invasion (GO:0042148), cAMP catabolic process (GO:0006198), DNA recombinase assembly (GO:0000730), positive regulation of production of miRNAs involved in gene silencing by miRNA (GO:1903800), response to vitamin D (GO:0033280), double-strand break repair via synthesis-dependent strand annealing (GO:0045003), cyclic nucleotide catabolic process (GO:0009214), response to ionizing radiation (GO:0010212), regulation of production of miRNAs involved in gene silencing by miRNA (GO:1903798); and top up-regulated are: muscle contraction (GO:0006936), regulation of viral entry into host cell (GO:0046596), regulation of cell migration involved in sprouting angiogenesis (GO:0090049), positive regulation of organelle organization (GO:0010638), regulation of mononuclear cell migration (GO:0071675), positive regulation of cell migration involved in sprouting angiogenesis (GO:0090050), positive regulation of blood vessel endothelial cell migration (GO:0043536), positive regulation of wound healing (GO:0090303), cellular response to decreased oxygen levels (GO:0036294), negative regulation of blood vessel morphogenesis (GO:2000181).

3.2.1 DNA damage increase

Following the enrichment analysis (Figure 3.5a), the observation of terms referring to DNA repair and strand-invasion suggested, together with the P63 being one of the results from the ChEA/ENCODE consensus suggested that DNA damage could be contributing to the observed increase in cell death of mESC *Cited2*-depleted cells. In fact, downregulation of *Rad51*c was speculated to be a mediator of *Cited2* during DNA repair events (Liu et al., 2015b), and upregulation of *Itgb4* was correlated with downregulation of *Cited2* in cells with a high level of DNA damage caused by ionizing irradiation (Bo et al., 2004). Therefore, to determine if *Cited2*-depleted cells showed higher DNA damage, an experiment was conducted to assess the increase of DNA damage compared to the control. For that, it was considered an indicator of DNA damage the increase of double-strand breaks visualized with the phosphorylated H2AX (or γH2AX) (Fernandez-Capetillo et al., 2004; Rogakou et al., 1998). In this experiment, the $C2^{fl/fl}$[cre] cells that allow the partial conditional knockout of *Cited2*, were treated for 16 hours and 48 hours with EtOH (control), or 4HT (*Cited2*-partial_KO); additionally, an insult with 100 µM of hydrogen peroxide was used as the positive control (Katsube et al., 2014) (Figure 3.6).

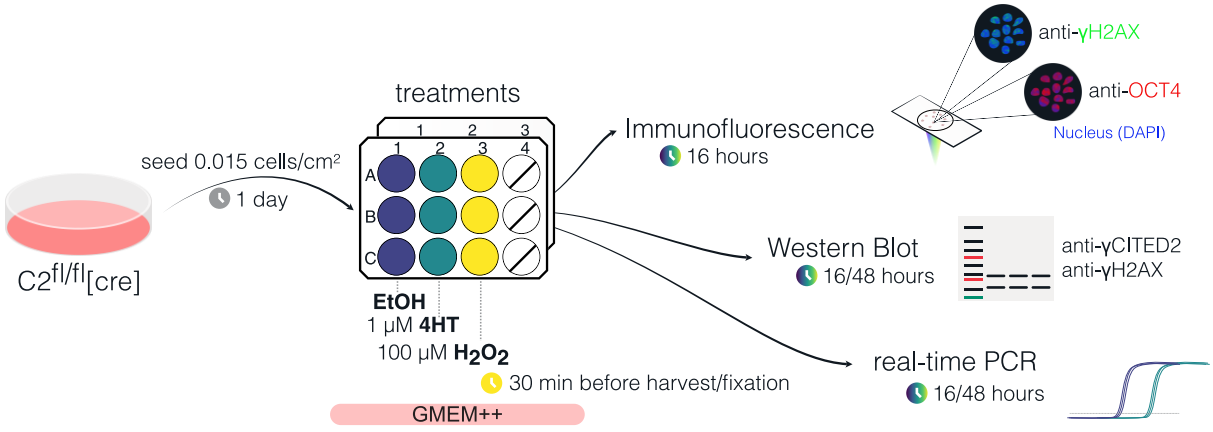

Figure 3.6 Experimental design to assess DNA damage. $C2^{fl/fl}$[cre] cells were seeded (0.015 cells/cm²) in 12-well and 6-well plates and allowed to grow for approximately one day. Next, a treatment with EtOH (control), 1 µM 4HT (*Cited2*-partial_KO) was applied for 16 or 48 hours. At 30 min before harvesting for RNA, protein isolation and fixation 100 µM of H_2O_2 (positive control) were applied to the respective wells. Fixed samples in 2% PFA were probed with anti-γH2AX, anti-OCT4, and nucleus stained with DAPI; samples were scoped under both a wide field fluorescence and a confocal microscope. The resulting images were quantified with a pipeline in Cell Profiler. The CITED2 protein level was verified at 48 hours; unlike γH2AX, which was verified at the two time points. The *Cited2* transcripts were analysed with real-time PCR. These experiments were repeated three times.

The decreased expression of *Cited2* was verified after 16 hours using qPCR (Figure 3.7), which is shown to be similar to the fold-change of 0.79 observed in the microarray experiment. In parallel, a group of cells was fixed and probed with antibodies anti-γH2AX and anti-OCT4. Before fixation, cells were observed under a phase contrast microscope to observe their

morphology and evidence of cell death (Figure 3.8). The results suggested spontaneous cell differentiation since there were more irregularly shaped colonies (Figure 3.8), thus deviating from the rounded mESC colonies (Mulas et al., 2019). Cell death in 4HT and H_2O_2 treatment was visible through a decrease in confluence and an increase in the number of small bright spots. Furthermore, the lower intensity of the OCT4 signal in some colonies suggests that they are differentiating (Figure 3.8). These results support the notion that, indeed, *Cited2*-partial_KO has more cell death and less cell growth than the control. However, the signal of γH2AX, at this magnification, did not allow the quantification (Figure 3.8).

Given that the labelling of γH2AX in a widefield microscope (Figure 3.8) was not conclusive, due to the high background levels, samples were scoped with a confocal microscope. Given the nature of the mESC colonies' morphology, a Z-stack of four images was taken, and then an image of its maximum projection was obtained. By doing this, it was possible to reduce the high background observed previously, and increase the resolution of the γH2AX speckles (or foci) (Figure 3.9a). Next, the images from confocal microscopy (Figure 3.9a) were used as input of a pipeline in Cell Profiler to quantify the γH2AX speckles. In this pipeline, both nuclei and speckles were segmented and quantified by area/shape and intensity (Figure 3.9b). The results showed that the average number of speckles per nucleus is unchanged in *Cited2*-partial_KO vs the control showing, respectively, 3.4 ± 0.2 vs 3.5 ± 0.2 (SEM) speckles per nucleus (Figure 3.9); while in the positive control there were 6.2 ± 0.3 (SEM) speckles per nucleus. However, when the speckle intensity is considered, the intensity of speckles in *Cited2*-partial_KO cells is higher than the control (0.045 ± 0.002 and 0.037 ± 0.002 (SEM) AU, respectively); positive control showed the highest intensity (0.06 ± 0.003 (SEM) AU). Moreover, given that not all cells showed speckles, the percentage of cells positive for γH2AX showed to be higher for *Cited2*-depleted cells than the control, and positive control: 89.4 %, 93.8 % and 89.3%, respectively.

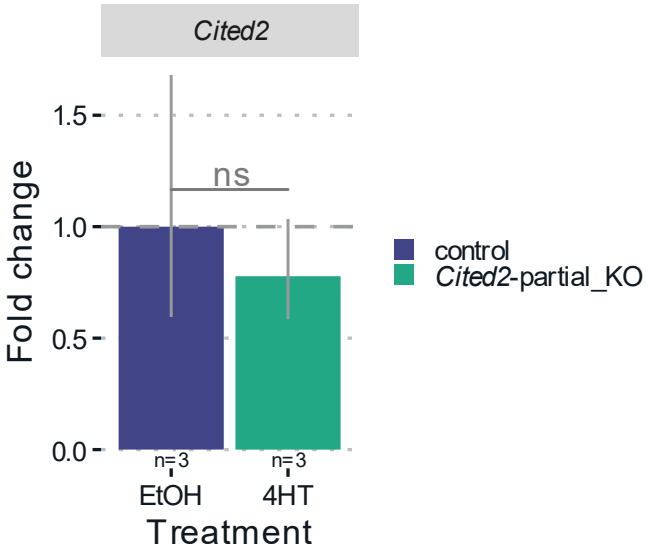

Figure 3.7 *Cited2* expression is down-regulated under undifferentiating conditions. Cultures of $C2^{fl/fl}$[cre] cells under pluripotency conditions were treated with EtOH (control) or 1 µM 4HT (*Cited2*-partial_KO) for 16 hours. Transcripts were analysed with the ddCt method and reported as fold-change relative to control; *Gapdh* was used as a reference gene. Results are shown as mean ± SEM from three experiments with "n" valid qPCR reads; the dCt means were compared to the control using the t-test considering the P-value threshold of 0.05 for significance: no statistically significant results (ns).

In addition to observing the γH2AX, in the microscope, its global levels were evaluated by Western blotting. Although microscopy allowed for the confirmation that this histone modification is present only in the nucleus, the observed/sampled region of a given cell is limited. Therefore, with western blot, a global evaluation of this histone modification is possible. These results showed that, although not statically significant, there is a tendency to increase phosphorylated H2AX levels in *Cited2*-partial_KO cells, as well as for the positive control (Figure 3.10). Therefore, this suggests that *Cited2*-partial_KO cells have increased levels of phosphorylated H2AX after 16 hours of treatment.

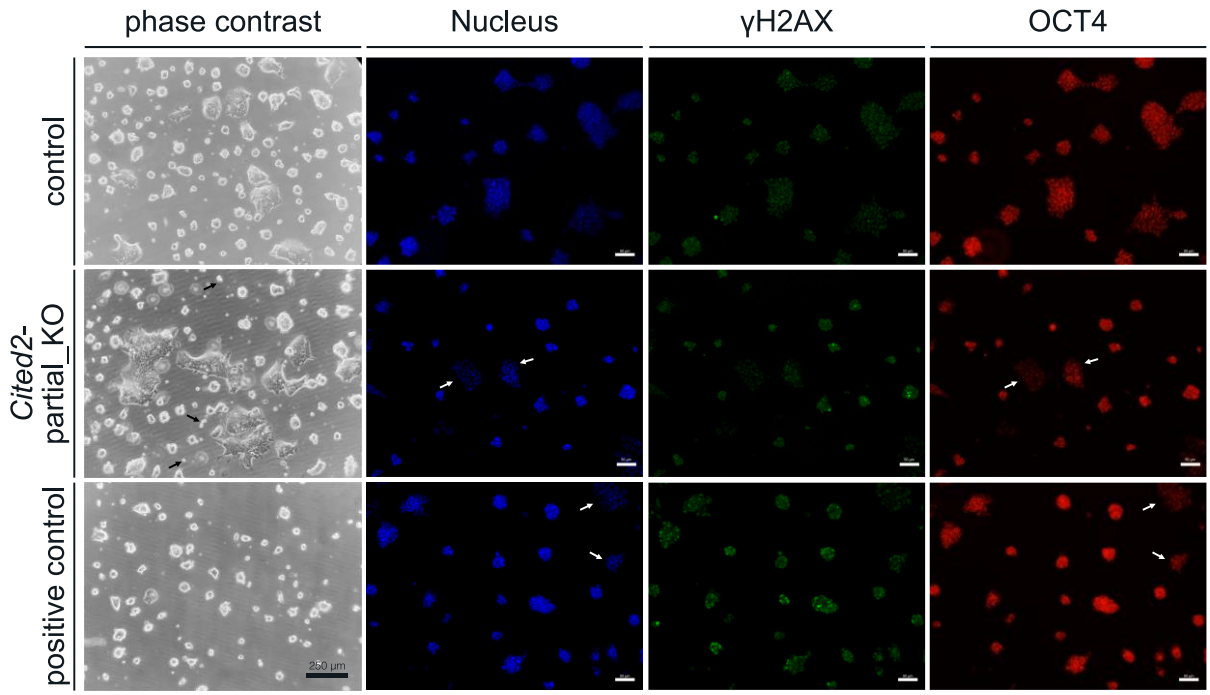

Figure 3.8 *Cited2*-partial_KO increases spontaneous differentiation and cell death. $C2^{fl/fl}$[cre] cells were cultured in pluripotency conditions in 12-well plates on glass coverslips, and treated with EtOH (control) or 1 µM 4HT (*Cited2*-partial_KO) for 16 hours, or 30 minutes before fixation with 100 µM hydrogen peroxide (positive control). Representative images with phase contrast of cells before fixation with 2% PFA were then probed with the primary antibody anti-γH2AX and anti-OCT4 followed by secondary incubation with Alexa Fluor A488 (green) and A594 (red), respectively. The slides were mounted with Flouromount-G containing DAPI for nuclear staining (blue). Samples were scoped with a wide-field microscope. The scale bar represents 250 µm and 50 µm for phase contrast (10x objective) and wide-field fluorescence (20x objective), respectively.

Next, 48 hours after treatment the protein levels of CITED2 and γH2AX were then evaluated by Western blotting. At this time point, as with the mRNA expression obtained with the microarray experiment, the protein levels were validated to be lower, although not statically significant (Figure 3.11). However, this result suggests that *Cited2* depletion was maintained for up to 48 hours. Furthermore, phosphorylated H2AX showed lower levels in *Cited2*-partial_KO cells than in the control (Figure 3.11). Together these results suggested that *Cited2* shows decreased expression, its protein levels are also decreased, and that γH2AX levels decreased over time in *Cited2*-partial_KO cells.,

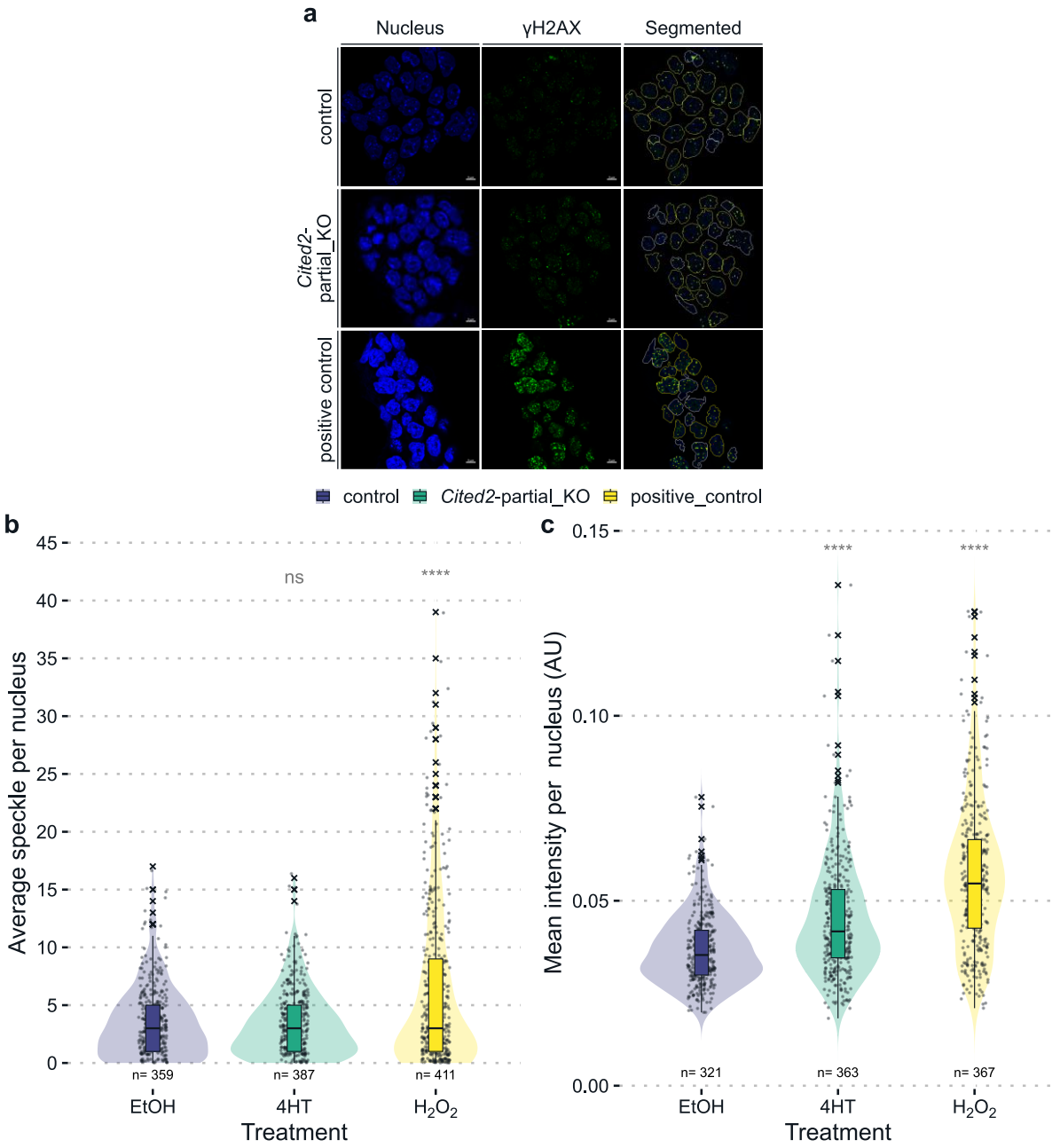

Figure 3.9 *Cited2*-partial_KO does not change γH2AX speckles number but increases their intensity. $C2^{fl/fl}$[cre] cells were cultured in pluripotency conditions in 12-well plates on glass coverslips, and treated with EtOH (control) or 1 µM 4HT (*Cited2*-) for 16 hours, or 30 minutes before fixation with 100 µM hydrogen peroxide (positive control). Representative images of cells probed with the primary antibody anti-γH2AX followed by secondary incubation with Alexa Fluor A488 (green). The slides were mounted with Flouromount-G containing DAPI for nuclear staining (blue). **(a)** Samples were scoped with a confocal microscope using Airyscan super-resolution to obtain four slices of 0.15 µm thickness from which the maximum intensity orthogonal projection was obtained. Then, this resulting image was used as input for a segmentation pipeline in Cell Profiler to identify the nuclei and the γH2AX speckles. **(b)** represents the number of γH2AX speckles per nucleus, while **(c)** represents the mean intensity of the γH2AX speckles per nucleus. Each dot represents a nucleus (n); crosses represent points outside the interquartile range. The nuclei were filtered by size and shape: the results shown with the white contours (○) represent the declined results, while the yellow contours (○) show the accepted results. The speckles were filtered by size and shape: the results shown with red contours (○) show declined results, while yellow contours (○) show accepted. The scale bar represents 5 µm (63x objective). Means were compared with the control condition using a t-test considering the P value threshold of 0.05 for significance; (ns): not significant and (****) ≤ 0.0001. The results are from three experiments.

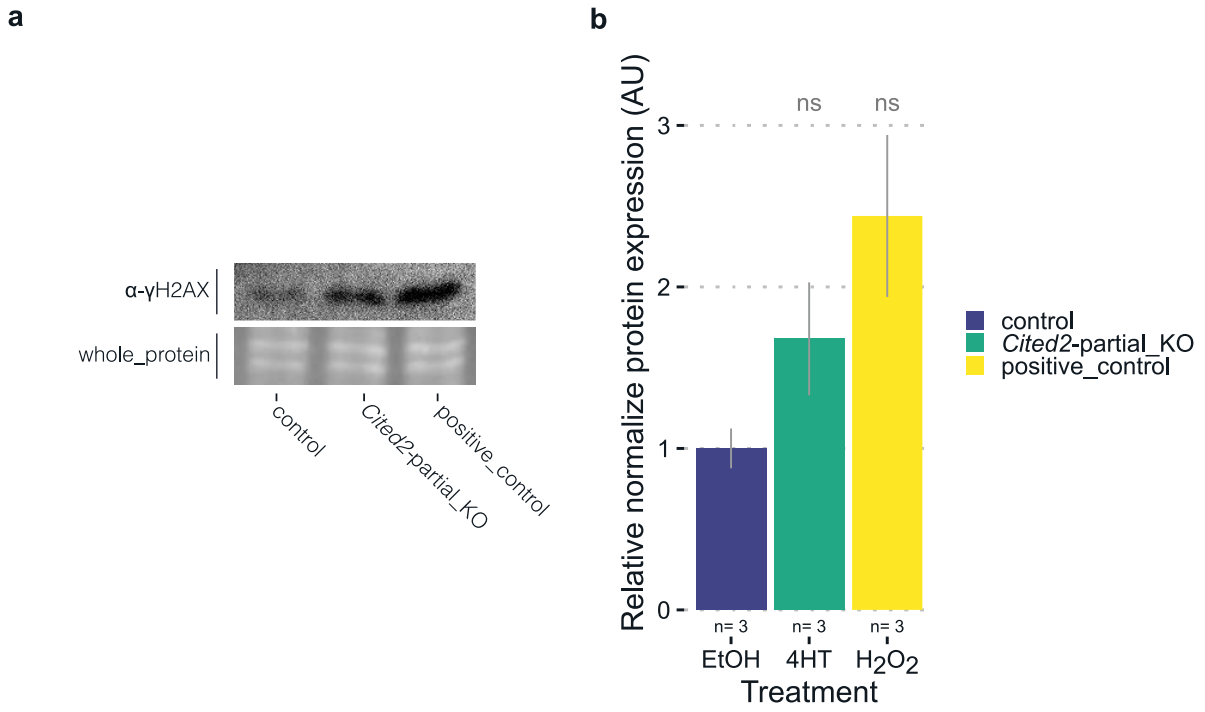

Figure 3.10 Increase in γH2AX protein levels in *Cited2*-partial_KO cells after 16 hours. Mouse embryonic stem cells ($C2^{fl/fl}$[cre]) were treated for 16 hours with EtOH (■ control), or 1 µM 4HT (■ *Cited2*), or 30 minutes before fixation 100 µM hydrogen peroxide (■ positive control). The whole protein was extracted, then immunoblotted and probed with anti-γH2AX (~15 kDa); loading control was performed with total protein in the lane (only ~50 kDa shown). The results were semi-quantified with a densiometric approach with ImageJ. Results of three experiments (n) are presented as normalized mean ± SEM expressed relative to control. Means were compared with the control condition using a t-test considering the P-value threshold of 0.05 for significance: (ns) not significant.

Next, the gene expression of known DNA damage/repair and apoptotic markers were analysed by qPCR. However, the genes chosen to be validated were those down-regulated in the microarray experiment (*Rad51c, Rad9b, Mdc1, Lin28a, Rbm24,*), and up-regulated (*Perp, Ptges, Plk2*). The expression of *p53* and *p21,* was also assessed since increased DNA damage could activate a p53-dependent cascade that can also drive cells to apoptosis and differentiation (Stambrook and Tichy, 2010). Therefore, the p53-effector p21 was evaluated since it is activated by p53 to induce cell cycle arrest, to attempt DNA repair (Blanpain et al., 2011). Lastly, the expression of *Casq2* was also validated, as it is associated with cardiomyocyte contractability function, since this protein handles calcium in the sarcoplasmic reticulum (Faggioni and Knollmann, 2012).

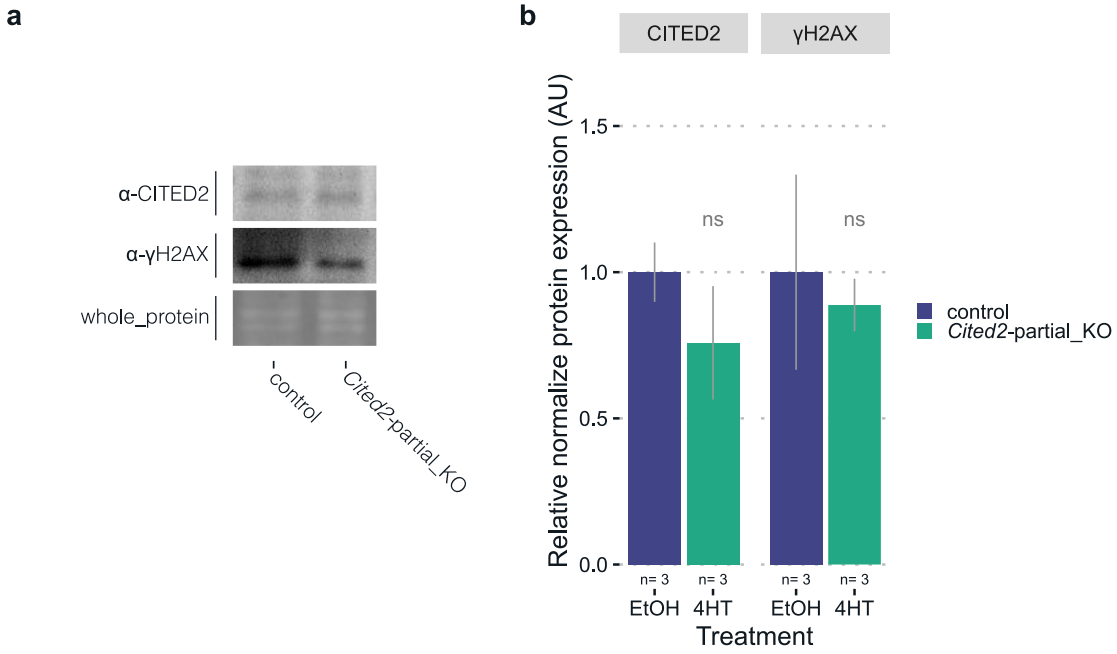

Figure 3.11 Suggested decreased γH2AX protein levels in *Cited2*-partial_KO cells after 48 hours. Mouse embryonic stem cells ($C2^{fl/fl}$[cre]) were treated for 48 hours with EtOH (■ control), 1 µM 4HT (■ *Cited2*). The whole protein was extracted, and immunoblotted and probed with anti-γH2AX (~15 kDa) and anti-CITED2 (~28 kDa); loading control was performed with total protein in the lane (only ~50 kDa shown). The results were semi-quantified with a densiometric approach with ImageJ, and the results are expressed relative to the loading control. Results of three experiments (n) are presented as normalized mean ± SEM expressed relative to control. Means were compared with the control condition using a t-test considering the P-value threshold of 0.05 for significance: (ns) not significant.

Therefore, $C2^{fl/fl}$[cre] cells were treated with EtOH (control) or 4HT (*Cited2*-partial_KO), and samples were harvested 48 hours after treatment (Figure 3.12). Compared to the control, *Cited2*-partial_KO cells showed downregulation of the expression of the DNA damage/repair marker *Rad51c* and a decreased expression of *Mdc1*, *Rad9b* (Figure 3.13). On the contrary, there was an upregulation of pro-apoptotic *p21* and *Ptges*, and *Plk2* and *Perp*, while the expression of *p53* was unchanged (Figure 3.13). Furthermore, biomarkers of cell growth and differentiation were investigated, and *Lin28a*, as well as *Rbm24*, showed decreased expression, while *Casq2* was up-regulated (Figure 3.13).

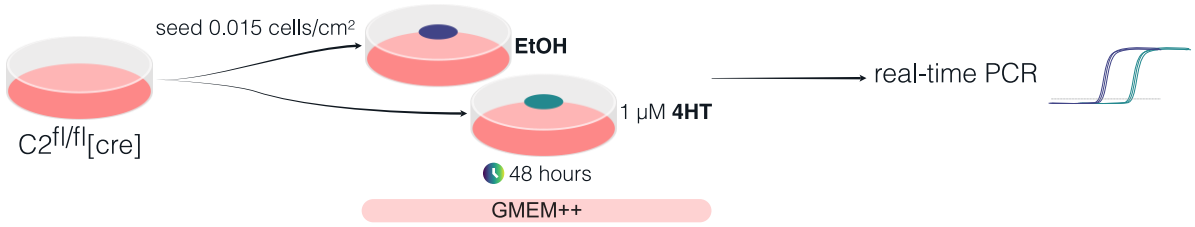

Figure 3.12 Experimental design of the validation of down-regulated and up-regulated genes in pluripotency. $C2^{fl/fl}$[cre] cells were seeded (0.015 cells/cm²) in 60 mm plates, treated with EtOH, 1 µM 4HT for 48 hours. The transcripts were analysed with real-time PCR. These experiments were repeated at least three times.

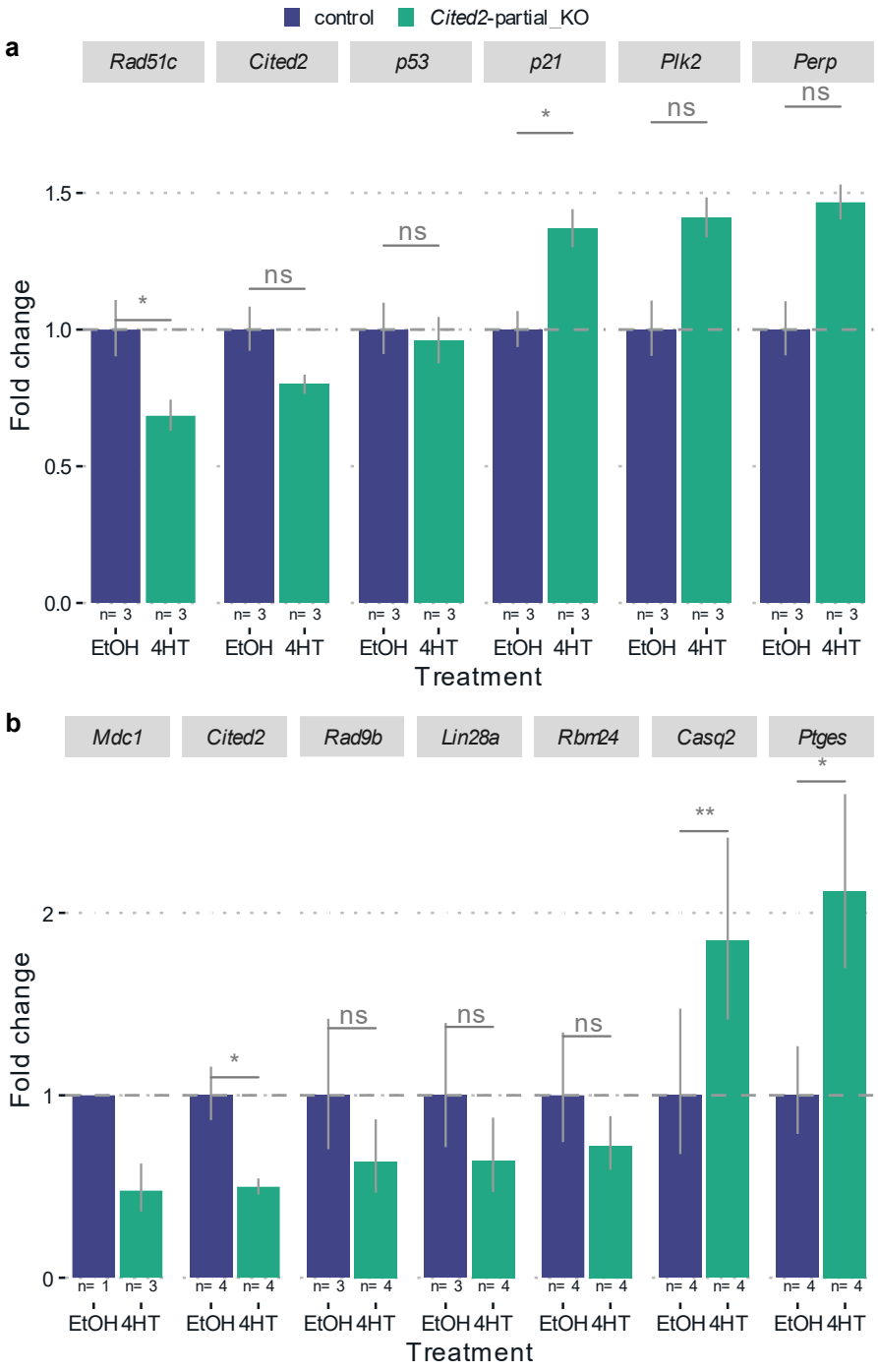

Figure 3.13 *Cited2*-partial_KO suggests an alteration of the DNA damage response, increased apoptosis, and unbalanced p53 response genes. Mouse embryonic stem cells ($C2^{fl/fl}$[cre]) were treated for 48 hours with EtOH (■ control), 1 µM 4HT (■ *Cited2*). Transcripts were analysed with ddCt method and reported as fold-change relative to control; *Gapdh* was used as a reference gene. In **(a)** results are shown for DNA damage and apoptotic genes while **(b)** it is showing the also DNA damage response genes and cardiac differentiation genes. Results are shown as mean ± SEM from three or more, experiments with "n" valid qPCR reads 'n'. The dCt means were compared to the control using the t-test considering the P-value threshold of 0.05 for significance: (ns) nonsignificant, (*) ≤ 0.05, (**) ≤ 0.01.

3.2.2 DNA damage rescue with recombinant Cited2

To understand whether *Cited2*-partial_KO increased γH2AX speckles intensity and levels of phosphorylation of H2AX, a rescue experiment with human recombinant CITED2 was performed (Figure 3.14). In this experiment, similar to what was done previously (Figure 3.6), $C2^{fl/fl}$[cre] cells were treated with EtOH or 4HT, or hydrogen peroxide, and to rescue *Cited2*-partial_KO cells the human recombinant (produced in-house and modified with eight arginines at the N-terminal (8R-CITED2) was also added to the culture medium (Nakase et al., 2004; Pacheco-Leyva et al., 2016). Additionally, 50 µM of hydrogen peroxide was added to the medium under all conditions (except for the positive control) based on the fact that it would increase the basal level of γH2AX, and thus the incubation time could be reduced from 16 hours to 6 hours.

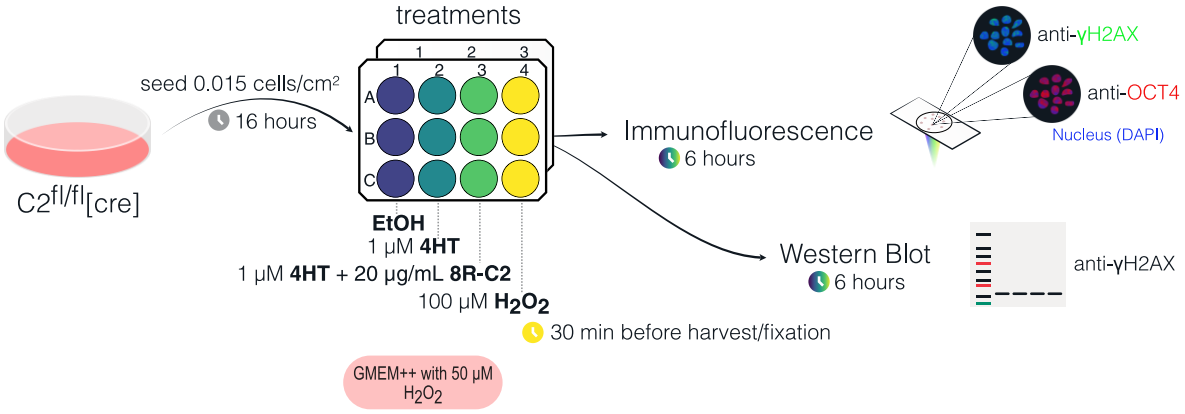

Figure 3.14 Experimental design to assess DNA damage, with the rescue of *Cited2*-partial_KO. $C2^{fl/fl}$[cre] cells were seeded (0.015 cells/cm²) in 12-well and 6-well plates and allowed to grow for 16 hours. Next, a treatment with EtOH (control), 1 µM 4HT (*Cited2*-partial_KO), or 1 µM 4HT + 20 µg/mL 8R-CITED2 (human recombinant protein) (rescue) was applied for 6 hours with cells in pluripotency medium with 50 µM of H_2O_2; 30 min before harvesting for protein isolation and fixation 100 µM of H_2O_2 (positive control) was added to the respective wells. Samples were fixed with 2% PFA, probed with anti-γH2AX, anti-OCT4, and nucleus stained with DAPI; samples were then scoped under both widefield fluorescence and confocal microscopes. The resulting images were quantified with a pipeline in Cell Profiler. γH2AX protein levels were verified. This experiment was performed once.

Similar to what was observed before in widefield microscopy (Figure 3.8) no noticeable differences were found between the four conditions, except that the positive control cells have higher confluency than the remaining conditions (Figure 3.15). However, when looking at the quantification of the speckles in confocal images (Figure 3.16) (processed as mentioned above), the number of speckles per nucleus is statistically significant lower in the rescue condition compared to the control (3.7 ± 0.2 and 4.4 ± 0.2 (SEM), respectively); while for the *Cited2*-partial_KO cells and the positive control, the averages of the speckles were respectively, 3.9 ± 0.2 and 4.6 ± 0.3 (SEM). Note that the addition of 50 µM of H_2O_2 during incubation resulted

in an increase in the number of speckles in the control condition compared to the previous experiment with treatment for 16 hours (Figure 3.9).

The mean intensity of the speckles per nucleus in the rescue condition showed the lowest intensity (0.043 ± 0.003 (SEM) AU) than the control and *Cited2*-partial_KO cells, respectively: 0.052 ± 0.003 and 0.045 ± 0.003 (SEM) AU). Conversely, the positive control showed the highest mean speckle intensity (0.055 ± 0.004 (SEM) AU). Additionally, the percentage of nuclei with speckles was similar between *Cited2*-partial_KO cells and rescue (93.4 % and 93.7 %, respectively), and both were higher than in control (89.1 %), as well as in the positive control (86.3 %). Lastly, the results of Western blot showed no differences in the phosphorylation levels of γH2AX between all conditions (Figure 3.17).

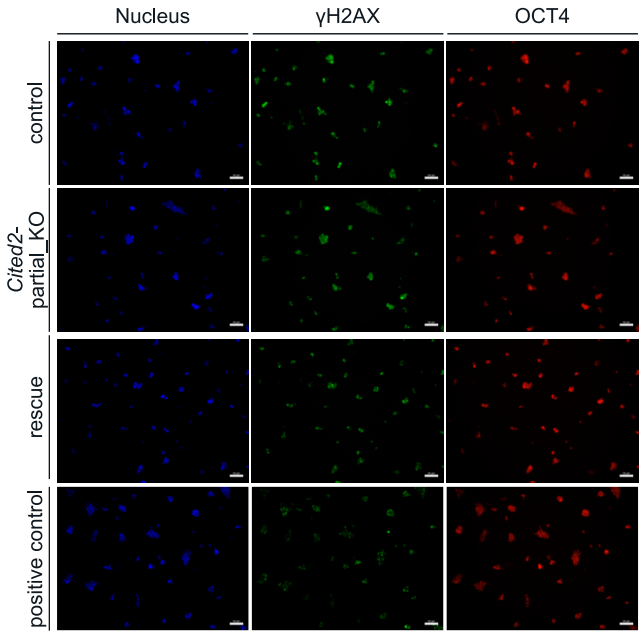

Figure 3.15 Wide-field fluorescence microscopy of γH2AX rescue experiment. $C2^{fl/fl}$[cre] cells were cultured in pluripotency conditions in 12-well plates on glass coverslips, treated with 50 µM hydrogen peroxide and EtOH (control), or 1 µM 4HT (*Cited2*-partial_KO), or 1 µM 4HT (*Cited2*-partial_KO) and 20 µg/mL human recombinant 8R-CITED2 (rescue) for 6 hours, or 30 minutes before fixation with 100 µM hydrogen peroxide (positive control). Representative images of cells probed with the primary antibody anti-γH2AX and anti-OCT4 followed by secondary incubation with Alexa Fluor A488 (green) and A594 (red), respectively. The slides were mounted with Flouromount-G containing DAPI for nuclear staining (blue). Samples were scoped with a wide-field microscope. Scale bar represents 50 µm (20x objective).

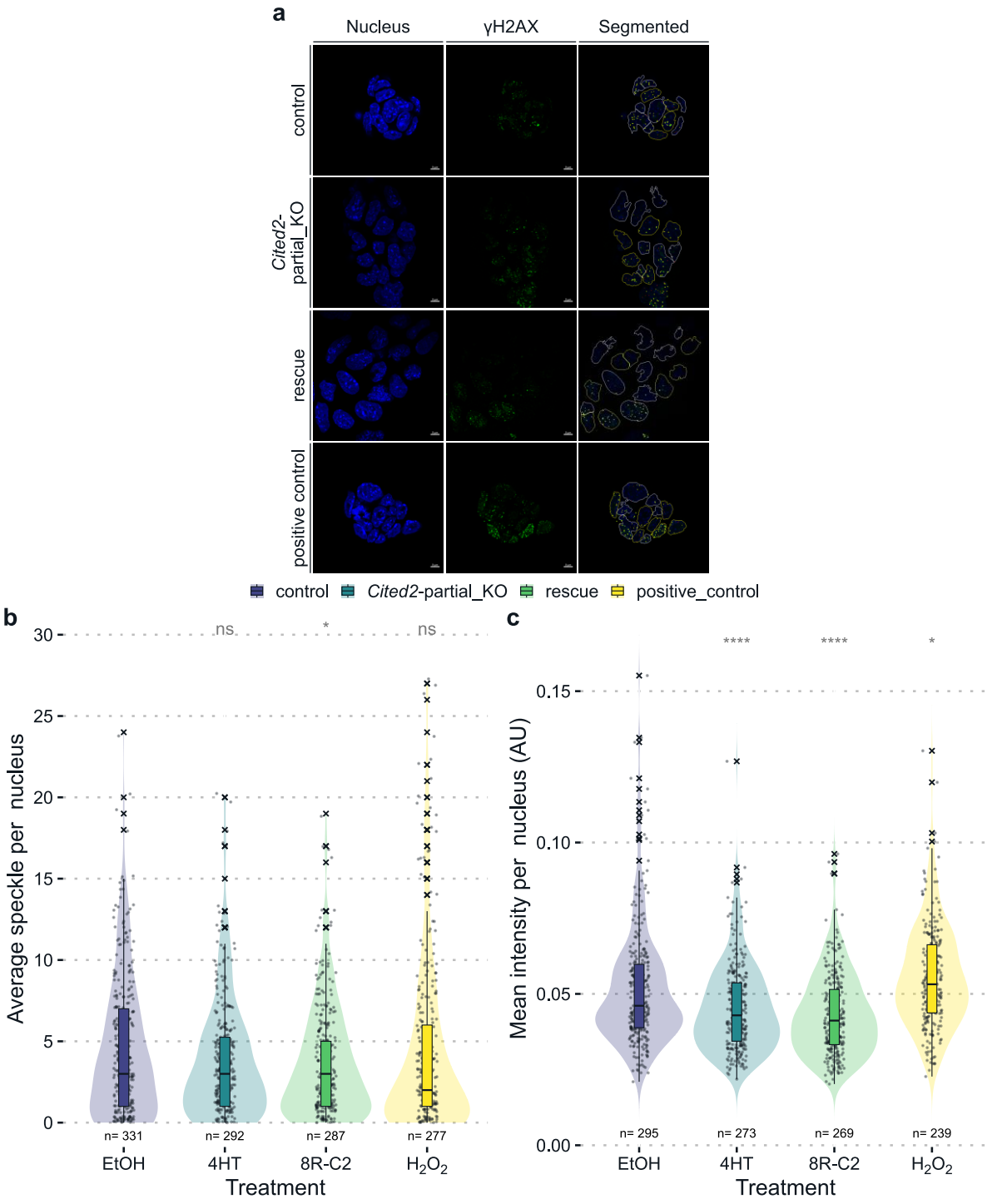

Figure 3.16 *Cited2*-partial_KO rescue with recombinant CITED2 appears to decrease the number of γH2AX speckles. $C2^{fl/fl}$[cre] cells were cultured in pluripotency conditions in 12-well plates on glass coverslips, treated with 50 µM hydrogen peroxide and EtOH (control), or 1 µM 4HT (Cited2-partial_KO), or 1 µM 4HT (Cited2-partial_KO) and 20 µg/mL human recombinant 8R-CITED2 (rescue) for 6 hours, or 30 minutes before fixation with 100 µM hydrogen peroxide (positive control). **(a)** Representative images of cells probed with the primary antibody anti-γH2AX followed by secondary incubation with Alexa Fluor A488 (green). The slides were mounted with Flouromount-G containing DAPI for nuclear staining (blue). The samples were scoped with a confocal microscope using Airyscan super solution to obtain four slices of 0.15 µm thickness which were then obtained as the maximum intensity orthogonal projection. Then, this resulting image was used as input for a segmentation pipeline in Cell Profiler to identify the nuclei and the γH2AX speckles. **(b)** represents the number of γH2AX speckles per nucleus, while **(c)** represents the mean intensity of the γH2AX speckles per nucleus. Each dot represents a nucleus (n); crosses represent points outside the interquartile range. The nuclei were filtered by size

and shape: the results shown with the white contours ( ) represent the declined results, while the yellow contours ( ) show the accepted results. The speckles were filtered by size and shape: the results shown with red contours ( ) show declined results, while yellow contours ( ) show accepted results. The scale bar represents 5 µm (63x objective). The mean was compared to the control condition using the t-test considering the P-value threshold of 0.05 for significance; (ns): not significant, (*) ≤ 0.05 and (****) ≤ 0.0001. The results are from three experiments.

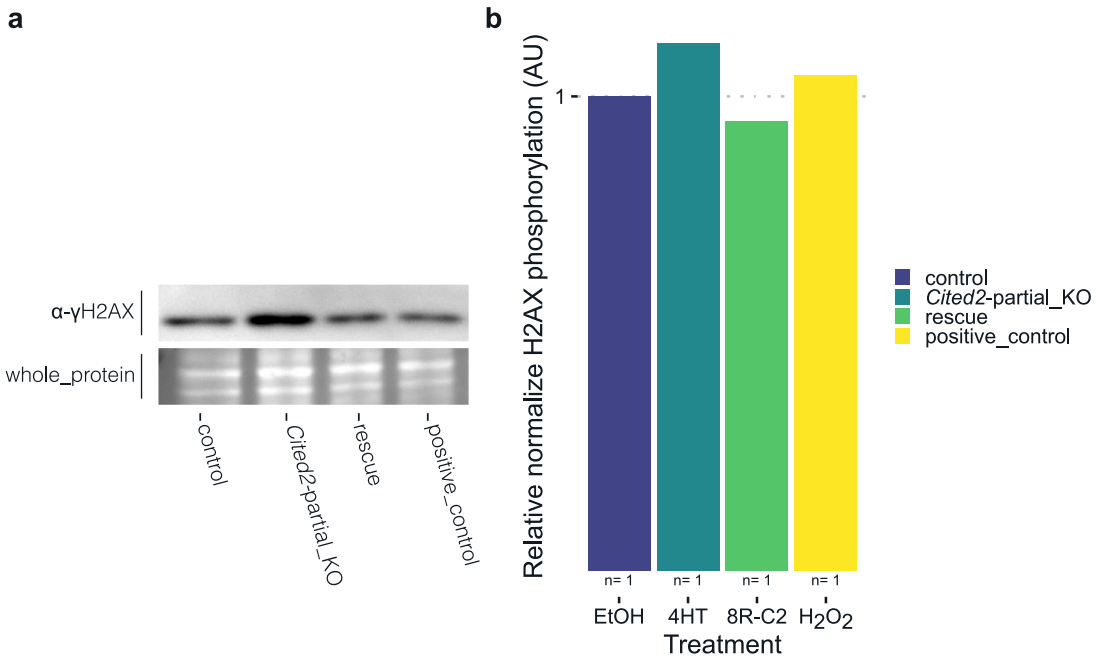

Figure 3.17 *Cited2*-partial_KO rescue shows unchanged γH2AX protein levels.C2$^{fl/fl}$[cre] cells were cultured in pluripotency conditions in 12-well plates on glass coverslips, treated with 50 µM hydrogen peroxide and EtOH (control), or 1 µM 4HT (*Cited2*-partial_KO), or 1 µM 4HT (Cited2-partial_KO) and 20 µg/mL human recombinant 8R-CITED2 (rescue) for 6 hours, or 30 minutes before fixation with 100 µM hydrogen peroxide (positive control). **(a)** The whole protein was extracted, then immunoblotted and probed with anti-γH2AX (~15 kDa); loading control was performed with total protein in the lane (only ~50 kDa shown). **(b)** Results from one experiment were semi-quantified with a densiometric approach with ImageJ, and the results are expressed relative to the loading control.

DNA damage under differentiation conditions

To better understand the role of *Cited2* in DNA repair and a possible dual role between pluripotency and differentiation, an experiment was performed in which cells were deprived of LIF in culture medium, to inhibit the maintenance of pluripotency. Given that mouse embryonic stem cells present more relaxed chromatin, which could be prone to more damage (Banáth et al., 2009), the contrary is expected in cells with more condensed chromatin (Meshorer and Misteli, 2006). Therefore, similarly to the above experiment (Figure 3.6), $C2^{fl/fl}$[cre] cells were treated with EtOH (control) and 4HT (*Cited2*-partial_KO), but in this experiment before treatments, cells were cultured for 48 hours in medium without LIF (GMEM+) (Figure 3.18).

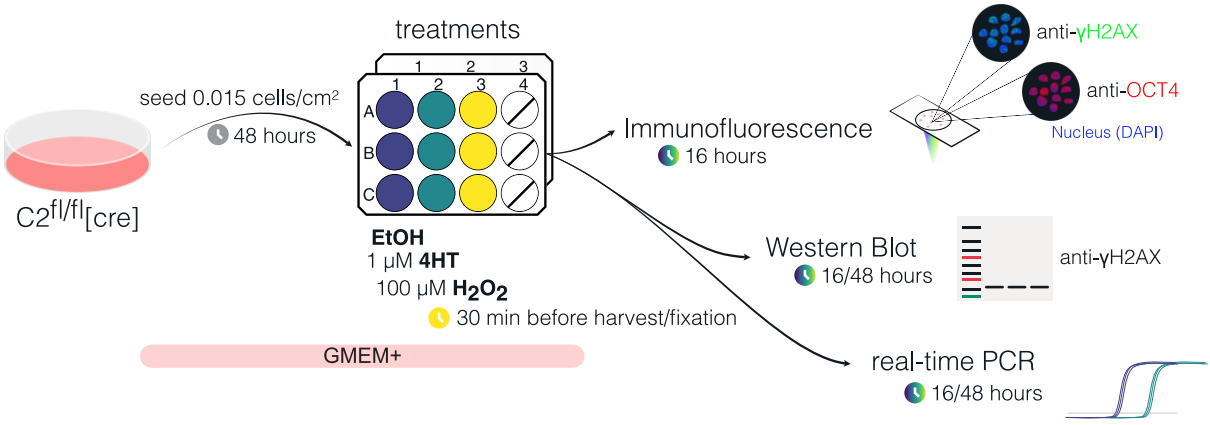

Figure 3.18 Experimental design to assess DNA damage in monolayer differentiation condition. $C2^{fl/fl}$[cre] cells were seeded (0.015 cells/cm^2) in 12-well and 6-well plates and allowed to grow for 48 hours in medium without LIF (GMEM+). Next a treatment with EtOH, 1 µM 4HT was applied for 16 or 48 hours, before harvesting for RNA and protein isolation and before fixation 100 µM of H_2O_2 (positive control) was added. Fixed samples in 2% PFA were probed with anti-γH2AX, anti-OCT4, and nucleus stained with DAPI; samples were scoped under both a widefield fluorescence and a confocal microscope. The resulting images were quantified with a pipeline in Cell Profiler. γH2AX protein was verified at both time points. These experiments were repeated three times.

After 16 hours of incubation, samples were fixed and probed with antibodies against γH2AX and OCT4. Before fixation cells were observed in phase contrast, and as expected, the morphology of the colonies changed from being round and domed-like to flatter and with irregular edges (Mulas et al., 2019) (Figure 3.19). This indicates that the cells do not maintain their undifferentiated state as when they were kept in medium with LIF (Figure 3.8). Consistent with this observation is the low signal of OCT4, which suggests that there is a downregulation of this pluripotency marker (Jang et al., 2014; Sugimoto et al., 2015; Ye et al., 2016) (Figure 3.19). No differences were observed between the control and *Cited2*-partial_KO cells.

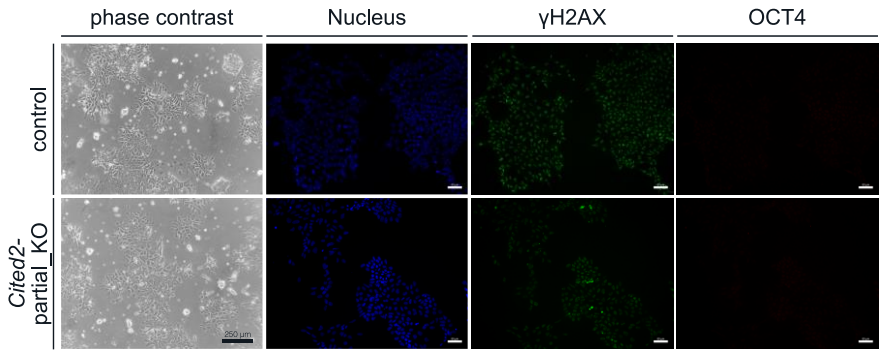

Figure 3.19 C2$^{fl/fl}$[cre] cells cultured in differentiation-inducing conditions (in medium without LIF). C2$^{fl/fl}$[cre] cells were cultured in culture medium without LIF for 48 hours in 12-well plates on glass coverslips, and then treated with EtOH (control) or 1 µM 4HT (*Cited2*-partial_KO) for 16 hours, or 30 minutes before fixation with 100 µM hydrogen peroxide (positive control). Representative images with phase contrast of cells before fixation with 2% PFA were then probed with the primary antibody anti-γH2AX and anti-OCT4 followed by secondary incubation with Alexa Fluor A488 (green) and A594 (red), respectively. The slides were mounted with Flouromount-G containing DAPI for nuclear staining (blue). Samples were scoped with a wide-field microscope. The scale bar represents 250 µm and 50 µm for phase contrast (10x objective) and wide-field fluorescence (20x objective), respectively.

Next, as before, the number of γH2AX speckles per nucleus and their intensity were quantified using confocal microscopy in a Cell Profiler pipeline (Figure 3.20). The results showed a decrease in the number of speckles per nucleus in the *Cited2*-partial_KO cells (3.8 ± 0.2 (SEM)) compared to the control (5.2 ± 0.3 (SEM)), and a decrease in the mean intensity of the speckles, 0.029 ± 0.002 vs 0.037 ± 0.002 (SEM) AU. No differences were observed in the positive control, where the average speckles per nucleus was 4.0 ± 0.5 (SEM) and the mean intensity was 0.035 ± 0.005 (SEM) AU. However, note that *Cited2*-partial_KO cells show a skew in the distribution of speckles towards zero. This is evident by the percentage of cells with speckles also being lower compared to the control: 78.2 % versus 94.7 %, respectively; 92.2 % observed for positive control.

As shown in the western blot results, *Cited2*-partial_KO cells decreased the phosphorylation levels of H2AX over time (Figure 3.21). As it can be seen in this figure *Cited2*-partial_KO cells showed a tendency to increase γH2AX levels after 16 hours, which decrease after 48 hours of treatment, when compared to the control. Furthermore, the levels of γH2AX over time in control cells show a tendency to increase, while the *Cited2*-partial_KO cells show the inverse. These results follow the same tendency of the cells maintained under pluripotency conditions (Figure 3.10 and Figure 3.11). However, in this culture conditions without LIF, the higher levels of expression do not seem to correlate with higher intensity. Lastly, the expression of *Cited2* was determined using qPCR, yet no differences in expression at both time points were detected (Figure 3.22).

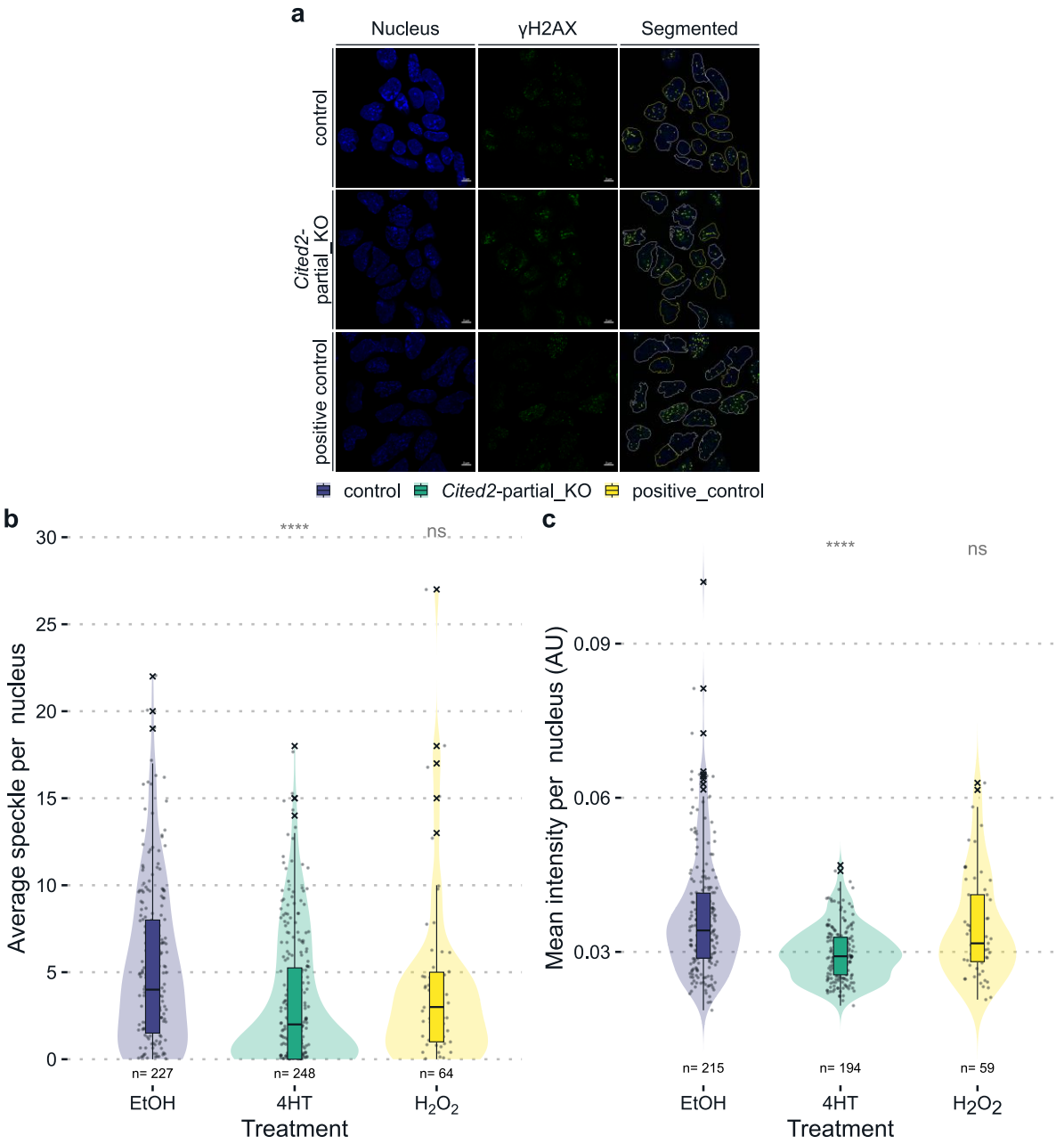

Figure 3.20 *Cited2*-partial_KO decreases γH2AX foci number and their intensity. $C2^{fl/fl}$[cre] cells were cultured in culture medium without LIF for 48 hours in 12-well plates on glass coverslips, and then treated with EtOH (control) or 1 µM 4HT (*Cited2*-partial_KO) for 16 hours, or 30 minutes before fixation with 100 µM hydrogen peroxide (positive control). Representative images of cells probed with the primary antibody anti-γH2AX followed by secondary incubation with Alexa Fluor A488 (green). The slides were mounted with Flouromount-G containing DAPI for nuclear staining (blue). **(a)** The samples were scoped with a confocal microscope using Airyscan super solution to obtain four slices of 0.15 µm thickness which were then obtained with the orthogonal projection was obtained. Then, this resulting image was used as input for a segmentation pipeline in Cell Profiler to identify the nuclei and the γH2AX speckles. **(b)** represents the number of γH2AX speckles per nucleus, while **(c)** represents the mean intensity of the γH2AX speckles per nucleus. Each dot represents a nucleus (n); crosses represent points outside the interquartile range. The nuclei were filtered by size and shape: the results shown with the white contours (◎) represent the declined results, while the yellow contours (◎) show the accepted results. The speckles were filtered by size and shape: the results shown with red contours (◎) show declined results, while yellow contours (◎) show accepted results. The scale bar represents 5 µm (63x objective). Means were compared with the control condition using a t-test considering the P-value threshold of 0.05 for significance; (ns): not significant and (****) ≤ 0.0001. The results are from three experiments.

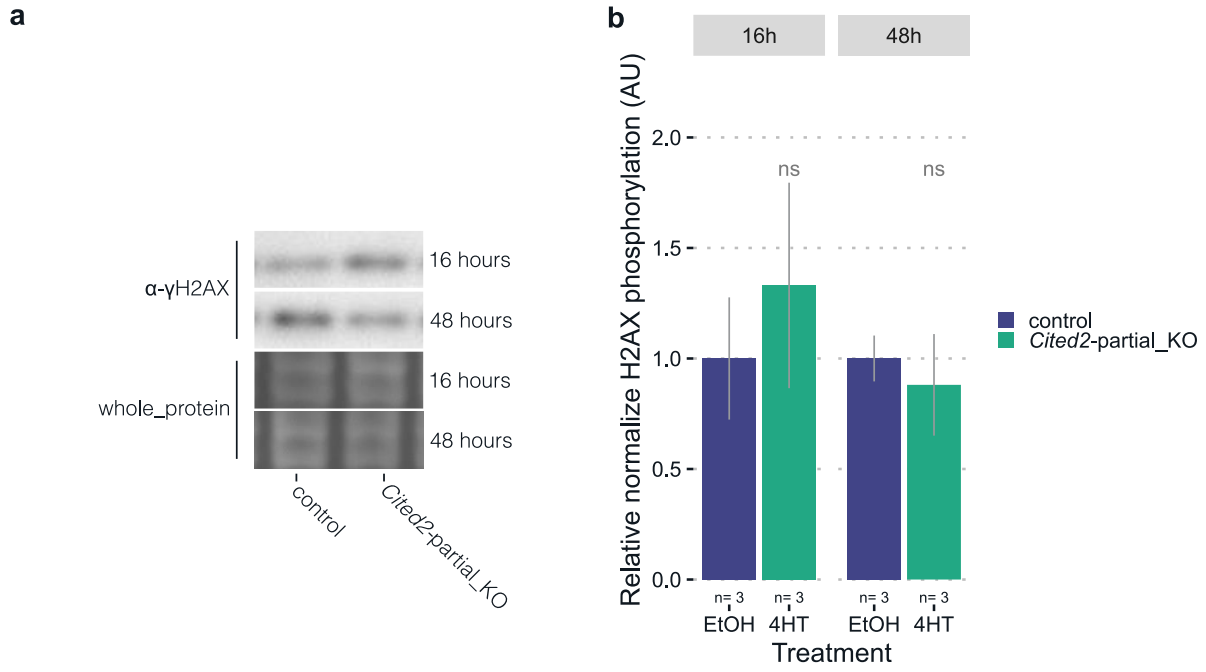

Figure 3.21 Suggestion that γH2AX levels decrease over time under *Cited2*-partial_KO in differentiating conditions. Mouse embryonic stem cells ($C2^{fl/fl}$[cre]) cultured 48 hours in medium without LIF were treated for 16 and 48 hours with EtOH (control) or 1 µM 4HT (*Cited2*-partial_KO). **(a)** The whole protein was extracted, then immunoblotted and probed with anti-γH2AX (~15 kDa) loading control was performed with total protein in the lane (only ~50 kDa shown). **(b)** Results of three experiments (n) are presented as normalized mean ± SEM expressed relative to control. The means were compared to the control condition of each time point using a t test considering the P-value threshold of 0.05 for significance: (ns) nonsignificant.

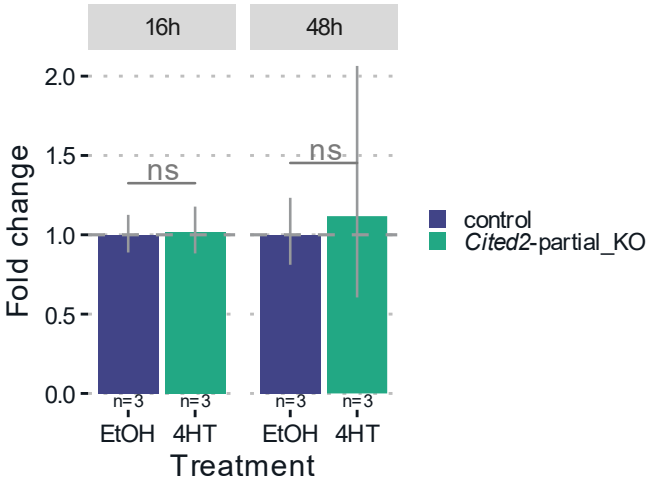

Figure 3.22 *Cited2* expression is unchanged under undifferentiating conditions at two time points. $C2^{fl/fl}$[cre] cells were cultured in culture medium without LIF for 48 hours in 12-well plates on glass coverslips and then treated with EtOH (control) or 1 µM 4HT (*Cited2*-partial_KO) for 16 hours and 48 hours. Transcripts were analysed with the ddCt method and reported as fold-change relative to control; *Gapdh* was used as a reference gene. Results are shown as mean ± SEM from three, or more, experiments with "n" valid qPCR reads; the dCt means were compared to the control using the t-test considering the P-value threshold of 0.05 for significance: no statistically significant results (ns).

3.2.4 Cited2-KO cells present downregulation of pro-apoptotic genes

As shown in previous results, the conditional partial knockout of *Cited2* in mESC leads cells to cell death and spontaneous differentiation. This suggested that when cells are *Cited2*-depleted, they activate pro-apoptotic responses, as suggested by the increased expression of p53-effectors such as *Perp*, and *p21*, and decrease expression of DNA repair genes (e.g., *Rad51c*). To investigate this possible correlation, similar to what was previously done, the expression of these markers was determined using a *Cited2* knockout cell line (*Cited2*-KO). Unlike the conditional knockout cell line used in the previous experiments, Cited2$^{-/-}$ cells maintain self-renewal, suggesting adaptation to the *Cited2* knockout (Kranc et al., 2015). Therefore, wild-type and *Cited2*-KO cells were cultured in pluripotency conditions for 48 hours (in GMEM++) and then harvested for transcript analysis by qPCR (Figure 3.23).

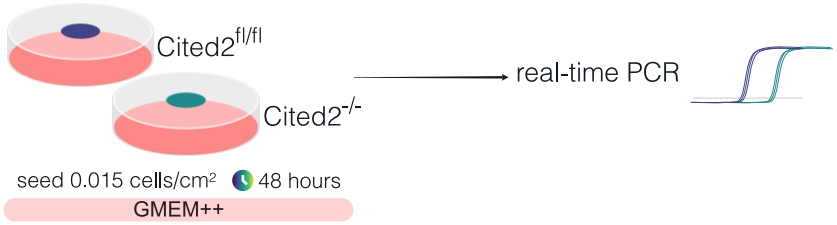

Figure 3.23 Experimental design to evaluate DNA damage and p53-response gene in *Cited2*-knockout cells. Cited2$^{fl/fl}$ (wildtype) and Cited$^{-/-}$ (*Cited2*-knockout) cells were seeded (0.015 cells/cm^2) in 60 mm plates, and allowed to grow for 48 hours. The transcripts were analysed with real-time PCR. These experiments were repeated three times.

The relative expression results showed a downregulation of *Plk2* and *p21*, while showing a decreased expression of *Perp* and *Mdc1* (Figure 3.24). Conversely, *Rad51c* and *p53* were not increased. These results suggest that acute loss of *Cited2* (as shown above) leads to cell death, while cells that adapted to the Cited2-KO are not expressing pro-apoptotic genes. This result was expected since these cells can maintain self-renewal.

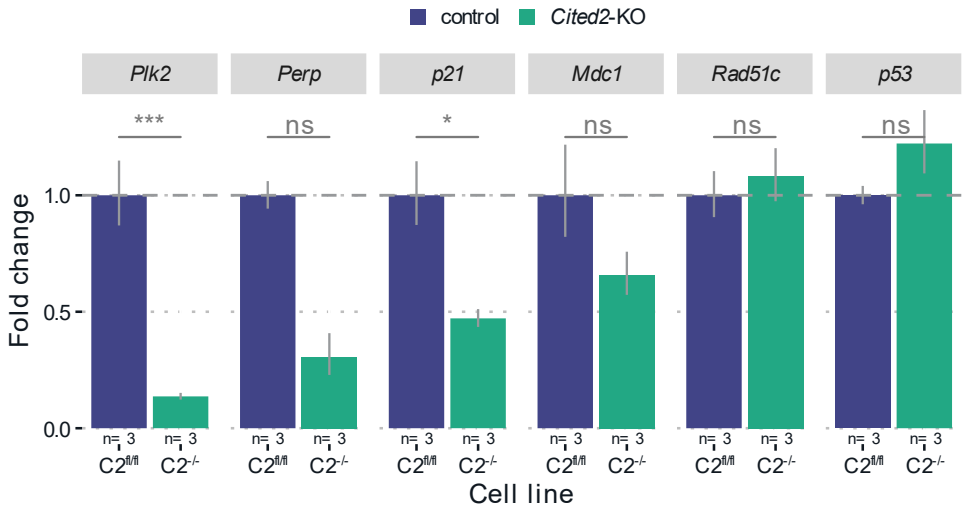

Figure 3.24 Downregulation of DNA damage response, and apoptotic genes in *Cited2*-KO cells. Cited2$^{fl/fl}$ (C2$^{fl/fl}$) and Cited2$^{-/-}$ (C2$^{-/-}$) cells were cultured under pluripotency conditions and 48 hours after plating they were harvested. Transcripts were analysed with the ddCt method and reported as fold-change relative to control; *Gapdh* was used as a reference gene. Results are shown as mean ± SEM from three, or more, experiments with "n" representing valid qPCR reads; the dCt means were compared to the control using the t-test considering the P-value threshold of 0.05 for significance: (ns): nonsignificant, (*) ≤ 0.05 and (***) ≤ 0. 001

3.3 Epigenetic regulation of differentiation (H3K27me3/ac)

Cited2 has been described as an important co-transcription factor for proper cardiac differentiation. Indeed, Cited2-knockout mice die in utero due to cardiac malformations (Bamforth et al., 2004; Wolfgang et al., 2005). Furthermore, at the molecular level, CITED2 is described as a negative modulator of HIF1α (Yin et al., 2002), and a partner/co-activator of *Isl1* (a secondary heart field marker) required for proper heart development and cardiac cells differentiation (Pacheco-Leyva et al., 2016). Previous work in our lab suggested that the role of *Cited2* is most important in the early stages of development, as its depletion in later differentiation days does not show impairment in cardiac differentiation, unlike at the onset of differentiation (Pacheco-Leyva et al., 2016). Therefore, the microarray experiment (Figure 3.1), opened the possibility to have a broad picture of how *Cited2* contributes to development, in addition to the comprehension of the role played by *Cited2* in pluripotency and self-renewal of ESC. Thus, as stated before for undifferentiated conditions: from the list of DEGs, the down-regulated and up-regulated genes were obtained considering the thresholds of $|log(fold\ change)| > 1.2$ and P-value < 0.05.

The depletion of *Cited2* at the beginning of differentiation results in the downregulation of more genes (a total of 322 genes) than those that were upregulated (236 genes) (Figure 3.25a). When considering the top ten down-regulated genes (Figure 3.25b), two genes are well distant from others: *Aplnr* and *Kdr*, which are both genes involved in cell signalling and heart development (Ema et al., 2006; Jackson et al., 2021). Furthermore, other genes important for mesoderm and cardiac differentiation, such as *Bmper*, *Rspo3*, and *Rasgrp3*, were also down-regulated (Chiapparo et al., 2016; Jackson et al., 2021; Osmanagic-Myers and Rezniczek, 2018; Zhou et al., 2020). When considering the top ten genes up-regulated, three genes involved in pluripotency appeared at the top positions, *Sox2*, *Dppa2*, and *Nr0b1* (or *Dax1*).

Next, similar to what was described above for undifferentiated cells, gene set enrichment analysis was performed using EnrichR (Chen et al., 2013; Kuleshov et al., 2016). The results from ChEA/ENCODE consensus database considering the list of down-regulated genes showed not only terms of epigenetic regulators such as SUZ12 and EZH2, but also terms of pluripotency factors such as NANOG, SOX2, POUF5F1 and TCF3; and cell cycle regulator TP53 (Figure 3.26a). From the upregulated list of genes, terms of pluripotency factors were also found: NANOG, SOX2, POU5F1 (OCT4), KLF4, SALL4 and TCF3 (Figure 3.26b). Furthermore, looking at the biological processes of gene ontology from the downregulated gene list, the term “heart development” was the top one, followed by “kidney development” and regulation of

"Wnt signalling pathway" (Figure 3.27a). However, from the up-regulated list of genes, there were no statistically significant terms when the adjusted P-value was considered. Nevertheless, the results suggest that the upregulation genes indicate biological processes such as "gonad development" and "regulation of transcription from RNA polymerase II promoter" (Figure 3.27b).

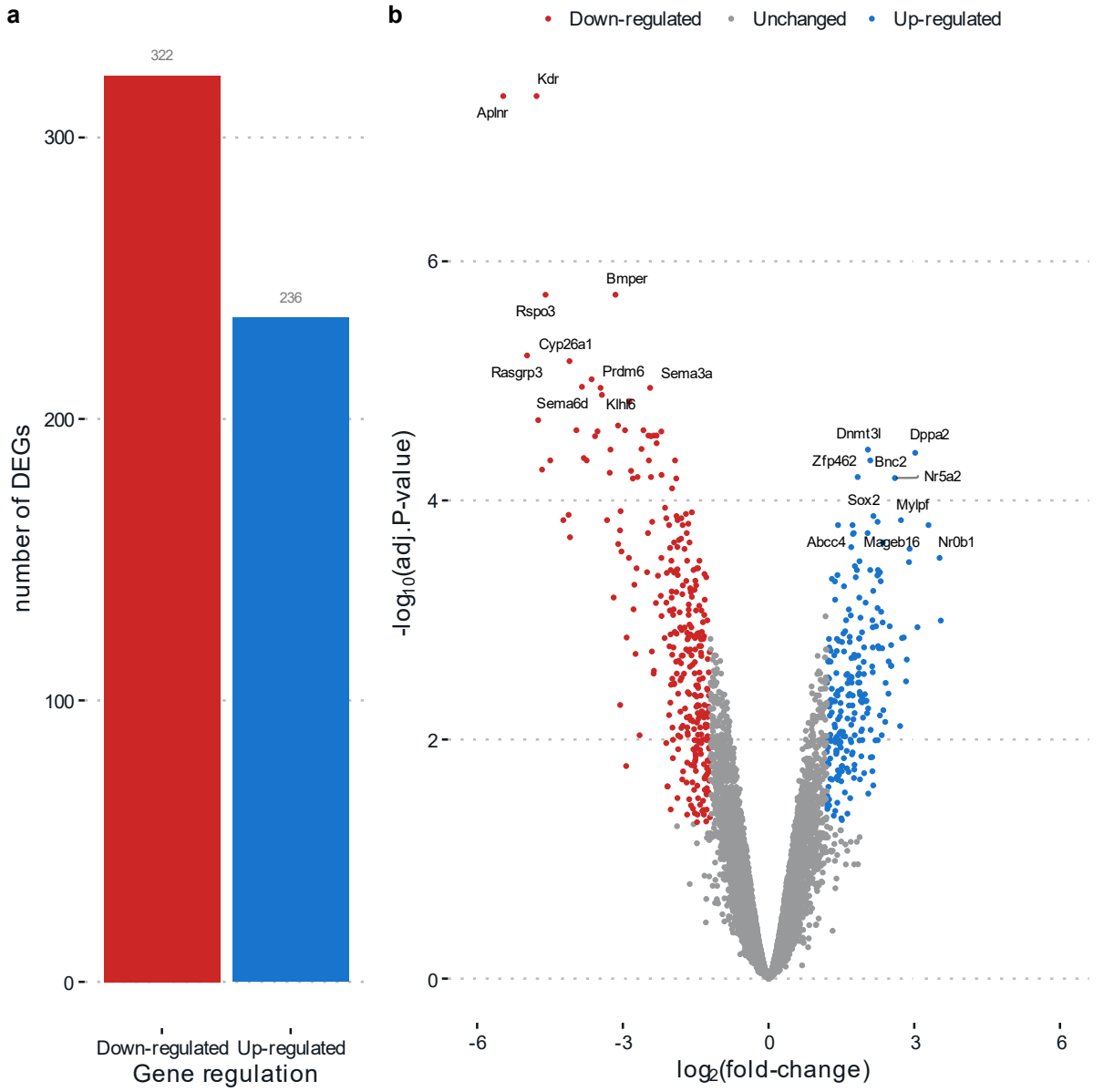

Figure 3.25 Different regulation of genes between cells that express and do not express *Cited2* in differentiation conditions on day 4. $C2^{fl/fl}$[cre] cells were cultured following the hanging drop method and treated with EtOH (control) or 4HT (*Cited2-partial_KO*) at the onset of differentiation, then harvested on day-4 and through microarray (Affymetrix) analysis the differentially expressed genes (DEGs) between the two conditions was obtained. **(a)** represents the total number of genes down-regulated and up-regulated between the two groups, represented as red (■) and blue (■), respectively. While in **(b)** represents the total number of genes (20291) where in grey (●) are the genes with unchanged expression, while in red (●) and blue (●) are, respectively represented, the down-regulated and up-regulated that crossed the threshold of log_2(fold-change) of 1.2 and the adjusted P-value of 0.05. The top ten most downregulated are labelled. The top down-regulated genes arranged by adjusted P-value are: *Aplnr, Kdr, Rspo3, Bmper, Rasgrp3, Cyp26a1, Prdm6, Sema6d, Klh16, Sema3a*; and top up-regulated are: *Dnmt3l, Dpp2a, Bnc2, Zfp462, Nr5a2, Sox2, Mylpf, Mageb16, Nr0b1, Abcc4*.

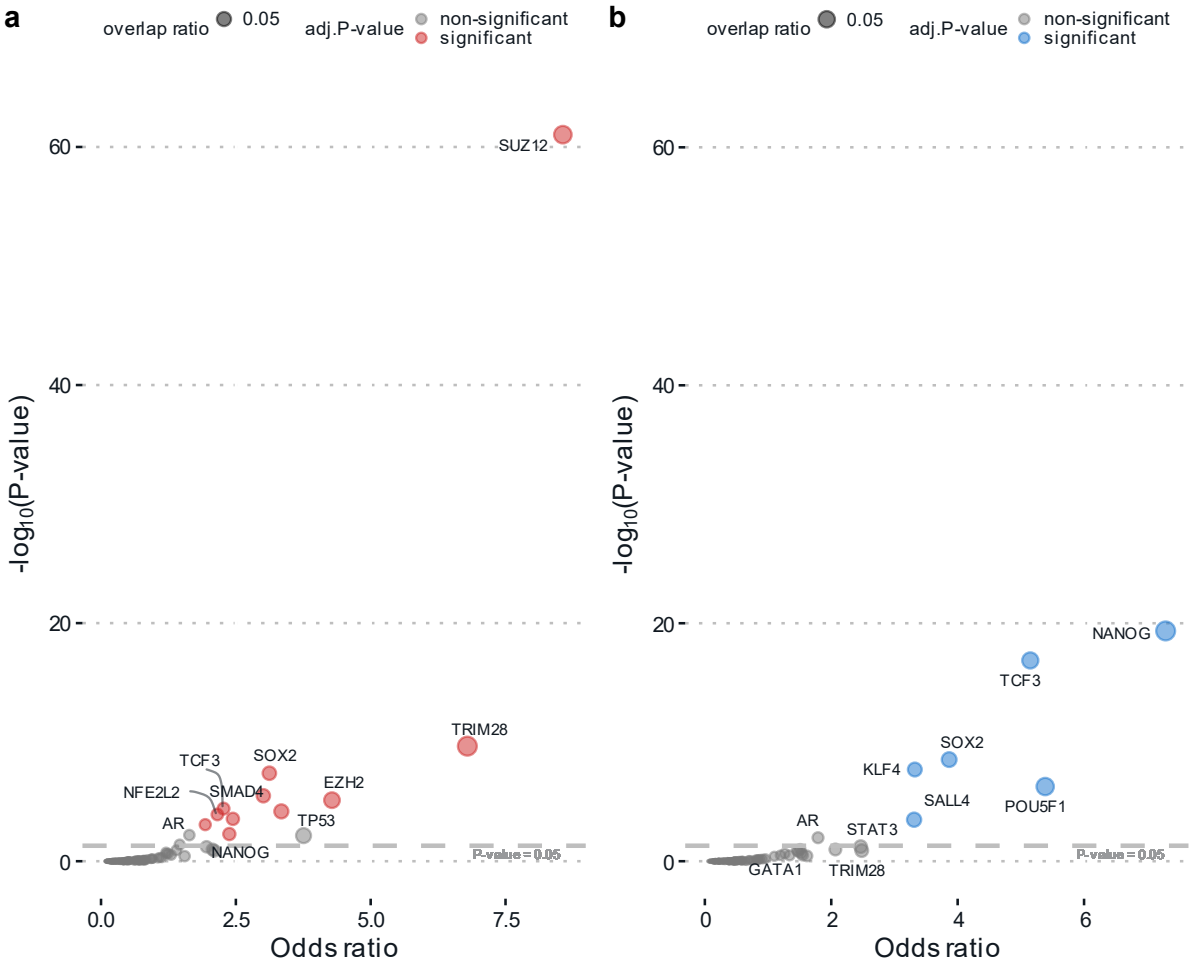

Figure 3.26 The depletion of *Cited2* reduces affects pluripotency transcription factors of ChEA/ENCODE database. The two lists of differentially expressed genes (322 downregulated and 236 up-regulated) in differentiation conditions were used to perform a gene set enrichment analysis for the CHEA/ENCODE transcription factor consensus; using tool EnrichR. The size of each point represents the overlap ratio, *i.e.* the number of genes in the list that are contributing to a term over the number of genes annotated for transcription factor term. In **(a)** the results of CHEA/ENCODE consensus terms are represented from the down-regulated list, and in **(b)** from the up-regulated list. The grey points (●) represent nonsignificant while the accent colour according to their regulation (down-regulated as red (●), and up-regulated as blue (●)) represents a smaller adjusted P-value than the threshold of 0.05. The dashed line (– –) represents the P-value threshold of 0.05. The top ten CHEA terms are labelled: top down-regulated are: SUZ12, TRIM28, SOX2, SMAD4, EZH2, TCF3, TP53, NFE2L2, NANOG, AR; and the top up-regulated are: NANOG, TCF3, SOX2, KLF4, POU5F1, SALL4, AR, STAT3, ATA1, TRIM28.

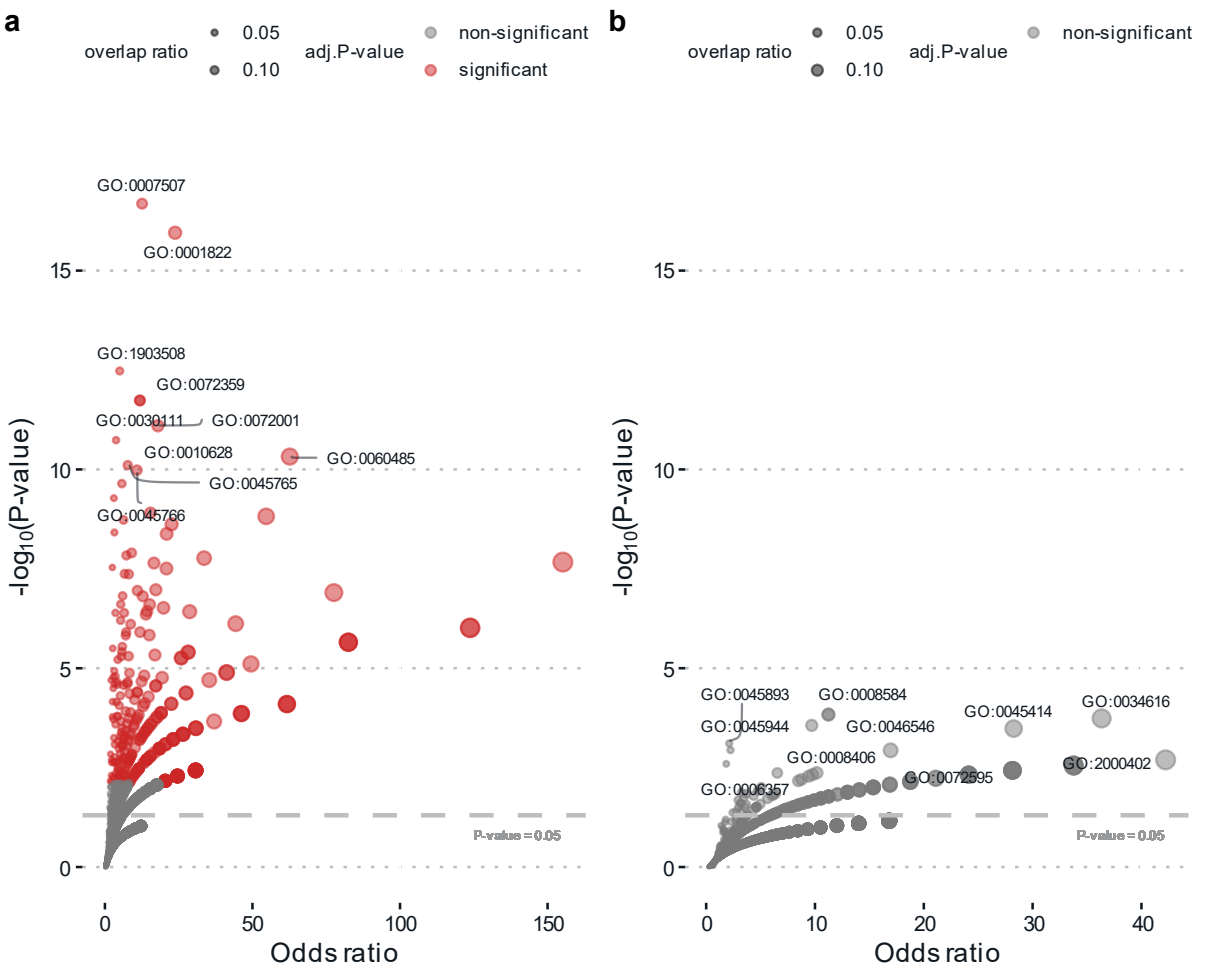

Figure 3.27 *Cited2* depletion affects heart development. The two lists of differentially expressed genes (322 down-regulated and 236 up-regulated) under differentiation conditions were used to perform a gene set enrichment analysis for Gene Ontology (GO): biological processes; using the EnrichR tool. The size of each point represents the overlap ratio, *i.e.* the number of genes in the list that are contributing to a term over the number of genes annotated for that gene ontology term. In **(a)** the results of GO terms from the down-regulated list, and in **(b)** they are represented from the up-regulated list. The grey points (●) represent nonsignificant while the accent colour according to their regulation (down-regulated as red (●), and up-regulated as blue (●)) represents a smaller adjusted P-value than the threshold of 0.05. The dashed line (– –) represents the P-value threshold of 0.05. The top ten terms are labelled. The top downregulated are: heart development (GO:0007507), kidney development (GO:0001822), positive regulation of nucleic acid-templated transcription (GO:1903508), circulatory system development (GO:0072359), regulation of Wnt signalling pathway (GO:0030111), renal system development (GO:0072001), positive regulation of gene expression (GO:0010628), mesenchyme development (GO:0060485), regulation of angiogenesis (GO:0045765), positive regulation of angiogenesis (GO:0045766); and top up-regulated are: male gonad of development (GO:0008584), development primary male sexual characteristics (GO:0046546), response to laminar fluid shear stress (GO:0034616), gonad development (GO:0008406), regulation of interleukin-8 biosynthetic process (GO:0045414), positive regulation of transcription DNA-templated (GO:0045893), positive regulation of transcription from RNA polymerase II promoter (GO:0045944), maintenance of protein localization in organelle (GO:0072595), negative regulation of lymphocyte migration (GO:2000402), regulation of transcription from RNA polymerase II promoter (GO:0006357).

The transcripts of the top down-regulated genes from embryoid bodies identified by microarrays were validated by qPCR. This validation of down-regulated genes in embryoid bodies showed that most of them were down-regulated (*Prdm6*, *Rasgrp3*, *Fgf10*, *Rspo3*, *Bmp5*, *Pcsk5*, *Cxcr4*, *Bmper*, *Asb4*, *Tbx20*, *Mex3b*) (Figure 3.28). However, some showed decreased

expression without statistical significance (*Wnt5a*, *Rbm24*, *Foxf1*, *Cxcr7*) (Figure 3.28). Overall, these down-regulated genes indicated players of pathways important for proper cardiac differentiation, such as: Wnt/β-catenin signalling (*Wnt5a*, *Rspo3*) (Ohkawara et al., 2011), chemokine signalling (*Cxcr4*, *Cxcr7*) (Chen et al., 2015), FGF signalling (*Fgf10*, *Foxf1*) (Katoh et al., 2018), and TGF-β/BMP signalling (*Bmp5*, and *Bmper*) (Fritsch et al., 2010; Osmanagic-Myers and Rezniczek, 2018). Furthermore, the remaining validated down-regulated genes seem to contribute indirectly to the pathways reference above. For example, *Pcsk5*, which is a proprotein convertase required for the activation of GDF15 (distant member of TGF-β pathway), is associated with patients with heart disease (Li et al., 2018) and heart failure (Rochette et al., 2021); *Tbx20*, acts as a modulator of BMP signalling in the myocardium (de Pater et al., 2012), and is important for the proliferation and regional specification during cardiogenesis (Cai et al., 2005); *Rasgrp3*, an identified *Mesp1* target gene during early events of cardiac progenitors' specifications (Chiapparo et al., 2016). Furthermore, regulation of gene expression through epigenetics can be altered in *Cited2*-depleted cells since: *Prdm6*, which was shown to be specific for vascular smooth muscle cells (Davis et al., 2006; Li et al., 2016) and an epigenetic modifier that controls heart development (Hong et al., 2022); *Mex3b* was found to be involved in downregulation of SUZ12 and its ubiquitination (Zhang et al., 2016a). The impairment of other embryonic tissues that contribute to cardiac differentiation during development appears to be modulated by *Cited2*, namely *Asb4*, which is described to participate in trophoblast differentiation (Townley-Tilson et al., 2014) and in endothelial differentiation in the placenta by regulation of HIF1α (Ferguson et al., 2007). Lastly, as verified under undifferentiated conditions (shown above), the downregulation of *Rbm24* is maintained, suggesting an impairment of mesoderm specification through p53 (Zhang et al., 2018) and cell contractibility (Poon et al., 2012).

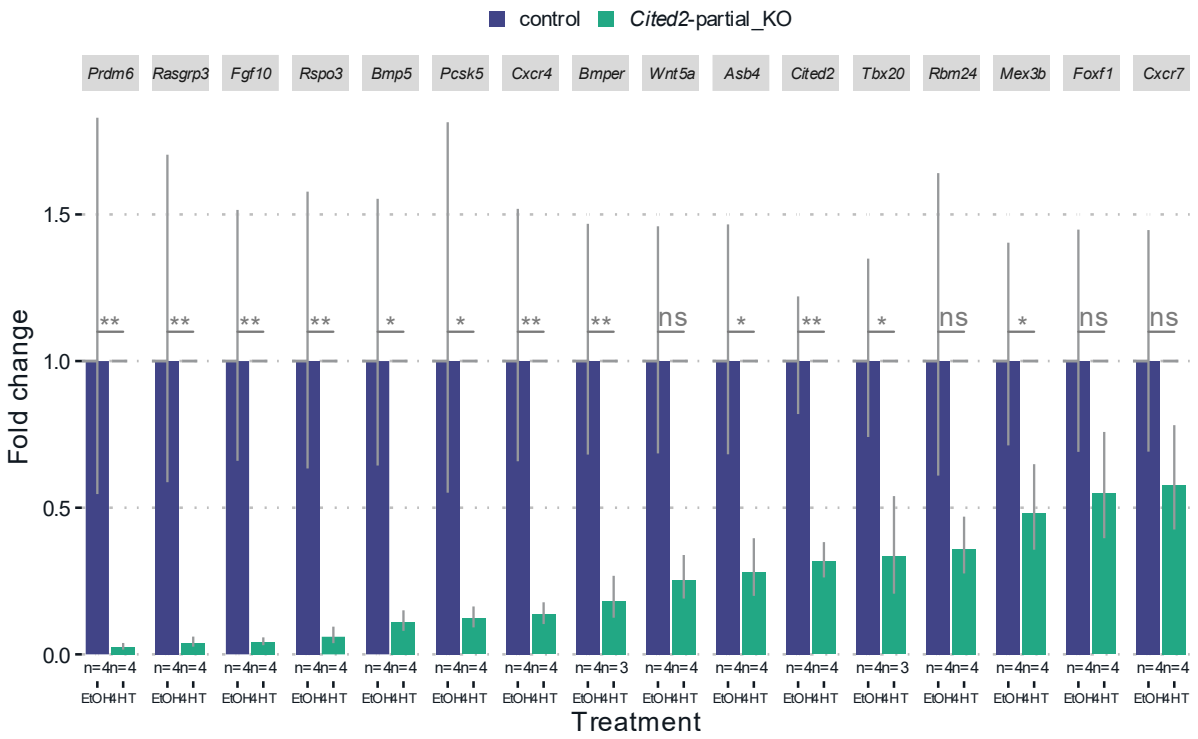

Figure 3.28 Validation of down-regulated genes in differentiation conditions obtained from microarrays. Mouse embryonic stem cells ($C2^{fl/fl}$[cre]) were treated for 48 hours with EtOH (■ control), 1 µM 4HT (■ *Cited2*-partial_KO). Transcripts were analysed with the ddCt method and reported as a fold-change relative to the control; *Gapdh* was used as reference gene. Results are shown as mean ± SEM from three experiments with "n" valid qPCR reads. The dCt means were compared to the control using the t-test considering the P-value threshold of 0.05 for significance: (ns) nonsignificant, (*) ≤ 0.05, (**) ≤ 0.01.

CITED2 was found to bind to the transcriptional coactivator p300 (Glenn and Maurer, 1999) that can acetylate lysine 27 of H3 (Martire et al., 2020). Therefore, the cooperation between p300 and CITED2 could be necessary for the acetylation of lysine 27 of H3 to allow the expression of cardiac mesoderm genes; similarly as shown by the interaction between p300 and BRACHYURY (Beisaw et al., 2018). The results of the microarray gene set enrichment analysis show the terms SUZ12 and EHZ2, which are proteins that belong to the PRC2 complex (Kuzmichev et al., 2005; Montgomery et al., 2005), further suggesting a possible role of Cited2 in epigenetics. In particular, *Cited2* could play a role in the regulation of the balance between the modifications of H3K27me3 and H3K27ac, which are histone modifications that are, respectively, associated with repression and activation of gene transcription (Piunti and Shilatifard, 2016). This hypothesised Cited2's role could, therefore, explain the delayed expression of mesoderm markers in *Cited2*-partial_KO cells previously observed (Santos et al., 2019). To investigate this possibility, a chromatin immunoprecipitation experiment was carried out with undifferentiated cells (kept under pluripotency conditions) and differentiated cells (as embryoid bodies at day-4 of differentiation) (Figure 3.29).

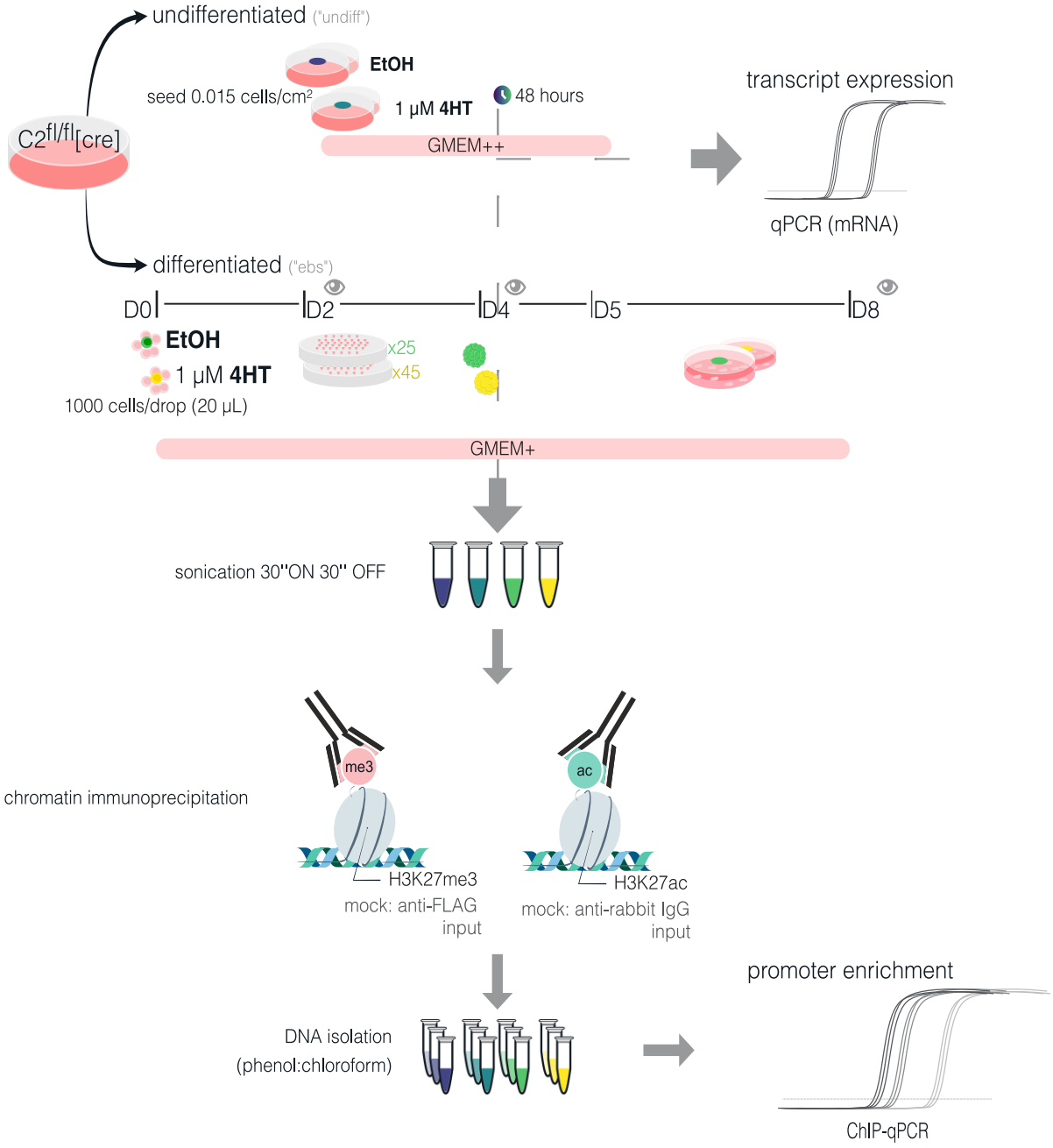

Figure 3.29 Experimental design to assess promoter enrichment of H3K27me3/ac. From C2$^{fl/fl}$[cre] two groups of cells were treated with EtOH (control) and 1 µm 4HT (*Cited2*-partial_KO): one group was cultured under pluripotency conditions (culture medium GMEM containing LIF), and the other group was culture in differentiation conditions following the hanging drop protocol; each drop of 20 µL contained 1000 cells in differentiation medium (GMEM+). Embryoid bodies were observed at three time points: day-2 (D2), day-4 (D4) and day-8 (D8), to measure their area and shape at the first two time points, and to evaluate the spontaneous differentiation in contractile cardiomyocyte at the last time point. For pluripotency cells, they were harvested after 48 hours, and the embryoid bodies were harvested on day-4 (D4) of differentiation. The plates were divided into three groups: (1) RNA used was isolated and transcripts analysed with qPCR (4 plates); (2) for the ChIP protocol 20 plates of EtOH, and 40 4HT plates of 4HT were harvested; lastly, (3) one plate was used for observation day-8. ChIP samples were sonicated 30'' ON 30'' OFF (3 cycles for undifferentiated cells, and 4 cycles for embryoid bodies), and then incubated with anti-H3K27me3, or anti-H3K27ac antibodies, the immune complex was captured with sepharose-G beads. The immunocaptured DNA in the DNA-histone-antibody complex was isolated with phenol:chloroform; the resulting fragments were analysed with qPCR, or 1.5 % agarose gel to evaluate the smear of sheared chromatin. This experiment was repeated three times for each histone modification. GMEM++, refers

to the culture medium supplemented and containing LIF, while GMEM+ refers to only supplemented medium. "D" stands for day.

Once with validated down-regulated genes modulated by *Cited2*, undifferentiated cells and embryoid bodies on day-4 of differentiation were then processed by chromatin immunoprecipitation (ChIP) targeting the two lysine 27 of histone 3 modifications: tri methylation and acetylation. Therefore, in ChIP experiments, cells were cultured under pluripotency conditions for 48 hours and observed before fixation with 1 % paraformaldehyde. As it can be seen, $C2^{fl/fl}$[cre] showed the same phenotype from the results described above (Figure 3.8): *Cited2*-partial_KO showed increased cell death (Figure 3.30). Similarly, the embryoid bodies were also observed on day-2 and harvesting day, the day-4 of differentiation (Figure 3.30). Phase-contrast images were processed in Cell Profiler to quantify the area and shape of embryoid bodies. The results showed that the *Cited2*-partial_KO embryoid bodies are smaller than the control at both time points, but increased over time (Figure 3.30). On day-2 of differentiation, control embryoid bodies showed on average an area of 0.0507 ± .0007 (SEM) μm^2 while the *Cited2*-partial_KO embryoid bodies showed 0.0329 ± 0.0006 (SEM) μm^2. Two days later, the embryoid bodies showed increased size and control showed on average 0.064 ± 0.001 (SEM) μm^2, while the *Cited2*-partial_KO embryoid bodies showed 0.0462 ± 0.0009 (SEM) μm^2. While their shape changes from a less to a more circular shape (form factor) on day-2 than the control (0.62 ± 0.01 vs 0.724 ± 0.008 (SEM) AU, respectively). However, they are similar to the control on day-4 (0.768 ± 0.008 vs 0.766 ± 0.008 (SEM) AU, respectively).

Furthermore, embryoid bodies were observed from the differentiation day-5 to day-8 and their capacity to differentiate was evaluated by the emergence of spontaneous beating foci. C*ited2*-partial_KO cells showed at least one beating foci two days later than *Cited2*-partial_KO cells, respectively, at differentiations day-8 versus day-6 (Figure 3.31). On day-8 of differentiation, the percentage of embryoid bodies showing spontaneous contractile activity was lower than the control, respectively: 9.74 ± 0.03 (SEM) and 88.09 ± 0.03 (SEM) %. Moreover, the average number of beating foci per embryoid body was also lower than the control, respectively: 0.21 ± 0.05 and 2.8 ± 0.1 (SEM). However, when only the embryoid bodies with beating foci are considered, the difference between *Cited2*-partial_KO and control is smaller: 1.1 beating foci per embryoid body); the observed values were, respectively, 2.1 ± 0.3 and 3.2 ± 0.1 (SEM). These results show evidence that the *Cited2*-partial_KO embryoid bodies seem to show impairment to undergo cardiac differentiation, specifically to be able to differentiate in functional cardiomyocytes as observed by a lower number of spontaneous beating embryoid bodies (Pacheco-Leyva et al., 2016; Santos et al., 2019).

Next, as mentioned above, sampled undifferentiated cells and embryoid bodies on day-4 were harvested, both control and Cited2-partial_KO cells. In total, the four sample groups were analysed according to the ChIP protocol. Thus, to evaluate the sheared chromatin, the DNA present in the sonicates was isolated and resolved in an agarose gel to confirm that the DNA smear peaked between 200-300 base pairs (Figure 3.32). The samples were incubated with antibody anti-H3K27me3 or anti-H3K27ac, and the isolated DNA fragments were analysed with qPCR. The promoter regions of the following genes were considered: *Cdx2, Dkk1, Isl1, Kdr, Mesp1* and *Wnt5a*.

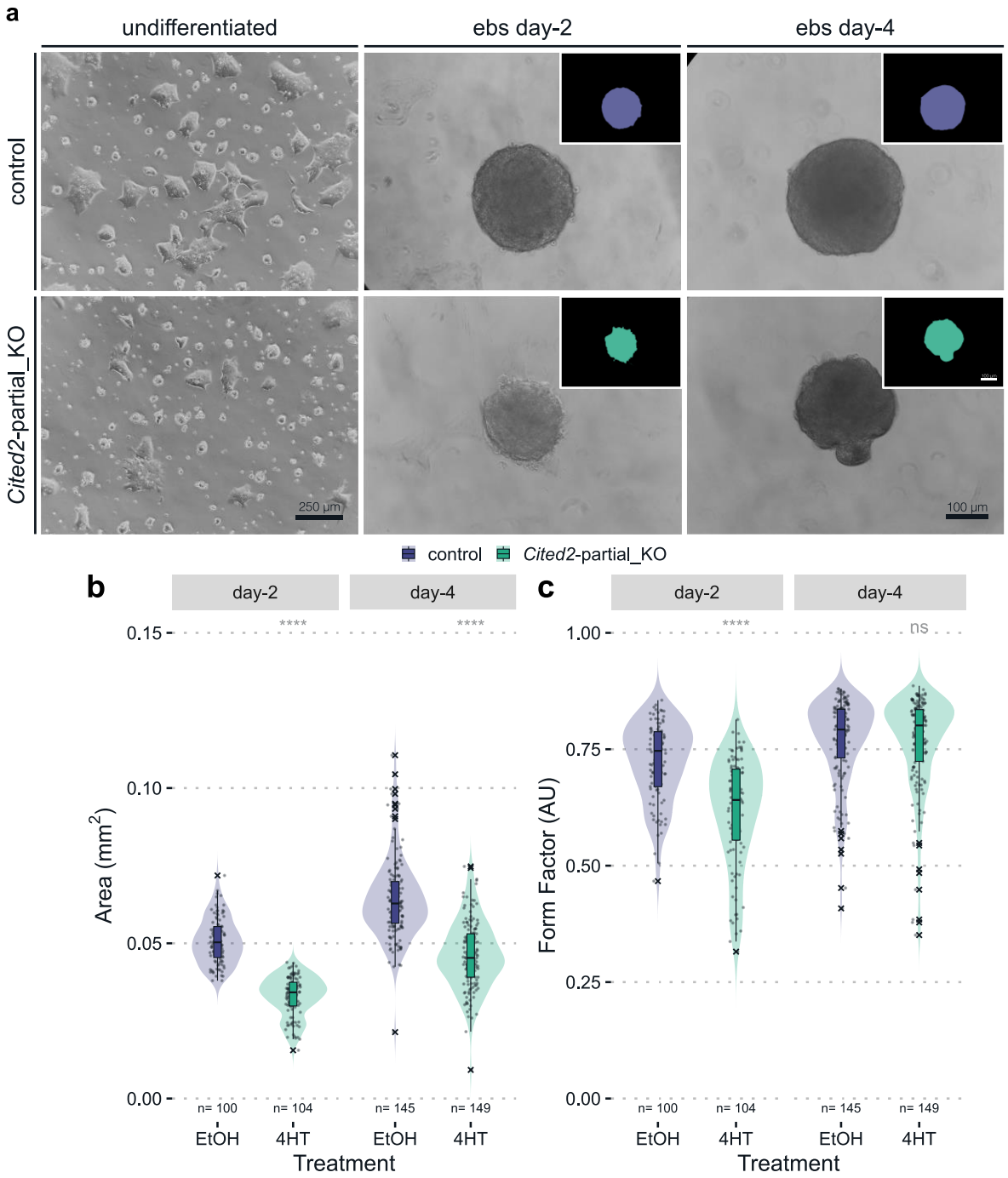

Figure 3.30 *Cited2*-partial_KO decreases the size and form factor of embryoid bodies. **(a)** Representative images of $C2^{fl/fl}$[cre] cultured under pluripotency and differentiation conditions and embryoid bodies generated using the hanging drop method were observed at two time-point: day-2 and day-4. The resulting images were used to quantify their **(b)** area and **(c)** shape features in a Cell Profiler pipeline; the inset on the embryoid bodies represents the segmentation results. Results of six experiments, where each dot represents an embryoid body (n). The scale bars of undifferentiated cells and embryoid bodies are 250 µm (10x objective) and 100 µm (20x objective), respectively. Means for each differentiation day were compared to the control using the t-test considering the P-value threshold of 0.05 for significance: (ns) nonsignificant, (****) ≤ 0.0001.

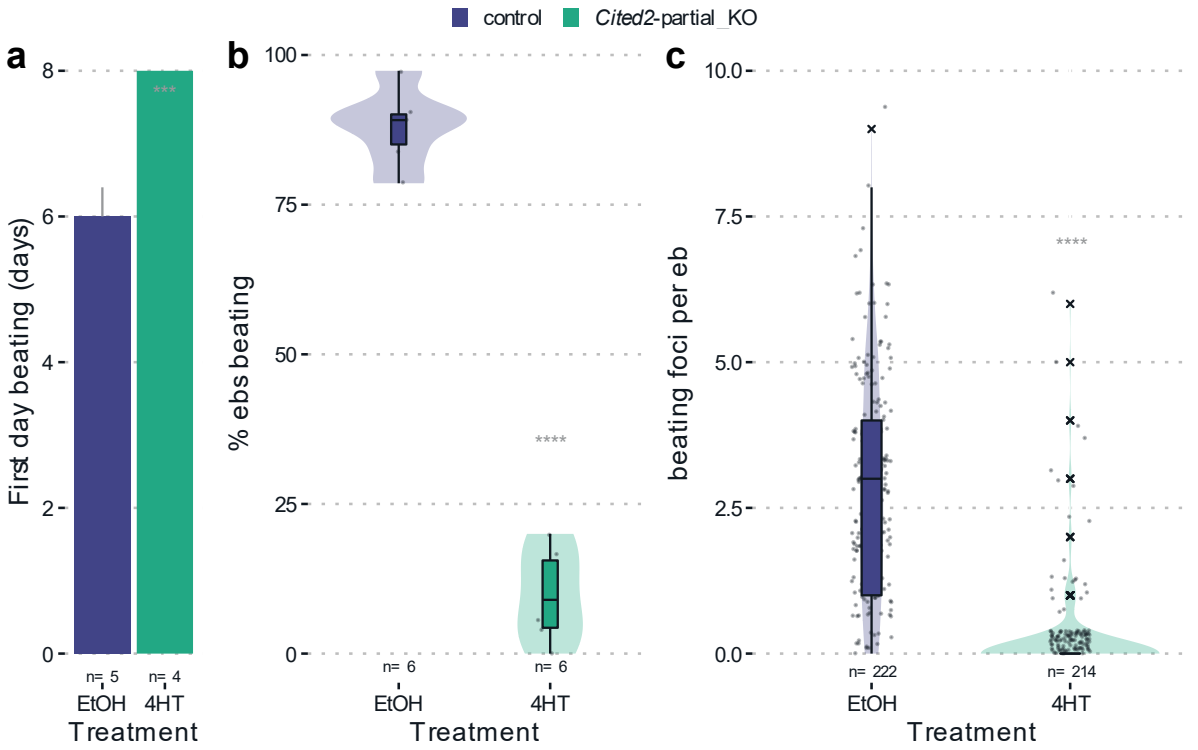

Figure 3.31 *Cited2*-partial_KO embryoid bodies show impaired cardiac differentiation. Embryoid bodies generated through the hanging drop method were **(a)** observed from day-6 to day-8 to find the first day a beating foci appeared (n, represents the number of experiments); and **(b)** shows the percentage of embryoid bodies beating, and **(c)** on day-8 the number of contractile foci per embryoid body (n) was counted. The results are from six experiments; in (a) it is represented as means ± SEM. Means were compared to the control using t-test considering the P-value threshold of 0.05 for significance: (ns) non-significant, (****) ≤ 0.0001.

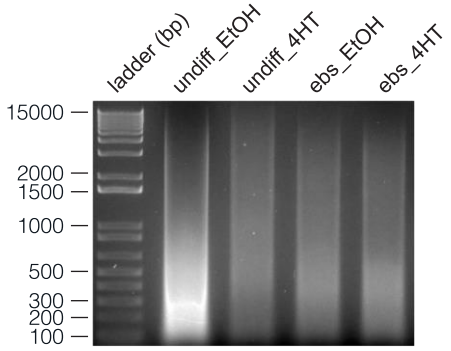

Figure 3.32 Representative image of the sheared chromatin smear. Undifferentiated cells cultured for 48 hours and embryoid bodies harvested on day-4 of differentiation, both treated with EtOH or 1 µM of 4HT, were lysed and sonicated respectively: 3 x 30" ON 30'' OFF, and 4 x 30" ON 30'' OFF. The isolated DNA was separated in a 1.5 % agarose gel. "bp" stands for base pairs, "undiff" for undifferentiated, and "ebs" for embryoid bodies.

The results show a suggestion of misregulation of H3K27me3 levels in *Cited2*-partial_KO cells compared to the control, although without statistically significant results (Figure 3.33). In undifferentiated cells, there is a tendency to increase repression marks for cardiac mesoderm genes (*Isl1* and *Mesp1*), but not for the mesoderm marker *Brachyury*. However, genes from signalling pathways showed reduced repression marks (*Dkk1*, and *Wnt5a*), as well as *Cdx2* and

Kdr. Under differentiation conditions, H3K27me3 levels appear to decrease for *Brachyury* and *Cdx2*, while they appear to increase for *Dkk1*. No changes were observed for the promoter regions of *Isl1*, *Kdr*, *Mesp1*, and *Wnt5a*. These results suggest that in *Cited2*-partial_KO cells cultured under undifferentiated conditions, it seems to have an increase in the repression mark in cardiac mesoderm-specific genes, when under differentiation conditions no changes were observed; except for the increase on *Dkk1*.

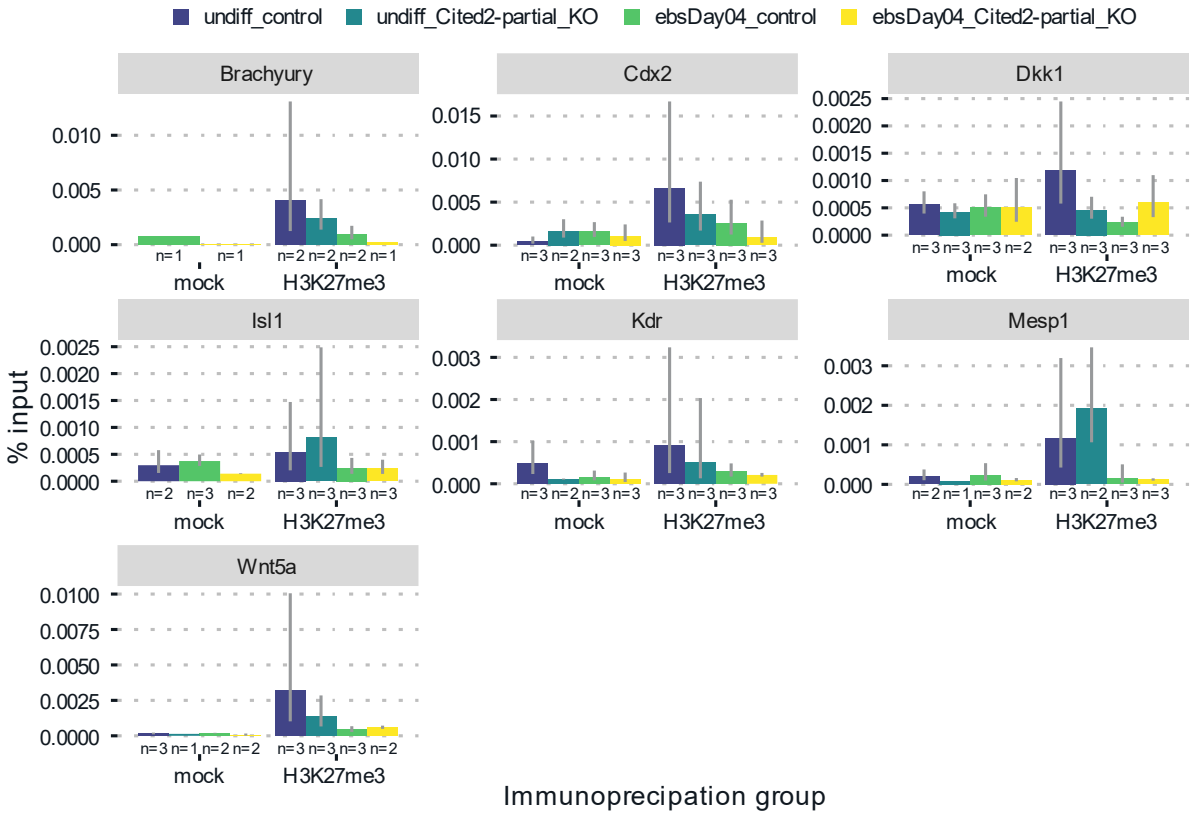

Figure 3.33 Suggestion that *Cited2*-partial_KO changes promoter enrichment levels of H3K27me3. From undifferentiated cells and embryoid bodies harvested on day-4, the samples were processed following the chromatin immunoprecipitation protocol using the antibody against H3K27me3; for the mock condition anti-FLAG was used, and 10 % (volume) of the input was sampled. The DNA fragments were then analysed by qPCR for the indicated target genes. The enrichment relative to the input was calculated using the dCt method, considering the 'input' condition as reference. Results are shown as mean ± SEM from three, experiments with "n" valid qPCR reads. Within the two groups of undifferentiated and embryoid bodies, the dCt means were compared with the control using the t-test considering the P-value threshold of 0.05 for significance: no significant results were obtained.

Next, the acetylation levels of the same promoters were also evaluated. A suggestion of increased levels of H3K27me3 is indicative of repression, and since the same lysine could be acetylated by p300 (Bedford and Brindle, 2012; Raisner et al., 2018), the working hypothesis is that acetylation is misregulated in *Cited2*-partial_KO cells. Therefore, it would be expected that for some promoters the acetylation levels would be lower than the control; complementary to this, the methylation levels would be increased; since this histone mark is considered the

reciprocal of H3K27me3 (Creyghton et al., 2010; Katoh et al., 2018). The samples were processed as previously stated, with the exception that the antibody used was anti-H3K27ac.

The results showed that similar to H3K27me3, it seems that H3K27ac levels are also misregulated in *Cited2*-partial_KO cells compared to the control, although without statistically significant results, except for the Wnt5a promoter in embryoid body samples (Figure 3.34). In undifferentiated cells, there is a suggestion of an increase in levels at the promoters of *Brachyury*, *Cdx2*, *Kdr* and *Mesp1*. Although it appears that there is no change for *Dkk1*, *Isl1*, and *Wnt5a*. Under differentiation conditions, the levels of H3K27ac decrease for *Dkk1*, *Isl1*, *Mesp1*, and *Wnt5a*. In contrast, it appears unchanged for *Cdx2* and *Brachyury*. These results suggest that in *Cited2*-partial_KO cells cultured under undifferentiated conditions, there is an increase in activation while a decrease was observed for differentiation conditions.

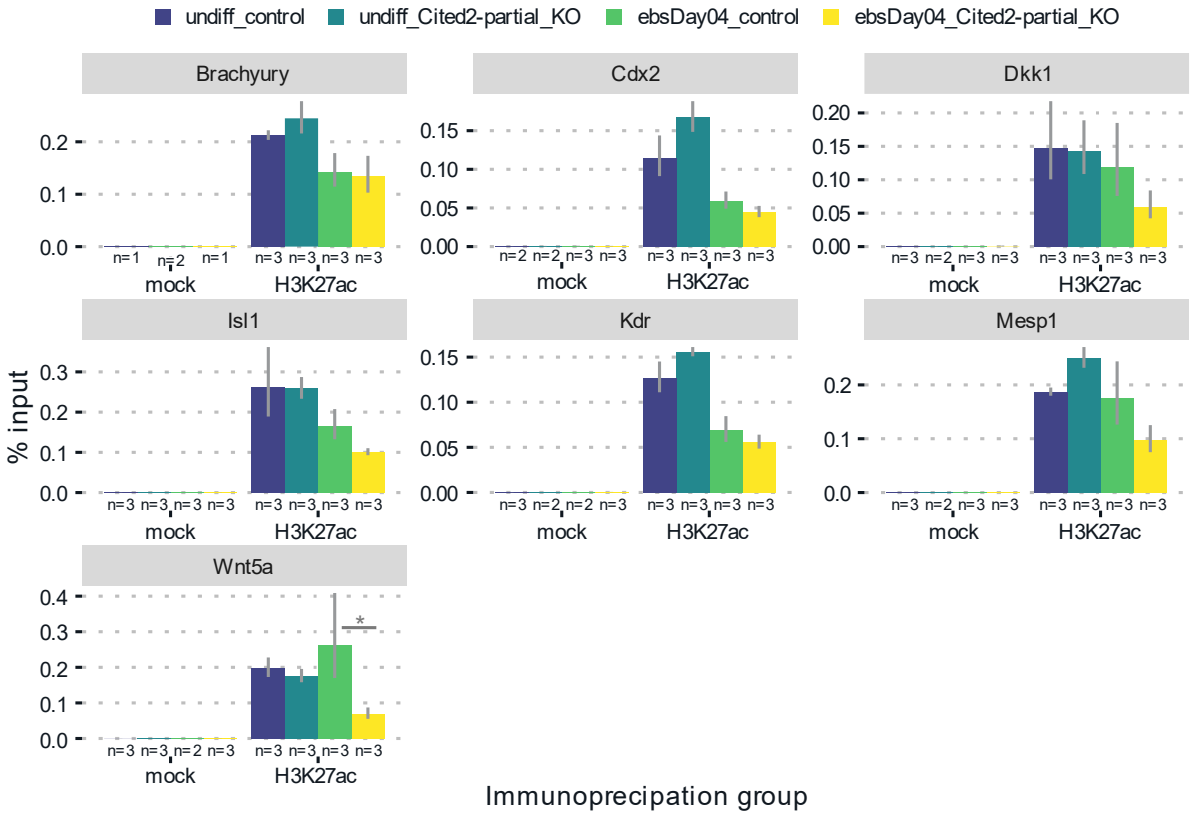

Figure 3.34 Suggestion that *Cited2*-partial_KO changes promoter enrichment levels of H3K27ac. From undifferentiated cells and embryoid bodies harvested on day-4, samples were processed following the chromatin immunoprecipitation protocol using the antibody against H3K27ac; for the mock condition anti-rabbit-IgG was used, and 10 % (volume) of the input was sampled. The DNA fragments were then analysed by qPCR for the indicated target genes. The enrichment relative to the input was calculated using the dCt method, considering the "input" condition as reference. Results are shown as mean ± SEM from three, experiments with "n" valid qPCR reads. Within the two groups of undifferentiated and embryoid bodies, the dCt means were compared with the control using the t-test considering the P-value threshold of 0.05 for significance: non-significant results not represented, (*) ≤ 0.05.

Next, to assess the regulation of the expression of the target genes by H3K27me3/ac their expression was evaluated by qPCR in both undifferentiated and differentiation conditions. The results showed that under undifferentiating conditions there is a tendency to increase expression, while under differentiation conditions there is a tendency to decrease expression. These results validate what was obtained from the microarrays. Note, that although in both conditions *Cited2* was depleted, the expression of the genes is different according to the context: undifferentiation or differentiation. However, the upregulation in undifferentiating conditions was not statistically significant for *Isl1* and *Brachyury*. While in differentiation conditions only the downregulation was not statistically significant for *Cdx2*, and *Kdr*. Furthermore, the genes with the highest up-regulated in undifferentiated cells were *Cdx2* and *Dkk1*, while the genes with the highest downregulation in differentiation conditions were *Mesp1* and Dkk1; *Mesp1*, a cardiac mesoderm marker, is the most down-regulated. Together, these results suggest that the misregulation of Wnt/signalling is constant between the two culture conditions in *Cited2*-depleted cells.

Figure 3.35 *Cited2*-partial_KO downregulates cardiac differentiation genes in differentiation conditions but upregulates in undifferentiation conditions. Mouse embryonic stem cells ($C2^{fl/fl}$[cre]) were treated with EtOH (control) or 1 µM 4HT (■ *Cited2*-partial_KO) under both pluripotency conditions and at the onset of differentiation and harvested respectively after 48 hours and at day-4. Transcripts were analysed with the ddCt

method and reported as a fold-change relative to the control; *Gapdh* was used as the reference gene. In **(a)**, the relative expression is shown for the undifferentiated cells and in **(b)** for the embryoid bodies at day-4. Results are shown as mean ± SEM from three, or more, experiments with "n" valid qPCR reads. The dCt means were compared with the control using the t-test considering the P-value threshold of 0.05 for significance: (ns) nonsignificant, (*) ≤ 0.05, (**) ≤ 0.01, (***) ≤ 0.001, (****) ≤ 0.0001.

3.3.1 Cited2 inhibits histone acetyltransferase activity

To better understand how *Cited2* could be influencing the acetylation of histone three, a histone acetyltransferase assay was performed between control and *Cited2*-partial_KO cells. Since *Cited2* interacts with p300, which is described to acetylate H3K27 (Raisner et al., 2018), the hypothesis for this experiment was that *Cited2*-partial_KO cells would have impairment to acetylated substrates. Therefore, undifferentiated cells were harvested after 48 hours of incubation and the whole protein extract was incubated with an anti-p300 antibody following the immunoprecipitation protocol. Thus, it was assumed that during p300 immunoprecipitation a complex would be pulled down, and in that complex, the control cells would contain CITED2, while in *Cited2*-partial_KO cells they would be deficient of CITED2 in that complex. Therefore, if CITED2 is required for acetylation then the immunoprecipitates of p300 from *Cited2*-depleted cells vs control would show reduced acetylation levels (Figure 3.36).

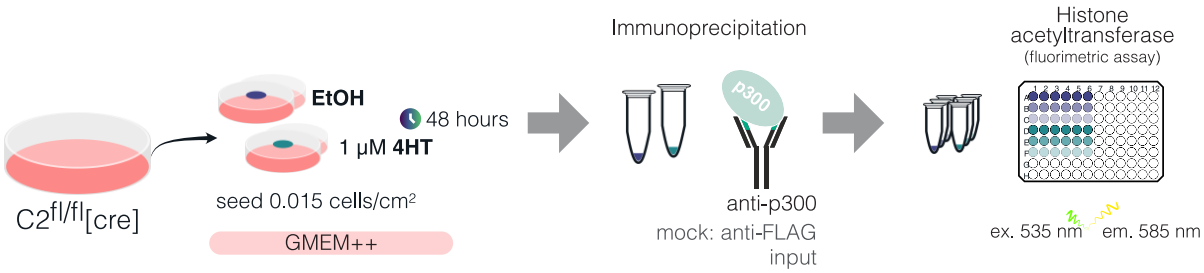

Figure 3.36 Experimental design to assess the ability of histone acetylation. Mouse embryonic stem cells ($C2^{fl/fl}$[cre]) were treated with EtOH (control), 1 µM 4HT (*Cited2*-partial_KO) under pluripotency conditions. The harvested cells were processed following the immunoprecipitation protocol using anti-p300 antibody, where the immune complex was captured with sepharose-G beads; for mock IP, anti-FLAG was used, and 10 % (volume) of input was sampled. The purified complex was eluted and loaded into a 96-well plate for the histone acetyltransferase fluorometric assay (excitation 535 nm and emission 585 nm). This experiment was repeated three times.

The results showed that for the whole lysate (input samples) the histone acetyltransferase activity tends to increase in *Cited2*-partial_KO cells. However, no differences were observed between the p300 immunoprecipitates (Figure 3.37). The Western blot of the immunoprecipitation of p300 was unsuccessful. These results suggest that, overall, *Cited2* depletion seems to increase the capacity of undifferentiated cells to acetylate histones, at least *in vitro*.

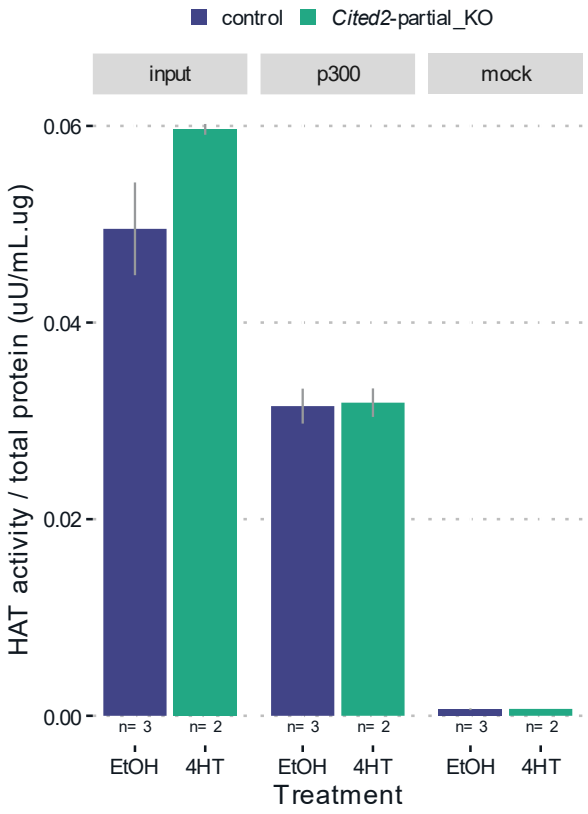

Figure 3.37 Undifferentiated *Cited2*-partial_KO cells suggested increased global histone acetyltransferase and unchanged acetylation by p300. Mouse embryonic stem cells ($C2^{fl/fl}$[cre]) were treated for 48 hours with EtOH (■ control), 1 µM 4HT (Cited2-partial_KO) and processed following the immunoprecipitation protocol with antibody against P300; the mock antibody used was anti-FLAG. The eluted purified protein was used to determine the histone acetyltransferase activity, which was then expressed relative to the amount of protein. Results are shown as mean ± SEM from two or more, experiments (n).

4 Discussion

In this study, we provide further evidence that, in mouse embryonic stem cells, *Cited2* depletion impairs not only the ability of cells to maintain self-renewal but also their ability to undergo cardiac differentiation. In the microarray expression screening, it was found that indeed gene expression regulation between the control and the *Cited2*-depleted cells, cultured under pluripotency and differentiation conditions, clustered separately, as evidenced by the principal component analysis. Previously published results by our group using part of these microarrays results group already elucidated this clustering, yet the *Cited2*-depleted group cultured in pluripotency conditions was not included (Santos et al., 2019). Therefore, in this study, when this group was considered in the present study, more information about the similarity between groups was obtained. For example, *Cited2*-depleted embryoid bodies showed global gene expression similar to undifferentiated control cells (pluripotent cells). This confirms that the initiation of differentiation is somewhat delayed by *Cited2* depletion, as previously reported, indicating that *Cited2* could play a role in the decision of cell fate (Santos et al., 2019). Furthermore, the gene expression of *Cited2*-depleted cells when maintained in undifferentiation conditions is different from that of embryoid body differentiation, suggesting that cells differentiate differently. While undifferentiated *Cited2*-depleted cells showed colonies with a morphology that is flatter than the control cells, the *Cited2*-depleted cells of embryoid bodies showed impairment in cardiac differentiation with a reduced number of spontaneous contracting foci, as observed previously (Kranc et al., 2015). These possible alternative differentiation paths were expected since two major factors are at play: the dimensionality of culture and the external queues. On the one hand, the induction of differentiation through a process that leads cells to form a 3D structure (embryoid body) will show different gene expression than if the same cells were induced to differentiate in a monolayer (Jeziorowska et al., 2017; Yang et al., 2021). On the other hand, the presence of LIF (an external factor) is also a contributing factor to the differentiation path (Murray and Edgar, 2001). In the presence of LIF an imbalance of germ layer specification favouring ectoderm and endoderm (Li et al., 2014) could be expected since *Cdx2* (trophectoderm marker) was found to be up-regulated when *Cited2* is down-regulated, and given that LIF contributes to the regulation of primitive and parietal endoderm (Murray and Edgar, 2001) in a concentration-dependent manner (Bader et al., 2001). However, no experiments were carried out using the hanging drop method with medium with LIF to better understand the role of *Cited2*. In conclusion, these PCA results demonstrated that different outcomes are expected when *Cited2* is depleted from mESC under

pluripotency and differentiation conditions. Therefore, to better understand the role of *Cited2*, experiments were carried out under both culturing conditions, based on a deeper analysis of the microarray results using gene set enrichment analysis.

One of the responses observed in mouse embryonic stem cells to DNA damage is spontaneous differentiation (Fortini et al., 2013; Sherman et al., 2011), which is also observed in *Cited2*-partial_KO cells (Kranc et al., 2015). In fact, even when cells are cultured in medium with LIF, which is acting as an external signal to maintain pluripotency, the expression of differentiation markers increases (*e.g. Brachyrury, Foxa2, and Sox17*) (Kranc et al., 2015). The microarray results also showed that there is misregulation of genes associated with differentiation genes described to be associated with *Cited2* and cardiac differentiation, namely *Lefty1* and *Lefty2* (Wolfgang et al., 2005) which are also associated with pluripotency (Kim et al., 2014; Meno et al., 1999). Furthermore, related to perturbations in cell cycle check points, which is also important for cell fate decision, it was observed in the microarrays that *Gadd45g* is upregulated, indicating cell cycle arrest in response to DNA damage (Salvador et al., 2013) and differentiation initiation (Zhang and Branciamore, 2021). The initiation of differentiation was supported by the confirmation of downregulation of pluripotency factors, for example, *Nanog* and *Oct4* (Kranc et al., 2015), and *Lin28a* (Zhang et al., 2016b), thus indicating loss of self-renewal and pluripotency. Further evidence was found from the gene set enrichment analysis of the list of down-regulated genes that showed mainly hits of transcription factors involved in the pluripotency network, for example, NANOG, SOX2, and OCT4. On the contrary, and as expected, analysis of the list of up-regulated genes showed hits of transcription factors that involve differentiation processes, for example, SMAD4, SUZ12, and TP63.

However, these observations from the microarrays suggest that *Cited2*-depleted cells differentiate even when kept under pluripotency conditions; this does not explain why they show increased cell death compared to the control cells. Moreover, the gene set enrichment analysis of Gene Ontology biological processes showed that down-regulated genes appear to be related to the DNA-repair mechanism. Therefore, *Cited2* was hypothesized to be involved in the regulation of the expression of genes involved in DNA repair in mouse embryonic stem cells. In fact, there is a suggestion that *CITED2* could be playing a role in DNA repair in human cells (Bo et al., 2004; Liu et al., 2015a). Human oesophageal cancer cells exposed to ionizing radiation showed downregulation of *CITED2* when *ITGB4* was up-regulated, which contributes to cell-cell and cell-matrix adhesion and cell growth (Bo et al., 2004). Although the present

study did not include irradiation experiments and the cells used were mouse embryonic stem cells, the same expression between these two genes was observed in the microarray results.

In this study, the role of *Cited2* in DNA repair was investigated, in mouse embryonic stem cells. To support this hypothesis, a detailed look at microarray results allowed the identification of downregulation of genes associated with DNA repair such as *Rad51c*, *Rad9b,* and *Mdc1*, which were validated in this work by qPCR. Although few studies are available on the role of Rad9b, it is suggested that it participates in various functions including DNA repair, cell cycle checkpoint control, and apoptosis (Leloup et al., 2010; Lieberman, 2006), while the roles of Mdc1 and Rad51c are well described.

When DNA damage is sensed by the cells and histone H2AX is phosphorylated (γH2AX), it is an indication of double-strand breaks in the DNA. It is thought that γH2AX recruits other repair factors that mediate the DNA damage response, such as *Mdc1* (Lou et al., 2006). This will result in the recruitment of Rad51c which plays a critical role in signalling the sister chromatid for homologous repair (Houtgraaf et al., 2006). Interestingly, RAD51 was suggested as a mediator of *Cited2* during DNA repair events in human cells treated with cisplatin (Liu et al., 2015b). Therefore, to investigate this hypothesis, the DNA damage in mESC was verified by the global levels of histone H2AX phosphorylation by western blot. It was found by Western blot that, indeed, there is a tendency for higher levels of this marker after 16 hours, followed by a decrease after 48 hours in *Cited2*-partial_KO cells; for cells cultured under undifferentiation conditions (with LIF) and differentiation conditions (without LIF). This is consistent with what was observed in other studies, in which histone H2AX phosphorylation decreases after radiation exposure (MacPhail et al., 2003). This decrease in γH2AX levels after the DNA damage experiment was attributed to the kinetics of the DNA repair which is dependent on the cell type and the amount of DNA damage induced (Bouquet et al., 2006). Nonetheless, other mechanisms can be involved, such as the dephosphorylation of γH2AX by the protein phosphatase 2 (PP2A) (Chowdhury et al., 2005).

Next, in an attempt to rescue the possible increase in DNA damage observed in *Cited2*-depleted cells maintained in undifferentiated conditions, an experiment using human recombinant *CITED2* fused with eight arginine at the N-terminal (8R-CITED2) was performed. However, the results were not conclusive, since all experimental conditions showed similar levels of phosphorylated H2AX between the experimental groups. This could be attributed to two main reasons: the shorter sampling time point of 6 hours (vs the 16 hours in the other two experiments), and the addition of hydrogen peroxide at the onset of the experiment. First, the

shorter incubation time point, below 16 hours, could not be enough induce the downregulation of *Cited2* by Cre recombinase (Feil et al., 1997; Kranc et al., 2015). Thus, it was not possible to rule out the possibility that the treatment with recombinant CITED2 rescued the depletion of *Cited2*. Second, the additional hydrogen peroxide at the onset could induce stress in cells that increases the DNA damage near a saturation point since it is similar to that of the positive control.

Although a correlation between western blot and immunofluorescence techniques using the same antibody cannot be performed due to possible epitope changes and protocol differences (Lund-Johansen and Browning, 2017), different information can be read from each technique. Therefore, histone phosphorylation was also observed, and speckle quantification was obtained. The results showed that under pluripotency conditions, the number of speckles remains unchanged between control cells and *Cited2*-partial_KO cells. However, the speckles intensity has increased in *Cited2*-partial_KO cells compared to the control. In the literature, it is suggested that the number of speckles correlates with the number of breaks (Kuo and Yang, 2008), and thus the amount of double-stranded DNA breaks present in a cell. Nonetheless, in mESC it is suggested that the number of speckles does not correlate with increased DNA damage, but instead with chromatin decondensation (Banáth et al., 2009) and pluripotency state (Turinetto et al., 2012). These observations can explain the results from the experiment in pluripotency with 16 hours where indeed *Cited2*-partial_KO cells are less pluripotent, and thus show fewer speckles. Furthermore, in the experiment without LIF, the reduction in speckles in *Cited2*-partial_KO cells was statistically significant and noticeably this was the condition with more cells presenting zero speckles. Complementary to the number of speckles is their intensity. In the literature, it is suggested that high intensity may be an indication of increased S-phase and apoptosis (Cleaver, 2011). In this study, it was found that indeed *Cited2*-partial_KO cells that showed the highest cell death also showed higher speckle intensity when cultured under pluripotency conditions for 16 hours; the same was not observed when cells were treated for 6 hours with 50 µM of H_2O_2 added to the medium, nor under non-pluripotency conditions. This suggests that although the cell line is the same, with different supplementation to the culture media the response to DNA could be different, similar to what was observed in a study that compares different cell lines (MacPhail et al., 2003).

To further explain apoptosis and the differentiation of *Cited2*-partial_KO cells, it was also considered after microarray analysis that p53 could be involved. As described in the literature, p53 acts as a check point for DNA integrity (Gurley and Kemp, 1996; Hirao et al., 2000;

Kuerbitz et al., 1992), but it can also play a role in determining cell fate (Fu et al., 2020; Li et al., 2012b; Lin et al., 2005; Zhang et al., 2018); of interest for this work is mesoderm differentiation (Shigeta et al., 2013). Although the results showed that the expression of p53 was unchanged in *Cited2*-partial_KO cells compared to the control. Nonetheless, some of the p53 effectors such as *p21*, *Plk2*, *Perp*, and *Ptges* were found to be upregulated, suggesting that the increased apoptosis previously described in (Kranc et al., 2015) for this cell line and in pluripotency conditions can be associated with p53. Furthermore, from experiments with *Cited2*$^{-/-}$ cells it was observed that the genes *Plk2, Perp, p21,* and *Mdc1* were negatively regulated, except *Rad51c* and *p53* which remained unchanged. These results suggested that these knockout cells overcame the apoptosis activation pathway that appears to be inducible by acute depletion of *Cited2*. The unaltered expression of p53 and the increased expression of its effectors could be explained by post-translational modifications. Indeed, an experiment in mice reported that although the expression of p53 remains unchanged, protein acetylation levels increase in *Cited2*$^{-/-}$ mice embryos (Massa et al., 2019), suggesting that the mechanism could be through protein modification rather than gene regulation. Similar observations were observed in the context of leukaemia cells and apoptosis in which *CITED2* was knockdown (Mattes et al., 2017).

The role of *Cited2* in pluripotency seems to be linked with its role in differentiation. As mentioned above, when *Cited2* is down-regulated, *Lefty1* and *Lefty2* are also down-regulated, which are genes important for cardiac development (Deng et al., 2014). Furthermore, the observed downregulation of *Rbm24*, a gene necessary for cardiac development, could be rescued with a deficiency of p53, since the observed heart defects were due to apoptosis of the endocardial cushion (Zhang et al., 2018). Interestingly, from the gene set enrichment analysis using the list of upregulated genes of undifferentiation conditions, terms associated with cardiac muscle contraction were frequent, suggesting that genes associated with these biological processes are up-regulated in *Cited2*-depleted conditions, for example, *Casq2* is important for the regulation of calcium and the contractility of cardiomyocytes (Flores et al., 2018; Rossi et al., 2021). These results suggest that Cited2 could be modulating the expression of genes associated with cardiac differentiation/development, since they appeared down-regulated even in pluripotency.

As mentioned above, *in vitro* differentiation of mESC with *Cited2*-depleted cells at the onset of differentiation affects cardiac differentiation (Pacheco-Leyva et al., 2016; Santos et al., 2019). Indeed, the global expression results analysed by PCA showed that the *Cited2*-depleted

embryoid bodies are close to undifferentiated control cells (pluripotent cells). This observation suggests that *Cited2*-depleted cells seem to be unable to initiate mesoderm differentiation at the same time point as the control cells, which is reflected in the delayed expression of mesoderm and cardiac mesoderm markers, such as *Brachyury*, *Mesp1* and *Mixl1* (Santos et al., 2019). Moreover, pluripotency seems to be upregulated in *Cited2*-partial_KO embryoid bodies on day-4 as indicated by the upregulation of pluripotency-associated genes (*e.g.* Nr0b1, Sox2, and Dppa2). Note that the ChEA/ENCODE gene set enrichment analysis from the up-regulated genes in embryoid bodies is similar to the list of downregulated genes in undifferentiated cells (Figure 3.4). Therefore, the proximity shown in the PCA plot between the *Cited2*-depleted embryoid bodies, and the undifferentiated control cells could be explained by the possible delay in the expression of differentiation genes.

To better understand what could be causing the delay, this work explored the role of *Cited2* in epigenetic regulation, particularly the regulation of histone modifications H3K27 tri-methylation and acetylation. Evidence for this hypothesis arose from the gene set enrichment analysis of ChEA/ENCODE consensus. The results showed that down-regulated genes in *Cited2*-depleted cells are genes previously shown to be associated not only with SUZ12, but also EZH2, which are both members of the PCR2 complex (Somorjai et al., 2012). This protein complex is associated with the methylation of lysine 27 of H3 indicates repression of gene expression. Therefore, it would be expected that the expression of the genes controlled by PRC2 will be down-regulated, namely mesoderm/cardiac mesoderm markers, such as *Brachyury*, *Isl1*, and *Mesp1* investigated in this work. Adding to those three genes, *Cdx2*, *Dkk1*, *Wnt5a* and *Kdr*, were also considered, as they are also down-regulated concomitantly with *Cited2*-depletion.

The results of promoter enrichment for H3K27me3 and H3K27ac in *Cited2*-partial_KO cells suggest a tendency for misregulation since there are on average enrichment level differences between the control and *Cited2*-partial_KO cells within the two groups (undifferentiated and differentiated). Although most of the observed differences observed did not reach statistically significant results. The exception was observed for H3K27ac in the promoter of *Wnt5a* on embryoid bodies. This result provides evidence of a new possible role for *Cited2* in the Wnt signalling pathway, in this case, epigenetic regulation of Wnt5a expression, which adds to previous evidence that human recombinant WNT5a/WNT11 rescued *Cited2*-depletion *in vitro* and *in vivo* (zebrafish) (Santos et al., 2019). Interestingly, the correct expression of Wnt5a in cattle embryos is necessary for the implantation and formation of extraembryonic tissues (Biase et al., 2013). Therefore, it appears that Cited2 defects could be rescued during early

development (pre-implantation), thus opening new doors for therapies targeting this time point, and possibly exploring supplementation of WNT5a (Hayashi et al., 2009; Rider et al., 2016).

Although the enrichment of these two histone modifications was not statistically significant, these experiments suggest that there is a tendency to see an increased enrichment of H3K27me3 at the *Isl1* and *Mesp1* promoters in undifferentiated *Cited2*-partial_KO cells compared to the control. Meanwhile, enrichment of H3K27ac at the same two promoters seems to remain unchanged. Similarly, at the promoters of *Wnt5a* and *Dkk1* both histone modifications show the same tendency of low enrichment in undifferentiated *Cited2*-partial_KO cells compared to the control. At the promoters of *Brachyury*, *Cdx2* and *Kdr*, the reciprocal functions between H3K27me3 and H3K27ac were observed in undifferentiated *Cited2*-partial_KO cells compared to the control (lower H3K27me3 and higher H3K27ac). However, for the same three genes, this reciprocity was not observed for the *Cited2*-partial_KO embryoid bodies, and in fact, it was observed a lower enrichment of both H3K27me3 and H3K27ac.

Overall, the promoter enrichment of the two histone modifications (H3K27me3 and H3K27ac) showed different tendencies. A trend was not observed for the H3K27me3 mark within undifferentiated cells or embryoid bodies. However, for H3K27ac there was a tendency to see increased enrichment in undifferentiated *Cited2*-partial_KO cells compared to the control, and a decrease in embryoid bodies *Cited2*-partial_KO cells compared to the control. Thus, the results obtained for H3K27ac enrichment levels, unlike those obtained for H3K27me3, agree with the expected mRNA transcript levels for the studied genes. That is, for the higher enrichment of H3K27ac in *Cited2*-partial_KO undifferentiated cells compared to the control, a tendency to increase expression was observed. Whereas, for the lower enrichment of H3K27ac in *Cited2*-partial_KO embryoid bodies compared to the control, a tendency to decreased expression was observed, as was known *a priori*.

The observation of increased enrichment of H3K27ac in undifferentiated conditions versus a decrease in differentiation conditions in *Cited2*-depleted cells compared to the control could indicate that, indeed, cells undergoing differentiation seem to have impaired capacity to acetylate H3K27. This could then be observed as a deficient expression of genes important for early mesoderm commitment, that lead to cardiac differentiation. Furthermore, considering this, and that under differentiation conditions in *Cited2*-partial_KO cells there was a tendency to equal or lower H3K27me3 enrichment of the promoters (except for *Dkk1*), suggests that the demethylation processes are not impaired while the acetylation seems to be. Alternatively, it is suggested that the promoters are under-methylated due to high acetylation, yet not enough to

induce the transcription of genes. Therefore, it can be speculated that *Cited2* could be playing a role in the acetylation of this H3K27 in a context-dependent manner. Indeed, in the histone acetyl transferase assay, undifferentiated *Cited2*-partial_KO cells showed an increase in acetylation, thus suggesting that overall acetylation increases when *Cited2* is decreased, at least *in vitro*. However, immunoprecipitated targeting p300 did not show differences, yet careful interpretations must be taken since the confirmation of immunoprecipitation of p300 by Western blot was unsuccessful, suggesting technical issues.

Moreover, given that there is high variability in the enrichment results overall, which not only can result from a technical standpoint, but also can be a result from the biological sample. For example, in both assays, the enrichment of histones at the promoter of undifferentiated cells showed a higher signal than the samples from embryoid bodies. This could be explained by the increased heterogeneity in the population of cells that arises during differentiation. That is, the population of cells kept in undifferentiated conditions is more homogeneous than cells cultured in differentiated conditions (Graf and Stadtfeld, 2008). Therefore, since the analysed sample is a pool of cells, in undifferentiated conditions epigenetic marks will be similar, thus resulting in increased signal and lower noise. Conversely, the pool of cells from embryoid bodies contains proportionally fewer cells in the same state, *i.e.* cells with similar histone modification on a given promoter, which leads to a decreased signal. Indeed, the mesoderm cells are a portion of the population that includes other germ layers (Kouskoff et al., 2005), and, as presented in another study, only about 5 % reached cardiac fate (Zandstra et al., 2003). Moreover, given that the undifferentiated cells were not synchronized, the spontaneous nature of the differentiation protocol could be noted as a major source of variations (Zhang et al., 2005). Nonetheless, this provides evidence of the intricate mechanisms at play in differentiation events that are well timely regulated (Paige et al., 2015; Rowton et al., 2021). Although the same timings were followed during the experiments, there is still visible variance in the enrichment of these histone modifications and the gene expression. Namely, the highest variance was observed for *Kdr* and *Brachyury*, which are genes that are modulated by Wnt signalling, which can be modulated by the size of the embryoid bodies (Yu-Shik et al., 2009); discussed below.

The validation of the down-regulated genes in differentiation conditions allowed the confirmation that not only Wnt signalling is affected by *Cited2*-depletion, but also other pathways are affected, such as FGF signalling, and TGF-β/BMP signalling.

As previously demonstrated in our lab Wnt signalling is misregulated in the absence of *Cited2*, yet the rescue of *Cited2*-depletion with recombinant WNT5A and WNT11 was successful both

in vitro experiment with mESC and *in vivo* with zebrafish (*Danio rerio*) (Santos et al., 2019). Moreover, indirectly the misregulation of the Wnt pathway can be linked to the top downregulated genes observed in the microarrays: *Aplnr* (Chen et al., 2019) and *Kdr* (Liu et al., 2012). Both these genes are associated with cell signalling processes that have been demonstrated to be important for differentiation events, namely angiogenesis (Helker et al., 2015; Pulkkinen et al., 2021; Zhou et al., 2020). The misregulation of *Kdr* could indicate that proper differentiation into mesendodermal cells is not occurring (Risau and Flamme, 1995), at least in the expected time window, which has been shown to be important for lineage commitment (Kouskoff et al., 2005). Furthermore, as observed for gene ontology biological processes analysis from undifferentiated cells, response to low oxygen levels was one of the terms found. This suggests that perhaps from an early stage of differentiation (day1-2) *Cited2*-partial_KO cells already have impaired the correct timing of the expression of *Kdr* that could be controlled by HIF1α (Yamakawa et al., 2003).

During the differentiation experiment, the embryoid bodies were observed on day-2 and on day-4 of differentiation to determine their area and shape. The results showed the under both conditions (control and *Cited2*-partial_KO) the embryoid bodies grew over time, yet the *Cited2*-partial_KO cells are smaller than the control. These results are expected, since, similarly to what is observed in undifferentiation conditions, there are some cells that die due to *Cited2*-depletion, which leads to a lower number of viable cells available to aggregate and form a sphere in the first two days of differentiation. This lower number of cells and the possible continuous death of cells during embryoid bodies growth could explain why the *Cited2*-partial_KO embryoid bodies are less regular and show a smaller form factor (circular shape) than the control. Nonetheless, on day-4 of differentiation, the form factor between control and *Cited2*-partial_KO cells is not statistically significant, which suggests that the *Cited2*-partial_KO embryoid bodies grew and became more round as observed for the control. This suggests that *Cited2*-partial_KO embryoid bodies were able to grow despite the initial loss of cells during the first two days of differentiation. However, cardiac differentiation was not as successful as control embryoid bodies, since the percentage of embryoid bodies showing beating foci was lower than control on day-8 of differentiation. Not only that, but the number of foci per embryoid body was on average lower in *Cited2*-partial_KO embryoid bodies than in control, which is consistent with previous work (Pacheco-Leyva et al., 2016; Santos et al., 2019). Other studies also demonstrated that the initial size of the embryoid bodies has

implications for differentiation trajectories (Pettinato et al., 2014). Especially in the ability of embryoid bodies to differentiate into the three germ layers, where smaller embryoid bodies showed increased expression of ectodermal markers than the bigger embryoid bodies that showed increased expression of mesodermal and endodermal markers (Park et al., 2007). Furthermore, the smaller size was demonstrated to be associated with higher expression of *Wnt5a*, which enhanced endothelial cell differentiation, while larger embryoid bodies showed increased *Wnt11* and enhanced cardiogenesis (Yu-Shik et al., 2009). Therefore, the observed differences in size and shape of *Cited2*-partial_KO embryoid bodies could be considered as morphological indicators that differentiation is impaired, when compared to the control.

However, the results presented here sometimes suffer considerable variations resulting from the fact that mouse embryonic stem cells die when *Cited2* is depleted. This could be due to the fact that when cells are treated with 4HT to induce *Cited2*-depletion. The best results are obtained after 48 hours, but by that time most of the cells that were indeed depleted of *Cited2* are no longer viable. For this reason, the term *Cited2*-partial_KO was used to better represent the heterogeneous population of sampled cells where some cells are not *Cited2*-depleted, others only one allele was excised, and others were depleted but did not enter apoptosis yet. This can be observed by the variation under *Cited2* expression under pluripotency conditions, as shown in the qPCR results. It can also be hypothesized that the degree of *Cited2* depletion or CITED2 levels, present in the cell can lead to different cell responses.

4.1 The proposed model and future perspectives

CITED2 is an interactor of p300/CBP, which can acetylate both histones (*e.g.* H3K27) and transcription factors (*e.g.* p53). Based on the results presented, it can be hypothesised, for future experimentation, that the dual role of Cited2 in pluripotency and differentiation could be to guide and modulate acetylation by p300/CBP (Figure 4.1). Therefore, Cited2 could be regulating p300/CBP acetyltransferase in a context-dependent fashion (pluripotency and differentiation), and in a time-dependent manner (which is intrinsically linked to the transition from pluripotency to differentiation).

In wild-type pluripotency conditions, the presence of *Cited2* promotes the maintenance of self-renewal. One of the mechanisms that could be at play is the inhibition of p53 acetylation by p300/CBP by CITED2 (Figure 4.1a). In this way, p53 is steady-stated that does not induce cell

death or spontaneous differentiation; the inverse would occur when *Cited2* is down-regulated. However, the possible direct connection between CITED2-p300 and p53 acetylation of p53 in the context of pluripotency in mouse embryonic stem cells remains unclear.

Nonetheless, the results presented in this work showed a tendency to increase histone acetylation in *Cited2*-depleted cells compared to the control, under pluripotency conditions. This suggests an inhibitory mechanism of CITED2 in the acetyltransferase activity of p300/CBP. Thus, one could predict that Cited2 expression would be lower at a given point to allow the acetylation of important genes for cardiac differentiation that are controlled by PRC2. Interestingly, downregulation of *Cited2* during differentiation is necessary for proper differentiation and it occurs at day-2 of differentiation.

Therefore, it could be hypothesised that differentiation conditions *Cited2* could partner with p300/CBP in recruiting other transcription factors to 'bookmark' cardiopoietic genes prior to differentiation (Figure 4.1b). Then, *Cited2* is required to be downregulated (on day-2) to allow the acetylation of H3K27, which, in turn, activates the transcription of the mesoderm and cardiac mesoderm genes. After this step, the expression of *Cited2* increases to levels comparable to those in pluripotency. The results presented in this work suggested that while under pluripotency conditions, downregulation of *Cited2* tended to increase the H3K27ac mark and cardiopoietic gene expression, the inverse was observed for differentiation conditions. However, in this study, it was not possible to establish a direct association of histone acetylation by p300 and *Cited2*. Furthermore, it remains to be understood if there is an initial increase in acetylation on day-1 of differentiation, that needs to be lowered down to levels comparable to pluripotency, from which cells can proceed with differentiation. Alternatively, the delayed expression of mesoderm makers is a consequence of the readaptation of cells to *Cited2* depletion, due to increased cell death during aggregation of the embryoid body.

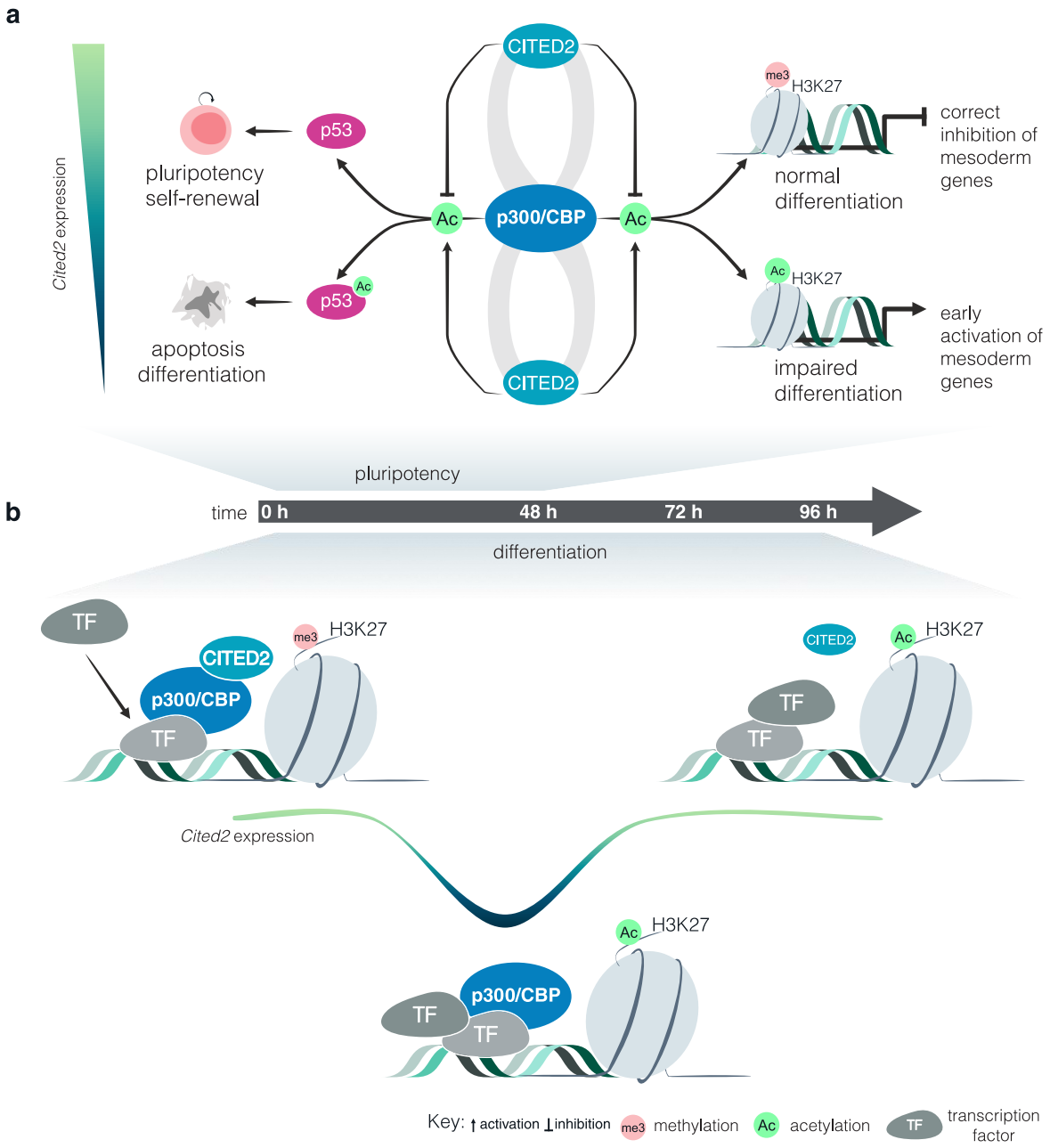

Figure 4.1 Simplified schematic representation of the proposed model of the role of Cited2 in pluripotency and differentiation. **(a)** Role of Cited2 in pluripotency and early hours of differentiation. When *Cited2* is downregulated, there is increased acetylation of p53 by p300/CBP which h stabilized p53 leading to increased cell death and spontaneous differentiation. In the early stages of differentiation, the downregulation of *Cited2* leads to increased acetylation of H3K27 activating the mesoderm genes ahead of time leading to an impairment of differentiation. **(b)** Role of CITED2 in normal differentiation. Before differentiation is initiated Cited2 partners with p300/CBP and other transcription factors to bind to regulatory regions of mesoderm/cardiopoietic genes. Then, *Cited2* is downregulated and these transcription factors along with p300/CBP bookmark-specific genes simultaneously occur the acetylation of H3K27 at the correct timing, to signal gene expression activation. Next, the expression of mesodermal and cardiopoietic genes is initiated, thus starting the cardiac differentiation, while *Cited2* transcript levels return to levels similar to pluripotency.

5 Conclusion

Evidence suggests that Cited2 could play a dual role in pluripotency and differentiation. In the present study, the role of Cited2 in pluripotency was investigated to better understand what leads to increased cell death after Cited2 depletion (or partial knockout). From the microarray experiment (Affymetrix) comparing the differentially expressed genes between Cited2-depleted and control cells, cultured under undifferentiated conditions, it was possible to identify several downregulated genes associated with DNA damage/repair, namely: *Rad51c*, *Rad9b*, *Mdc1*. At the same time, upregulation of p53 effects was also verified, such as *p21*, and *Ptges*. Therefore, DNA damage was assessed by looking at both the foci and the total levels (by Western blot) of γH2AX. Although the results failed to demonstrate a clear and statistically significant difference between the control and the *Cited2*-depleted cells, a time-dependent response of γH2AX. After 16 hours of *Cited2*-depletion, the γH2AX levels increased, while at 48 hours the levels decreased when compared to the control. However, given the difficulties in maintaining *Cited2*-depleted cells in culture, it was not possible to demonstrate that the increase in cell death is caused by an increase in DNA damage. Therefore, other methods should be applied to better understand. As an example, the single-cell comet assay would allow gain resolution from the population to the cell and reduce background noise.

Moreover, it was also hypothesized that the cause of increased cell death in *Cited2*-depleted cells could be attributed to improper regulation of p53, since similar roles were also observed in the context of cancer. However, it was not possible to demonstrate a clear link between *Cited2* downregulation and post-translational modifications to p53. For example, increased acetylation of p53, could be mediated by p300/CBP.

Cited2-depletion in mouse embryonic stem cells causes delayed expression of important mesoderm and cardiac mesoderm markers (*Brachyury, Kdr, Mesp1, Isl1*), as well as other genes important for the proper differentiation process (*Cdx2*, *Dkk1*, *Wnt5a*). To better understand this delayed expression, it was hypothesized that *Cited2* could play a role in the epigenetic regulation of the expression of these genes. The results of the chromatin immunoprecipitation experiment from embryoid bodies harvested on day 4 of differentiation, which were evaluated by qPCR, showed that although not statistically significant there is a decrease in the H3K27ac mark, while the H3k27me3 mark is not always consistent with the respective H3K27ac, as expected. Hence, the results from the H3K27ac mark were better predictors of gene expression under both experimental conditions of pluripotency and differentiation.

Overall, this work explored the hypothesis that could explain the role of *Cited2* in pluripotency and differentiation. In pluripotency, the results suggest that the role of *Cited2* might be associated with the regulation of DNA repair, while the apoptosis mediated by p53 remains unclear. However, the results cannot rule out the direct association of Cited2, DNA repair/damage and p53-induced apoptosis. In differentiation, the results support the hypothesis that Cited2 could play a role in the regulation of H3K27 epigenetic modification that precedes the expression of cardiopoietic genes during the early events of differentiation, which could begin while cells are pluripotent.

6 References

Abu-Issa, R., and Kirby, M.L. (2007). Heart field: from mesoderm to heart tube. Annu Rev Cell Dev Biol *23*, 45-68.

Acharya, A., Brungs, S., Henry, M., Rotshteyn, T., Singh Yaduvanshi, N., Wegener, L., Jentzsch, S., Hescheler, J., Hemmersbach, R., Boeuf, H., *et al.* (2018). Modulation of Differentiation Processes in Murine Embryonic Stem Cells Exposed to Parabolic Flight-Induced Acute Hypergravity and Microgravity. Stem Cells and Development *27*, 838-847.

Ahmed, M., and Kim, D.R. (2018). pcr: an R package for quality assessment, analysis and testing of qPCR data. PeerJ *6*, e4473.

Ahuja, A.K., Jodkowska, K., Teloni, F., Bizard, A.H., Zellweger, R., Herrador, R., Ortega, S., Hickson, I.D., Altmeyer, M., Mendez, J., *et al.* (2016). A short G1 phase imposes constitutive replication stress and fork remodelling in mouse embryonic stem cells. Nature Communications *7*, 10660.

Arnold, S.J., and Robertson, E.J. (2009). Making a commitment: cell lineage allocation and axis patterning in the early mouse embryo. Nat Rev Mol Cell Biol *10*, 91-103.

Asp, P. (2020). Chapter Fourteen - The chromatin immunoprecipitation (ChIP) assay and ChIP-qPCR. In Epigenetics Methods, T. Tollefsbol, ed. (Academic Press), pp. 281-296.

Bader, A., Gruss, A., Höllrigl, A., Al-Dubai, H., Capetanaki, Y., and Weitzer, G. (2001). Paracrine promotion of cardiomyogenesis in embryoid bodies by LIF modulated endoderm. Differentiation *68*, 31-43.

Bamforth, S.D., Bragança, J., Eloranta, J.J., Murdoch, J.N., Marques, F.I.R., Kranc, K.R., Farza, H., Henderson, D.J., Hurst, H.C., and Bhattacharya, S. (2001). Cardiac malformations, adrenal agenesis, neural crest defects and exencephaly in mice lacking Cited2, a new Tfap2 co-activator. Nature Genetics *29*, 469-474.

Bamforth, S.D., Bragança, J., Farthing, C.R., Schneider, J.E., Broadbent, C., Michell, A.C., Clarke, K., Neubauer, S., Norris, D., Brown, N.A., *et al.* (2004). Cited2 controls left-right patterning and heart development through a Nodal-Pitx2c pathway. Nature Genetics *36*, 1189-1196.

Banáth, J.P., Bañuelos, C.A., Klokov, D., MacPhail, S.M., Lansdorp, P.M., and Olive, P.L. (2009). Explanation for excessive DNA single-strand breaks and endogenous repair foci in pluripotent mouse embryonic stem cells. Experimental Cell Research *315*, 1505-1520.

Barrero, M.J., and Izpisua Belmonte, J.C. (2008). Epigenetic Mechanisms Controlling Mesodermal Specification. In StemBook (Cambridge (MA): Harvard Stem Cell Institute).

Batalov, I., and Feinberg, A.W. (2015). Differentiation of Cardiomyocytes from Human Pluripotent Stem Cells Using Monolayer Culture. Biomark Insights *10*, 71-76.

Beddington, R.S., and Robertson, E.J. (1989). An assessment of the developmental potential of embryonic stem cells in the midgestation mouse embryo. Development *105*, 733-737.

Bedford, D.C., and Brindle, P.K. (2012). Is histone acetylation the most important physiological function for CBP and p300? Aging (Albany NY) *4*, 247-255.

Beisaw, A., Tsaytler, P., Koch, F., Schmitz, S.U., Melissari, M.-T., Senft, A.D., Wittler, L., Pennimpede, T., Macura, K., Herrmann, B.G., *et al.* (2018). BRACHYURY directs histone acetylation to target loci during mesoderm development. EMBO reports *19*, 118-134.

Belo, J.A., Bachiller, D., Agius, E., Kemp, C., Borges, A.C., Marques, S., Piccolo, S., and De Robertis, E.M. (2000). Cerberus-like is a secreted BMP and nodal antagonist not essential for mouse development. Genesis *26*, 265-270.

Belo, J.A., Bouwmeester, T., Leyns, L., Kertesz, N., Gallo, M., Follettie, M., and De Robertis, E.M. (1997). Cerberus-like is a secreted factor with neutralizing activity expressed in the anterior primitive endoderm of the mouse gastrula. Mechanisms of Development *68*, 45-57.

Bernardo, A.S., Faial, T., Gardner, L., Niakan, K.K., Ortmann, D., Senner, C.E., Callery, E.M., Trotter, M.W., Hemberger, M., Smith, J.C., *et al.* (2011). BRACHYURY and CDX2 mediate BMP-induced differentiation of human and mouse pluripotent stem cells into embryonic and extraembryonic lineages. Cell Stem Cell *9*, 144-155.
Bhattacharya, S., Michels, C.L., Leung, M.K., Arany, Z.P., Kung, A.L., and Livingston, D.M. (1999). Functional role of p35srj, a novel p300/CBP binding protein, during transactivation by HIF-1. Genes Dev *13*, 64-75.
Biase, F.H., Rabel C Fau - Guillomot, M., Guillomot M Fau - Sandra, O., Sandra O Fau - Andropolis, K., Andropolis K Fau - Olmstead, C., Olmstead C Fau - Oliveira, R., Oliveira R Fau - Wallace, R., Wallace R Fau - Le Bourhis, D., Le Bourhis D Fau - Richard, C., Richard C Fau - Campion, E., *et al.* (2013). Changes in WNT signaling-related gene expression associated with development and cloning in bovine extra-embryonic and endometrial tissues during the peri-implantation period. Mol Reprod Dev *80*, 977-987.
Bishopric, N.H. (2005). Evolution of the heart from bacteria to man. Ann N Y Acad Sci *1047*, 13-29.
Blanpain, C., Mohrin, M., Sotiropoulou, P.A., and Passegué, E. (2011). DNA-Damage Response in Tissue-Specific and Cancer Stem Cells. Cell Stem Cell *8*, 16-29.
Blue, G.M., Kirk, E.P., Sholler, G.F., Harvey, R.P., and Winlaw, D.S. (2012). Congenital heart disease: current knowledge about causes and inheritance. Med J Aust *197*, 155-159.
Bo, H., Ghazizadeh, M., Shimizu, H., Kurihara, Y., Egawa, S., Moriyama, Y., Tajiri, T., and Kawanami, O. (2004). Effect of ionizing irradiation on human esophageal cancer cell lines by cDNA microarray gene expression analysis. J Nippon Med Sch *71*, 172-180.
Boege, Y., Malehmir, M., Healy, M.E., Bettermann, K., Lorentzen, A., Vucur, M., Ahuja, A.K., Böhm, F., Mertens, J.C., Shimizu, Y., *et al.* (2017). A Dual Role of Caspase-8 in Triggering and Sensing Proliferation-Associated DNA Damage, a Key Determinant of Liver Cancer Development. Cancer Cell *32*, 342-359 e310.
Boettger, T., Braun, T., and van Rooij, E. (2012). A New Level of Complexity. Circulation Research *110*, 1000-1013.
Bomsztyk, K., Mar, D., An, D., Sharifian, R., Mikula, M., Gharib, S.A., Altemeier, W.A., Liles, W.C., and Denisenko, O. (2015). Experimental acute lung injury induces multi-organ epigenetic modifications in key angiogenic genes implicated in sepsis-associated endothelial dysfunction. Crit Care *19*, 225.
Bondue, A., Lapouge, G., Paulissen, C., Semeraro, C., Iacovino, M., Kyba, M., and Blanpain, C. (2008). Mesp1 acts as a master regulator of multipotent cardiovascular progenitor specification. Cell Stem Cell *3*, 69-84.
Boroviak, T., Stirparo, G.G., Dietmann, S., Hernando-Herraez, I., Mohammed, H., Reik, W., Smith, A., Sasaki, E., Nichols, J., and Bertone, P. (2018). Single cell transcriptome analysis of human, marmoset and mouse embryos reveals common and divergent features of preimplantation development. Development *145*, dev167833.
Bouquet, F., Muller, C., and Salles, B. (2006). The loss of gammaH2AX signal is a marker of DNA double strand breaks repair only at low levels of DNA damage. Cell Cycle *5*, 1116-1122.
Boyer, L.A., Lee, T.I., Cole, M.F., Johnstone, S.E., Levine, S.S., Zucker, J.P., Guenther, M.G., Kumar, R.M., Murray, H.L., Jenner, R.G., *et al.* (2005). Core transcriptional regulatory circuitry in human embryonic stem cells. Cell *122*, 947-956.
Boyer, L.A., Mathur, D., and Jaenisch, R. (2006). Molecular control of pluripotency. Current Opinion in Genetics & Development *16*, 455-462.
Bradford, M.M. (1976). A rapid and sensitive method for the quantitation of microgram quantities of protein utilizing the principle of protein-dye binding. Anal Biochem *72*, 248-254.

Braganca, J., Lopes, J.A., Mendes-Silva, L., and Almeida Santos, J.M. (2019). Induced pluripotent stem cells, a giant leap for mankind therapeutic applications. World J Stem Cells *11*, 421-430.
Bragança, J., Mendes-Silva, L., and Lopes, J.A.C. (2019). CITED Proteins in the Heart of Pluripotent Cells and in Heart's Full Potential. Regenerative Medicine Frontiers.
Brennan, J., Lu, C.C., Norris, D.P., Rodriguez, T.A., Beddington, R.S., and Robertson, E.J. (2001). Nodal signalling in the epiblast patterns the early mouse embryo. Nature *411*, 965-969.
Brown, M.A., Rajamarthandan, S., Francis, B., O'Leary-Kelly, M.K., and Sinha, P. (2020). Update on stem cell technologies in congenital heart disease. J Card Surg *35*, 174-179.
Bruneau, B.G., Nemer, G., Schmitt, J.P., Charron, F., Robitaille, L., Caron, S., Conner, D.A., Gessler, M., Nemer, M., Seidman, C.E., *et al.* (2001). A murine model of Holt-Oram syndrome defines roles of the T-box transcription factor Tbx5 in cardiogenesis and disease. Cell *106*, 709-721.
Buckingham, M., Meilhac, S., and Zaffran, S. (2005). Building the mammalian heart from two sources of myocardial cells. Nat Rev Genet *6*, 826-835.
Buikema, J.W., Mady, A.S., Mittal, N.V., Atmanli, A., Caron, L., Doevendans, P.A., Sluijter, J.P., and Domian, I.J. (2013). Wnt/beta-catenin signaling directs the regional expansion of first and second heart field-derived ventricular cardiomyocytes. Development *140*, 4165-4176.
Cai, C.-L., Liang, X., Shi, Y., Chu, P.-H., Pfaff, S.L., Chen, J., and Evans, S. (2003). Isl1 identifies a cardiac progenitor population that proliferates prior to differentiation and contributes a majority of cells to the heart. Developmental Cell *5*, 877-889.
Cai, C.-L., Zhou, W., Yang, L., Bu, L., Qyang, Y., Zhang, X., Li, X., Rosenfeld, M.G., Chen, J., and Evans, S. (2005). T-box genes coordinate regional rates of proliferation and regional specification during cardiogenesis. Development *132*, 2475-2487.
Cai, C., Yu, Q.C., Jiang, W., Liu, W., Song, W., Yu, H., Zhang, L., Yang, Y., and Zeng, Y.A. (2014). R-spondin1 is a novel hormone mediator for mammary stem cell self-renewal. Genes Dev *28*, 2205-2218.
Cao, L.L., Guan, P.P., Liang, Y.Y., Huang, X.S., and Wang, P. (2019). Calcium Ions Stimulate the Hyperphosphorylation of Tau by Activating Microsomal Prostaglandin E Synthase 1. Front Aging Neurosci *11*.
Carvalho, B.S., and Irizarry, R.A. (2010). A framework for oligonucleotide microarray preprocessing. Bioinformatics *26*, 2363-2367.
Cha, J.M., Bae, H., Sadr, N., Manoucheri, S., Edalat, F., Kim, K., Kim, S.B., Kwon, I.K., Hwang, Y.-S., and Khademhosseini, A. (2015). Embryoid body size-mediated differential endodermal and mesodermal differentiation using polyethylene glycol (PEG) microwell array. Macromolecular Research *23*, 245-255.
Charneca, J., Matias, A.C., Escapa, A.L., Fernandes, C., Alves, A., Santos, J.M.A., Nascimento, R., and Braganca, J. (2017). Ectopic expression of CITED2 prior to reprogramming, promotes and homogenises the conversion of somatic cells into induced pluripotent stem cells. Experimental Cell Research *358*, 290-300.
Chatterjee, N., and Walker, G.C. (2017). Mechanisms of DNA damage, repair and mutagenesis. Environ Mol Mutagen *58*, 235-263.
Chazaud, C., Yamanaka, Y., Pawson, T., and Rossant, J. (2006). Early Lineage Segregation between Epiblast and Primitive Endoderm in Mouse Blastocysts through the Grb2-MAPK Pathway. Developmental Cell *10*, 615-624.
Chen, C.M., Bentham, J., Cosgrove, C., Braganca, J., Cuenda, A., Bamforth, S.D., Schneider, J.E., Watkins, H., Keavney, B., Davies, B., *et al.* (2012). Functional significance of SRJ domain mutations in CITED2. PLOS ONE *7*, e46256.

Chen, D., Xia, Y., Zuo, K., Wang, Y., Zhang, S., Kuang, D., Duan, Y., Zhao, X., and Wang, G. (2015). Crosstalk between SDF-1/CXCR4 and SDF-1/CXCR7 in cardiac stem cell migration. Scientific Reports *5*.
Chen, E.Y., Tan, C.M., Kou, Y., Duan, Q., Wang, Z., Meirelles, G.V., Clark, N.R., and Ma'ayan, A. (2013). Enrichr: interactive and collaborative HTML5 gene list enrichment analysis tool. BMC Bioinformatics *14*, 128.
Chen, H., Wong, C.-C., Liu, D., Go, M.Y.Y., Wu, B., Peng, S., Kuang, M., Wong, N., and Yu, J. (2019). APLN promotes hepatocellular carcinoma through activating PI3K/Akt pathway and is a druggable target. Theranostics *9*, 5246-5260.
Chen, L., Yabuuchi, A., Eminli, S., Takeuchi, A., Lu, C.-W., Hochedlinger, K., and Daley, G.Q. (2009). Cross-regulation of the Nanog and Cdx2 promoters. Cell Research *19*, 1052-1061.
Chen, X., Xu, H., Yuan, P., Fang, F., Huss, M., Vega, V.B., Wong, E., Orlov, Y.L., Zhang, W., Jiang, J., *et al.* (2008). Integration of external signaling pathways with the core transcriptional network in embryonic stem cells. Cell *133*, 1106-1117.
Chen, Y., Haviernik, P., Bunting, K.D., and Yang, Y.-C. (2007). Cited2 is required for normal hematopoiesis in the murine fetal liver. Blood *110*, 2889-2898.
Chiapparo, G., Lin, X., Lescroart, F., Chabab, S., Paulissen, C., Pitisci, L., Bondue, A., and Blanpain, C. (2016). Mesp1 controls the speed, polarity, and directionality of cardiovascular progenitor migration. The Journal of Cell Biology *213*, 463-477.
Chinn, A., Fitzsimmons, J., Shepard, T.H., and Fantel, A.G. (1989). Congenital heart disease among spontaneous abortuses and stillborn fetuses: prevalence and associations. Teratology *40*, 475-482.
Chowdhury, D., Keogh, M.-C., Ishii, H., Peterson, C.L., Buratowski, S., and Lieberman, J. (2005). gamma-H2AX dephosphorylation by protein phosphatase 2A facilitates DNA double-strand break repair. Molecular Cell *20*, 801-809.
Chuykin, I.A., Lianguzova, M.S., Pospelova, T.V., and Pospelov, V.A. (2008). Activation of DNA damage response signaling in mouse embryonic stem cells. Cell Cycle *7*, 2922-2928.
Cleaver, J.E. (2011). gamma H2Ax: Biomarker of Damage or Functional Participant in DNA Repair "All that Glitters Is not Gold!". Photochemistry and Photobiology *87*, 1230-1239.
ClinicalTrials.gov. https://clinicaltrials.gov/.
Creyghton, M.P., Cheng, A.W., Welstead, G.G., Kooistra, T., Carey, B.W., Steine, E.J., Hanna, J., Lodato, M.A., Frampton, G.M., Sharp, P.A., *et al.* (2010). Histone H3K27ac separates active from poised enhancers and predicts developmental state. Proceedings of the National Academy of Sciences *107*, 21931-21936.
Currie, G., and Delles, C. (2018). Precision Medicine and Personalized Medicine in Cardiovascular Disease. Adv Exp Med Biol *1065*, 589-605.
D'Angelo, W., Chen, B., Gurung, C., and Guo, Y.L. (2018). Characterization of embryonic stem cell-differentiated fibroblasts as mesenchymal stem cells with robust expansion capacity and attenuated innate immunity. In Stem Cell Res Ther.
Dahle, Ø., Kumar, A., and Kuehn, M.R. (2010). Nodal signaling recruits the histone demethylase Jmjd3 to counteract polycomb-mediated repression at target genes. Sci Signal *3*, ra48.
Dahm-Daphi, J., Sass, C., and Alberti, W. (2000). Comparison of biological effects of DNA damage induced by ionizing radiation and hydrogen peroxide in CHO cells. Int J Radiat Biol *76*, 67-75.
David, R., Jarsch, V.B., Schwarz, F., Nathan, P., Gegg, M., Lickert, H., and Franz, W.-M. (2011). Induction of MesP1 by Brachyury(T) generates the common multipotent cardiovascular stem cell. Cardiovascular Research *92*, 115-122.
Davis, C.A., Haberland, M., Arnold, M.A., Sutherland, L.B., McDonald, O.G., Richardson, J.A., Childs, G., Harris, S., Owens, G.K., and Olson, E.N. (2006). PRISM/PRDM6, a

transcriptional repressor that promotes the proliferative gene program in smooth muscle cells. Molecular and Cellular Biology *26*, 2626-2636.
De Guzman, R.N., Martinez-Yamout, M.A., Dyson, H.J., and Wright, P.E. (2004). Interaction of the TAZ1 Domain of the CREB-Binding Protein with the Activation Domain of CITED2: REGULATION BY COMPETITION BETWEEN INTRINSICALLY UNSTRUCTURED LIGANDS FOR NON-IDENTICAL BINDING SITES. Journal of Biological Chemistry *279*, 3042-3049.
de Pater, E., Ciampricotti, M., Priller, F., Veerkamp, J., Strate, I., Smith, K., Lagendijk, A.K., Schilling, T.F., Herzog, W., Abdelilah-Seyfried, S., *et al.* (2012). Bmp signaling exerts opposite effects on cardiac differentiation. Circulation Research *110*, 578-587.
Deng, X., Zhou, J., Li, F.-F., Yan, P., Zhao, E.-Y., Hao, L., Yu, K.-J., and Liu, S.-L. (2014). Characterization of nodal/TGF-lefty signaling pathway gene variants for possible roles in congenital heart diseases. PLOS ONE *9*, e104535.
Dinant, C., Houtsmuller, A.B., and Vermeulen, W. (2008). Chromatin structure and DNA damage repair. Epigenetics & Chromatin *1*, 9.
Dunwoodie, S.L., Rodriguez, T.A., and Beddington, R.S. (1998). Msg1 and Mrg1, founding members of a gene family, show distinct patterns of gene expression during mouse embryogenesis. Mechanisms of Development *72*, 27-40.
Edupuganti, R.R., Harikumar, A., Aaronson, Y., Biran, A., Sailaja, B.S., Nissim-Rafinia, M., Azad, G.K., Cohen, M.A., Park, J.E., Shivalila, C.S., *et al.* (2017). Alternative SET/TAFI Promoters Regulate Embryonic Stem Cell Differentiation. Stem Cell Reports *9*, 1291-1303.
Ema, M., Takahashi, S., and Rossant, J. (2006). Deletion of the selection cassette, but not cis-acting elements, in targeted Flk1-lacZ allele reveals Flk1 expression in multipotent mesodermal progenitors. Blood *107*, 111-117.
Encode (2022). Gene: CITED2 (ENSG00000164442) - Gene tree - Homo_sapiens - Ensembl genome browser 106. https://wwwensemblorg/Homo_sapiens/Gene/Compara_Tree?collapse=5140331,5140424,5140380,5140337,5140500,5140476,5140463,5140366,5140427,5140480,5140323,5140154,5140344,5140465,5140501,5140558;db=core;g=ENSG00000164442;r=6:139371807-139374648.
Eurocat (2022). European Platform on Rare Disease Registration. https://eu-rd-platformjrceceuropaeu
https://eu-rd-platformjrceceuropaeu/eurocat/eurocat-data/prevalence_en?$0-0$1-$-1-39,29,2,90,21,3,60,88,81,66,5,34,33,49,10,79,18,104,8,23,13,59,67,28,30,93,86,20,62,72,73,84,68,57,70,92,95$Cprevalence_table$X0_-1-a$X0_9-pre

Evans, M.J., and Kaufman, M.H. (1981). Establishment in culture of pluripotential cells from mouse embryos. Nature *292*, 154-156.
Faggioni, M., and Knollmann, B.C. (2012). Calsequestrin 2 and arrhythmias.
Fahed, A.C., and Nemer, G.M. (2012). Genetic Causes of Syndromic and Non-Syndromic Congenital Heart Disease (IntechOpen).
Faucherre, A., and Jopling, C. (2013). The heart's content-renewable resources. International journal of cardiology *167*.
Fei, Q., Yang, X., Jiang, H., Wang, Q., Yu, Y., Yi, W., Zhou, S., Chen, T., Lu, C., Atadja, P., *et al.* (2015). SETDB1 modulates PRC2 activity at developmental genes independently of H3K9 trimethylation in mouse ES cells. Genome Research *25*, 1325-1335.

Feil, R., Wagner, J.r., Metzger, D., and Chambon, P. (1997). Regulation of Cre Recombinase Activity by Mutated Estrogen Receptor Ligand-Binding Domains. Biochemical and Biophysical Research Communications *237*, 752-757.
Ferguson, J.E., Wu, Y., Smith, K., Charles, P., Powers, K., Wang, H., and Patterson, C. (2007). ASB4 is a hydroxylation substrate of FIH and promotes vascular differentiation via an oxygen-dependent mechanism. Molecular and Cellular Biology *27*, 6407-6419.
Fernandez-Capetillo, O., Lee, A., Nussenzweig, M., and Nussenzweig, A. (2004). H2AX: the histone guardian of the genome. DNA Repair *3*, 959-967.
Ferraro, F., Celso, C.L., and Scadden, D. (2010). Adult Stem Cells and Their Niches. Adv Exp Med Biol *695*, 155-168.
Fischer, L.A., Khan, S.A., and Theunissen, T.W. (2022). Induction of Human Naïve Pluripotency Using 5i/L/A Medium. Methods in Molecular Biology (Clifton, NJ) *2416*, 13-28.
Fiuza-Luces, C., Santos-Lozano, A., Joyner, M., Carrera-Bastos, P., Picazo, O., Zugaza, J.L., Izquierdo, M., Ruilope, L.M., and Lucia, A. (2018). Exercise benefits in cardiovascular disease: beyond attenuation of traditional risk factors. Nat Rev Cardiol *15*, 731-743.
Flores, D.J., Duong, T., Brandenberger, L.O., Mitra, A., Shirali, A., Johnson, J.C., Springer, D., Noguchi, A., Yu, Z.-X., Ebert, S.N., *et al.* (2018). Conditional ablation and conditional rescue models for Casq2 elucidate the role of development and of cell-type specific expression of Casq2 in the CPVT2 phenotype. Human Molecular Genetics *27*, 1533-1544.
Fortini, P., Ferretti, C., and Dogliotti, E. (2013). The response to DNA damage during differentiation: pathways and consequences. Mutat Res *743-744*, 160-168.
Freedman, S.J., Sun, Z.Y.J., Kung, A.L., France, D.S., Wagner, G., and Eck, M.J. (2003). Structural basis for negative regulation of hypoxia-inducible factor-1 alpha by CITED2. Nat Struct Biol *10*, 504-512.
Fritsch, C., Lanfear, R., and Ray, R.P. (2010). Rapid evolution of a novel signalling mechanism by concerted duplication and divergence of a BMP ligand and its extracellular modulators. Development Genes and Evolution *220*, 235-250.
Fu, X., Wu, S., Li, B., Xu, Y., and Liu, J. (2020). Functions of p53 in pluripotent stem cells. Protein Cell *11*, 71-78.
Fujimori, H., Asahina, K., Shimizu-Saito, K., Ikeda, R., Tanaka, Y., Teramoto, K., Morita, I., and Teraoka, H. (2008). Vascular endothelial growth factor promotes proliferation and function of hepatocyte-like cells in embryoid bodies formed from mouse embryonic stem cells. J Hepatol *48*, 962-973.
Garrido, C., Galluzzi, L., Brunet, M., Puig, P.E., Didelot, C., and Kroemer, G. (2006). Mechanisms of cytochrome c release from mitochondria. Cell Death Differ *13*, 1423-1433.
Ghimire, S., Mantziou, V., Moris, N., and Martinez Arias, A. (2021). Human gastrulation: The embryo and its models. Developmental Biology *474*, 100-108.
Gilbert, S.F. (2000). Early Mammalian Development. Developmental Biology 6th edition.
Glenn, D.J., and Maurer, R.A. (1999). MRG1 binds to the LIM domain of Lhx2 and may function as a coactivator to stimulate glycoprotein hormone alpha-subunit gene expression. The Journal of Biological Chemistry *274*, 36159-36167.
Godin, S.K., Sullivan, M.R., and Bernstein, K.A. (2016). Novel insights into RAD51 activity and regulation during homologous recombination and DNA replication. Biochem Cell Biol *94*, 407-418.
Graf, T., and Stadtfeld, M. (2008). Heterogeneity of Embryonic and Adult Stem Cells. Cell Stem Cell *3*, 480-483.
Granier, C.J., Wang, W., Tsang, T., Steward, R., Sabaawy, H.E., Bhaumik, M., and Rabson, A.B. (2014). Conditional inactivation of PDCD2 induces p53 activation and cell cycle arrest. Biology Open *3*, 821-831.

Gu, W., and Roeder, R.G. (1997). Activation of p53 sequence-specific DNA binding by acetylation of the p53 C-terminal domain. Cell *90*, 595-606.
Gurley, K.E., and Kemp, C.J. (1996). p53 induction, cell cycle checkpoints, and apoptosis in DNAPK- deficient scid mice. Carcinogenesis *17*, 2537-2542.
Haun, C., Alexander, J., Stainier, D.Y., and Okkema, P.G. (1998). Rescue of Caenorhabditis elegans pharyngeal development by a vertebrate heart specification gene. Proceedings of the National Academy of Sciences of the United States of America *95*, 5072-5075.
Hayashi, K., Erikson, D.W., Tilford, S.A., Bany, B.M., Maclean, J.A., Rucker, E.B., Johnson, G.A., and Spencer, T.E. (2009). Wnt Genes in the Mouse Uterus: Potential Regulation of Implantation. Biol Reprod *80*, 989-1000.
Heid, C.A., Stevens, J., Livak, K.J., and Williams, P.M. (1996). Real time quantitative PCR. Genome Research *6*, 986-994.
Helker, C.S.M., Schuermann, A., Pollmann, C., Chng, S.C., Kiefer, F., Reversade, B., and Herzog, W. (2015). The hormonal peptide Elabela guides angioblasts to the midline during vasculogenesis. Elife *4*.
Hirao, A., Kong, Y.Y., Matsuoka, S., Wakeham, A., Ruland, J., Yoshida, H., Liu, D., Elledge, S.J., and Mak, T.W. (2000). DNA damage-induced activation of p53 by the checkpoint kinase Chk2. Science *287*, 1824-1827.
Hoffman, J.I.E. (2013). The global burden of congenital heart disease. Cardiovasc J Afr *24*, 141-145.
Holmqvist, P.-H., Boija, A., Philip, P., Crona, F., Stenberg, P., and Mannervik, M. (2012). Preferential genome targeting of the CBP co-activator by Rel and Smad proteins in early Drosophila melanogaster embryos. PLoS genetics *8*, e1002769.
Holmqvist, P.-H., and Mannervik, M. (2013). Genomic occupancy of the transcriptional co-activators p300 and CBP. Transcription *4*, 18-23.
Hong, L., Li, N., Gasque, V., Mehta, S., Ye, L., Wu, Y., Li, J., Gewies, A., Ruland, J., Hirschi, K.K., *et al.* (2022). Prdm6 controls heart development by regulating neural crest cell differentiation and migration. JCI Insight *7*, e156046.
Houtgraaf, J.H., Versmissen, J., and van der Giessen, W.J. (2006). A concise review of DNA damage checkpoints and repair in mammalian cells. Cardiovasc Revasc Med *7*, 165-172.
Hu, Z., Liu, Y., Zhang, C., Zhao, Y., He, W., Han, L., Yang, L., Hopkins, K.M., Yang, X., Lieberman, H.B., *et al.* (2008). Targeted deletion of Rad9 in mouse skin keratinocytes enhances genotoxin-induced tumor development. Cancer Research *68*, 5552-5561.
Huang, D., Guo, G., Yuan, P., Ralston, A., Sun, L., Huss, M., Mistri, T., Pinello, L., Ng, H.H., Yuan, G., *et al.* (2017). The role of Cdx2 as a lineage specific transcriptional repressor for pluripotent network during the first developmental cell lineage segregation. Scientific Reports *7*, 17156.
Hyatt, B.A., and Yost, H.J. (1998). The left-right coordinator: the role of Vg1 in organizing left-right axis formation. Cell *93*, 37-46.
Ichikawa, T., Nakazato, K., Keller, P.J., Kajiura-Kobayashi, H., Stelzer, E.H.K., Mochizuki, A., and Nonaka, S. (2013). Live Imaging of Whole Mouse Embryos during Gastrulation: Migration Analyses of Epiblast and Mesodermal Cells. PLOS ONE *8*, e64506.
Ivanova, N., Dobrin, R., Lu, R., Kotenko, I., Levorse, J., DeCoste, C., Schafer, X., Lun, Y., and Lemischka, I.R. (2006). Dissecting self-renewal in stem cells with RNA interference. Nature *442*, 533-538.
Jackson, M., Fidanza, A., Taylor, A.H., Rybtsov, S., Axton, R., Kydonaki, M., Meek, S., Burdon, T., Medvinsky, A., and Forrester, L.M. (2021). Modulation of APLNR Signaling Is Required during the Development and Maintenance of the Hematopoietic System. Stem Cell Reports *16*, 727-740.

Jang, H.J., Kim, J.S., Choi, H.W., Jeon, I., Choi, S., Kim, M.J., Song, J., and Do, J.T. (2014). Neural stem cells derived from epiblast stem cells display distinctive properties. Stem Cell Research *12*, 506-516.
Jeziorowska, D., Fontaine, V., Jouve, C., Villard, E., Dussaud, S., Akbar, D., Letang, V., Cervello, P., Itier, J.-M., Pruniaux, M.-P., *et al.* (2017). Differential Sarcomere and Electrophysiological Maturation of Human iPSC-Derived Cardiac Myocytes in Monolayer vs. Aggregation-Based Differentiation Protocols. International Journal of Molecular Sciences *18*, E1173.
Johnson, T.M., Yu, Z.X., Ferrans, V.J., Lowenstein, R.A., and Finkel, T. (1996). Reactive oxygen species are downstream mediators of p53-dependent apoptosis. Proceedings of the National Academy of Sciences of the United States of America *93*, 11848-11852.
Jumper, J., Evans, R., Pritzel, A., Green, T., Figurnov, M., Ronneberger, O., Tunyasuvunakool, K., Bates, R., Zidek, A., Potapenko, A., *et al.* (2021). Highly accurate protein structure prediction with AlphaFold. Nature *596*, 583-589.
Kapinas, K., Grandy, R., Ghule, P., Medina, R., Becker, K., Pardee, A., Zaidi, S.K., Lian, J., Stein, J., van Wijnen, A., *et al.* (2013). The abbreviated pluripotent cell cycle. Journal of Cellular Physiology *228*, 9-20.
Kashyap, V., Rezende, N.C., Scotland, K.B., Shaffer, S.M., Persson, J.L., Gudas, L.J., and Mongan, N.P. (2009). Regulation of Stem Cell Pluripotency and Differentiation Involves a Mutual Regulatory Circuit of the Nanog, OCT4, and SOX2 Pluripotency Transcription Factors With Polycomb Repressive Complexes and Stem Cell microRNAs. Stem Cells and Development *18*, 1093-1108.
Kassambara, A. (2020). ggpubr: 'ggplot2' based publication ready plots.
Kassambara, A. (2021). rstatix: Pipe-friendly framework for basic statistical tests.
Katoh, N., Kuroda, K., Tomikawa, J., Ogata-Kawata, H., Ozaki, R., Ochiai, A., Kitade, M., Takeda, S., Nakabayashi, K., and Hata, K. (2018). Reciprocal changes of H3K27ac and H3K27me3 at the promoter regions of the critical genes for endometrial decidualization. Epigenomics *10*, 1243-1257.
Katsu, K., N, T., D, N., K, Y., and Y, Y. (2013). Multi-modal effects of BMP signaling on Nodal expression in the lateral plate mesoderm during left-right axis formation in the chick embryo. Developmental Biology *374*.
Katsube, T., Mori, M., Tsuji, H., Shiomi, T., Wang, B., Liu, Q., Nenoi, M., and Onoda, M. (2014). Most hydrogen peroxide-induced histone H2AX phosphorylation is mediated by ATR and is not dependent on DNA double-strand breaks. J Biochem *156*, 85-95.
Kemp, C., Willems, E., Abdo, S., Lambiv, L., and Leyns, L. (2005). Expression of all Wnt genes and their secreted antagonists during mouse blastocyst and postimplantation development. Dev Dyn *233*, 1064-1075.
Keramari, M., Razavi, J., Ingman, K.A., Patsch, C., Edenhofer, F., Ward, C.M., and Kimber, S.J. (2010). Sox2 Is Essential for Formation of Trophectoderm in the Preimplantation Embryo. PLOS ONE *5*, e13952.
Kim, D.-K., Cha, Y., Ahn, H.-J., Kim, G., and Park, K.-S. (2014). Lefty1 and lefty2 control the balance between self-renewal and pluripotent differentiation of mouse embryonic stem cells. Stem Cells and Development *23*, 457-466.
Kimbrel, E.A., and Lanza, R. (2015). Current status of pluripotent stem cells: moving the first therapies to the clinic. Nat Rev Drug Discov *14*, 681-692.
Kitajima, S., Takagi, A., Inoue, T., and Saga, Y. (2000). MesP1 and MesP2 are essential for the development of cardiac mesoderm. Development *127*, 3215-3226.
Kivimäki, M., and Steptoe, A. (2018). Effects of stress on the development and progression of cardiovascular disease. Nat Rev Cardiol *15*, 215-229.

Koga, M., Matsuda, M., Kawamura, T., Sogo, T., Shigeno, A., Nishida, E., and Ebisuya, M. (2014). Foxd1 is a mediator and indicator of the cell reprogramming process. Nature Communications *5*, 3197.
Kouskoff, V., Lacaud, G., Schwantz, S., Fehling, H.J., and Keller, G. (2005). Sequential development of hematopoietic and cardiac mesoderm during embryonic stem cell differentiation. Proceedings of the National Academy of Sciences of the United States of America *102*, 13170-13175.
Kranc, K.R., Oliveira, D.V., Armesilla-Diaz, A., Pacheco-Leyva, I., Catarina Matias, A., Luisa Escapa, A., Subramani, C., Wheadon, H., Trindade, M., Nichols, J., *et al.* (2015). Acute loss of Cited2 impairs Nanog expression and decreases self-renewal of mouse embryonic stem cells. Stem Cells *33*, 699-712.
Kranc, K.R., Schepers, H., Rodrigues, N.P., Bamforth, S., Villadsen, E., Ferry, H., Bouriez-Jones, T., Sigvardsson, M., Bhattacharya, S., Jacobsen, S.E., *et al.* (2009). Cited2 is an essential regulator of adult hematopoietic stem cells. Cell Stem Cell *5*, 659-665.
Krishnan, A., Samtani, R., Dhanantwari, P., Lee, E., Yamada, S., Shiota, K., Donofrio, M.T., Leatherbury, L., and Lo, C.W. (2014). A Detailed Comparison of Mouse and Human Cardiac Development. Pediatric research *76*, 500-507.
Kuerbitz, S.J., Plunkett, B.S., Walsh, W.V., and Kastan, M.B. (1992). Wild-type p53 is a cell cycle checkpoint determinant following irradiation. Proceedings of the National Academy of Sciences of the United States of America *89*, 7491-7495.
Kuleshov, M.V., Jones, M.R., Rouillard, A.D., Fernandez, N.F., Duan, Q., Wang, Z., Koplev, S., Jenkins, S.L., Jagodnik, K.M., Lachmann, A., *et al.* (2016). Enrichr: a comprehensive gene set enrichment analysis web server 2016 update. Nucleic Acids Research *44*, W90-97.
Kuo, L.J., and Yang, L.X. (2008). Gamma-H2AX - a novel biomarker for DNA double-strand breaks. In Vivo *22*, 305-309.
Kurtenbach, S., Reddy, R., and Harbour, J.W. (2019). ChIPprimersDB: a public repository of verified qPCR primers for chromatin immunoprecipitation (ChIP). Nucleic Acids Research *47*, D46-D49.
Kuzmichev, A., Margueron, R., Vaquero, A., Preissner, T.S., Scher, M., Kirmizis, A., Ouyang, X., Brockdorff, N., Abate-Shen, C., Farnham, P., *et al.* (2005). Composition and histone substrates of polycomb repressive group complexes change during cellular differentiation. Proceedings of the National Academy of Sciences of the United States of America *102*, 1859-1864.
Lee, T., and Pelletier, J. (2017). Dependence of p53-deficient cells on the DHX9 DExH-box helicase. In Oncotarget, pp. 30908-30921.
Lee, T.I., Jenner, R.G., Boyer, L.A., Guenther, M.G., Levine, S.S., Kumar, R.M., Chevalier, B., Johnstone, S.E., Cole, M.F., Isono, K.-i., *et al.* (2006). Control of developmental regulators by Polycomb in human embryonic stem cells. Cell *125*, 301-313.
Leloup, C., Hopkins, K.M., Wang, X., Zhu, A., Wolgemuth, D.J., and Lieberman, H.B. (2010). Mouse Rad9b is essential for embryonic development and promotes resistance to DNA damage. Dev Dyn *239*, 2837-2850.
Li, J.J., Liu, J., Lupino, K., Liu, X., Zhang, L., and Pei, L. (2018). Growth Differentiation Factor 15 Maturation Requires Proteolytic Cleavage by PCSK3, -5, and -6. Molecular and Cellular Biology *38*, e00249-00218.
Li, M., He, Y., Dubois, W., Wu, X., Shi, J., and Huang, J. (2012a). Distinct regulatory mechanisms and functions of p53-activated and p53-repressed DNA damage response genes in embryonic stem cells. Molecular Cell *46*, 30-42.
Li, N., Subrahmanyan, L., Smith, E., Yu, X., Zaidi, S., Choi, M., Mane, S., Nelson-Williams, C., Behjati, M., Kazemi, M., *et al.* (2016). Mutations in the Histone Modifier PRDM6 Are

Associated with Isolated Nonsyndromic Patent Ductus Arteriosus. Am J Hum Genet *98*, 1082-1091.
Li, Q., Hakimi, P., Liu, X., Yu, W.-M., Ye, F., Fujioka, H., Raza, S., Shankar, E., Tang, F., Dunwoodie, S.L., *et al.* (2014). Cited2, a transcriptional modulator protein, regulates metabolism in murine embryonic stem cells. The Journal of Biological Chemistry *289*, 251-263.
Li, Q., Ramírez-Bergeron, D.L., Dunwoodie, S.L., and Yang, Y.-C. (2012b). Cited2 gene controls pluripotency and cardiomyocyte differentiation of murine embryonic stem cells through Oct4 gene. The Journal of Biological Chemistry *287*, 29088-29100.
Lian, X., Hsiao, C., Wilson, G., Zhu, K., Hazeltine, L.B., Azarin, S.M., Raval, K.K., Zhang, J., Kamp, T.J., and Palecek, S.P. (2012). Robust cardiomyocyte differentiation from human pluripotent stem cells via temporal modulation of canonical Wnt signaling. Proceedings of the National Academy of Sciences of the United States of America *109*, E1848-1857.
Lieberman, H.B. (2006). Rad9, an evolutionarily conserved gene with multiple functions for preserving genomic integrity. J Cell Biochem *97*, 690-697.
Lin, T., Chao, C., Saito, S.i., Mazur, S.J., Murphy, M.E., Appella, E., and Xu, Y. (2005). p53 induces differentiation of mouse embryonic stem cells by suppressing Nanog expression. Nature Cell Biology *7*, 165-171.
Liu, C., Wang, R., He, Z., Osteil, P., Wilkie, E., Yang, X., Chen, J., Cui, G., Guo, W., Chen, Y., *et al.* (2018a). Suppressing Nodal Signaling Activity Predisposes Ectodermal Differentiation of Epiblast Stem Cells. Stem Cell Reports *11*, 43-57.
Liu, F., Kang, I., Park, C., Chang, L.-W., Wang, W., Lee, D., Lim, D.-S., Vittet, D., Nerbonne, J.M., and Choi, K. (2012). ER71 specifies Flk-1+ hemangiogenic mesoderm by inhibiting cardiac mesoderm and Wnt signaling. Blood *119*, 3295-3305.
Liu, L., Scolnick, D.M., Trievel, R.C., Zhang, H.B., Marmorstein, R., Halazonetis, T.D., and Berger, S.L. (1999a). p53 Sites Acetylated In Vitro by PCAF and p300 Are Acetylated In Vivo in Response to DNA Damage. Molecular and Cellular Biology *19*, 1202-1209.
Liu, P., Dou, X., Liu, C., Wang, L., Xing, C., Peng, G., Chen, J., Yu, F., Qiao, Y., Song, L., *et al.* (2015a). Histone deacetylation promotes mouse neural induction by restricting Nodal-dependent mesendoderm fate. Nature Communications *6*, 6830.
Liu, P., Wakamiya, M., Shea, M.J., Albrecht, U., Behringer, R.R., and Bradley, A. (1999b). Requirement for Wnt3 in vertebrate axis formation. Nature Genetics *22*, 361-365.
Liu, S., Liu, J., Tang, J., Ji, J., Chen, J., and Liu, C. (2009). Environmental risk factors for congenital heart disease in the Shandong Peninsula, China: a hospital-based case-control study. J Epidemiol *19*, 122-130.
Liu, X., Huang, J., Chen, T., Wang, Y., Xin, S., Li, J., Pei, G., and Kang, J. (2008). Yamanaka factors critically regulate the developmental signaling network in mouse embryonic stem cells. Cell Research *18*, 1177-1189.
Liu, Y., Chen, S., Zühlke, L., Black, G.C., Choy, M.-K., Li, N., and Keavney, B.D. (2019). Global birth prevalence of congenital heart defects 1970-2017: updated systematic review and meta-analysis of 260 studies. Int J Epidemiol *48*, 455-463.
Liu, Y.C., Chang, P.Y., and Chao, C.C. (2015b). CITED2 silencing sensitizes cancer cells to cisplatin by inhibiting p53 trans-activation and chromatin relaxation on the ERCC1 DNA repair gene. Nucleic Acids Research *43*, 10760-10781.
Liu, Y.W., Chen, B., Yang, X., Fugate, J.A., Kalucki, F.A., Futakuchi-Tsuchida, A., Couture, L., Vogel, K.W., Astley, C.A., Baldessari, A., *et al.* (2018b). Human embryonic stem cell-derived cardiomyocytes restore function in infarcted hearts of non-human primates. Nat Biotechnol *36*, 597-605.
Livak, K.J., and Schmittgen, T.D. (2001). Analysis of relative gene expression data using real-time quantitative PCR and the 2(-Delta Delta C(T)) Method. Methods *25*, 402-408.

Loh, K.M., Ang, L.T., Zhang, J., Kumar, V., Ang, J., Auyeong, J.Q., Lee, K.L., Choo, S.H., Lim, C.Y.Y., Nichane, M., *et al.* (2014). Efficient endoderm induction from human pluripotent stem cells by logically directing signals controlling lineage bifurcations. Cell Stem Cell *14*, 237-252.
Loh, K.M., Lim, B., and Ang, L.T. (2015). Ex Uno Plures: Molecular Designs for Embryonic Pluripotency. Physiological Reviews *95*, 245-295.
Loh, K.M., van Amerongen, R., and Nusse, R. (2016). Generating Cellular Diversity and Spatial Form: Wnt Signaling and the Evolution of Multicellular Animals. Developmental Cell *38*, 643-655.
Lombard, D.B., Beard, C., Johnson, B., Marciniak, R.A., Dausman, J., Bronson, R., Buhlmann, J.E., Lipman, R., Curry, R., Sharpe, A., *et al.* (2000). Mutations in the WRN Gene in Mice Accelerate Mortality in a p53-Null Background. Molecular and Cellular Biology *20*, 3286-3291.
Lou, Z., Minter-Dykhouse, K., Franco, S., Gostissa, M., Rivera, M.A., Celeste, A., Manis, J.P., van Deursen, J., Nussenzweig, A., Paull, T.T., *et al.* (2006). MDC1 maintains genomic stability by participating in the amplification of ATM-dependent DNA damage signals. Molecular Cell *21*, 187-200.
Lowndes, N.F., and Toh, G.W. (2005). DNA repair: the importance of phosphorylating histone H2AX. Curr Biol *15*, R99-R102.
Lund-Johansen, F., and Browning, M.D. (2017). Should we ignore western blots when selecting antibodies for other applications? Nature Methods *14*, 215-215.
Lyons, I., Parsons, L.M., Hartley, L., Li, R., Andrews, J.E., Robb, L., and Harvey, R.P. (1995). Myogenic and morphogenetic defects in the heart tubes of murine embryos lacking the homeo box gene Nkx2-5. Genes Dev *9*, 1654-1666.
Lyublinskaya, O.G., Ivanova, J.S., Pugovkina, N.A., Kozhukharova, I.V., Kovaleva, Z.V., Shatrova, A.N., Aksenov, N.D., Zenin, V.V., Kaulin, Y.A., Gamaley, I.A., *et al.* (2017). Redox environment in stem and differentiated cells: A quantitative approach. Redox Biol *12*, 758-769.
MacPhail, S.H., Banath, J.P., Yu, T.Y., Chu, E.H., Lambur, H., and Olive, P.L. (2003). Expression of phosphorylated histone H2AX in cultured cell lines following exposure to X-rays. Int J Radiat Biol *79*, 351-358.
Mannino, G., Russo, C., Maugeri, G., Musumeci, G., Vicario, N., Tibullo, D., Giuffrida, R., Parenti, R., and Lo Furno, D. (2022). Adult stem cell niches for tissue homeostasis. Journal of Cellular Physiology *237*, 239-257.
Martire, S., Gogate, A.A., Whitmill, A., Tafessu, A., Nguyen, J., Teng, Y.-C., Tastemel, M., and Banaszynski, L.A. (2019). Phosphorylation of histone H3.3 at serine 31 promotes p300 activity and enhancer acetylation. Nature Genetics *51*, 941-946.
Martire, S., Nguyen, J., Sundaresan, A., and Banaszynski, L.A. (2020). Differential contribution of p300 and CBP to regulatory element acetylation in mESCs. BMC Mol and Cell Biol *21*, 55.
Martyn, I., Siggia, E.D., and Brivanlou, A.H. (2019). Mapping cell migrations and fates in a gastruloid model to the human primitive streak. Development *146*, dev179564.
Massa, V., Avagliano, L., Grazioli, P., De Castro, S.C.P., Parodi, C., Savery, D., Vergani, P., Cuttin, S., Doi, P., Bulfamante, G., *et al.* (2019). Dynamic acetylation profile during mammalian neurulation. Birth Defects Res.
Mattes, K., Berger, G., Geugien, M., Vellenga, E., and Schepers, H. (2017). CITED2 affects leukemic cell survival by interfering with p53 activation. Cell Death & Disease *8*, e3132.
Maynard, S., Keijzers, G., Akbari, M., Ezra, M.B., Hall, A., Morevati, M., Scheibye-Knudsen, M., Gonzalo, S., Bartek, J., and Bohr, V.A. (2019). Lamin A/C promotes DNA base excision repair. Nucleic Acids Research.

McQuin, C., Goodman, A., Chernyshev, V., Kamentsky, L., Cimini, B.A., Karhohs, K.W., Doan, M., Ding, L.Y., Rafelski, S.M., Thirstrup, D., *et al.* (2018). CellProfiler 3.0: Next-generation image processing for biology. PLOS Biology *16*.
Melo, I.S., Braz, P., Roquette, R., Sousa, P., Nunes, C., and Dias, C. (2020). Congenital Heart Disease Prevalence in Portugal in 2015: Data from the National Register of Congenital Anomalies. Acta Med Port *33*, 491-499.
Menaissy, Y., Alkady, H., and El-Saiedi, S. (2019). Rescue Cardiac Surgeries After Pediatric Catheter-Based Interventions: A Ten-Year Retrospective Study. World J Pediatr Congenit Heart Surg *10*, 539-542.
Mendjan, S., Mascetti, V.L., Ortmann, D., Ortiz, M., Karjosukarso, D.W., Ng, Y., Moreau, T., and Pedersen, R.A. (2014). NANOG and CDX2 pattern distinct subtypes of human mesoderm during exit from pluripotency. Cell Stem Cell *15*, 310-325.
Meno, C., Gritsman, K., Ohishi, S., Ohfuji, Y., Heckscher, E., Mochida, K., Shimono, A., Kondoh, H., Talbot, W.S., Robertson, E.J., *et al.* (1999). Mouse Lefty2 and zebrafish antivin are feedback inhibitors of nodal signaling during vertebrate gastrulation. Molecular Cell *4*, 287-298.
Meshorer, E., and Misteli, T. (2006). Chromatin in pluripotent embryonic stem cells and differentiation. Nat Rev Mol Cell Biol *7*, 540-546.
Miller, A.J., Roman, B., and Norstrom, E. (2016). A method for easily customizable gradient gel electrophoresis. Analytical Biochemistry *509*, 12-14.
Milne, E., Royle, J.A., Miller, M., Bower, C., de Klerk, N.H., Bailey, H.D., van Bockxmeer, F., Attia, J., Scott, R.J., Norris, M.D., *et al.* (2010). Maternal folate and other vitamin supplementation during pregnancy and risk of acute lymphoblastic leukemia in the offspring. Int J Cancer *126*, 2690-2699.
Miyanari, Y., and Torres-Padilla, M.-E. (2012). Control of ground-state pluripotency by allelic regulation of Nanog. Nature *483*, 470-473.
Molè, M.A., Weberling, A., and Zernicka-Goetz, M. (2020). Comparative analysis of human and mouse development: From zygote to pre-gastrulation. Current Topics in Developmental Biology *136*, 113-138.
Montgomery, N.D., Yee, D., Chen, A., Kalantry, S., Chamberlain, S.J., Otte, A.P., and Magnuson, T. (2005). The murine polycomb group protein Eed is required for global histone H3 lysine-27 methylation. Curr Biol *15*, 942-947.
Moretti, A., Caron, L., Nakano, A., Lam, J.T., Bernshausen, A., Chen, Y., Qyang, Y., Bu, L., Sasaki, M., Martin-Puig, S., *et al.* (2006). Multipotent embryonic isl1+ progenitor cells lead to cardiac, smooth muscle, and endothelial cell diversification. Cell *127*, 1151-1165.
Morey, L., Aloia, L., Cozzuto, L., Benitah, S.A., and Di Croce, L. (2013). RYBP and Cbx7 define specific biological functions of polycomb complexes in mouse embryonic stem cells. Cell Reports *3*, 60-69.
Morgan, M.A.J., and Shilatifard, A. (2020). Reevaluating the roles of histone-modifying enzymes and their associated chromatin modifications in transcriptional regulation. Nature Genetics *52*, 1271-1281.
Morgani, S., Nichols, J., and Hadjantonakis, A.-K. (2017). The many faces of Pluripotency: in vitro adaptations of a continuum of in vivo states. BMC Developmental Biology *17*, 7.
Morris, S.A., Teo, R.T.Y., Li, H., Robson, P., Glover, D.M., and Zernicka-Goetz, M. (2010). Origin and formation of the first two distinct cell types of the inner cell mass in the mouse embryo. Proceedings of the National Academy of Sciences of the United States of America *107*, 6364-6369.
Morrison, S.J., and Kimble, J. (2006). Asymmetric and symmetric stem-cell divisions in development and cancer. Nature *441*, 1068-1074.

Morrison, S.J., and Scadden, D.T. (2014). The bone marrow niche for haematopoietic stem cells. Nature *505*, 327-334.
Muhr, J., and Ackerman, K.M. (2022). Embryology, Gastrulation (StatPearls Publishing).
Mulas, C., Kalkan, T., von Meyenn, F., Leitch, H.G., Nichols, J., and Smith, A. (2019). Correction: Defined conditions for propagation and manipulation of mouse embryonic stem cells (doi:10.1242/dev.173146). Development *146*.
Müller, F., and O'Rahilly, R. (2004). The primitive streak, the caudal eminence and related structures in staged human embryos. Cells Tissues Organs *177*, 2-20.
Müller, P., Lemcke, H., and David, R. (2018). Stem Cell Therapy in Heart Diseases - Cell Types, Mechanisms and Improvement Strategies. Cell Physiol Biochem *48*, 2607-2655.
Murray, P., and Edgar, D. (2001). The regulation of embryonic stem cell differentiation by leukaemia inhibitory factor (LIF). Differentiation *68*, 227-234.
Nakase, I., Niwa, M., Takeuchi, T., Sonomura, K., Kawabata, N., Koike, Y., Takehashi, M., Tanaka, S., Ueda, K., Simpson, J.C., *et al.* (2004). Cellular uptake of arginine-rich peptides: roles for macropinocytosis and actin rearrangement. Mol Ther *10*, 1011-1022.
Nascimento, R. (2015). Recombinant protein in diffrentiation of stem cells (Faro: Universidade do Algarve), pp. 90.
Ng, S.Y., Wong, C.K., and Tsang, S.Y. (2010). Differential gene expressions in atrial and ventricular myocytes: insights into the road of applying embryonic stem cell-derived cardiomyocytes for future therapies. Am J Physiol Cell Physiol *299*, C1234-1249.
Nichols, J., Silva, J., Roode, M., and Smith, A. (2009). Suppression of Erk signalling promotes ground state pluripotency in the mouse embryo. Development *136*, 3215-3222.
Nichols, J., and Smith, A. (2009). Naive and primed pluripotent states. Cell Stem Cell *4*, 487-492.
Nichols, J., Zevnik, B., Anastassiadis, K., Niwa, H., Klewe-Nebenius, D., Chambers, I., Schöler, H., and Smith, A. (1998). Formation of pluripotent stem cells in the mammalian embryo depends on the POU transcription factor Oct4. Cell *95*, 379-391.
Noe, A. (2004). The human embryo collection. Centennial history of the Carnegie Institution of Washington *5*, 21-61.
Noor, N., Shapira, A., Edri, R., Gal, I., Wertheim, L., and Dvir, T. (2019). 3D Printing of Personalized Thick and Perfusable Cardiac Patches and Hearts. Adv Sci *6*.
Obeid, R., Holzgreve, W., and Pietrzik, K. (2019). Folate supplementation for prevention of congenital heart defects and low birth weight: an update. Cardiovasc Diagn Ther *9*, S424-S433.
Oh, H. (2017). Cell Therapy Trials in Congenital Heart Disease. Circulation Research *120*, 1353-1366.
Ohkawara, B., Glinka, A., and Niehrs, C. (2011). Rspo3 binds syndecan 4 and induces Wnt/PCP signaling via clathrin-mediated endocytosis to promote morphogenesis. Developmental Cell *20*, 303-314.
Osmanagic-Myers, S., and Rezniczek, G.A. (2018). Arteriovenous specification: BMPER and TWSG1 determine endothelial cell fate via activation of synergistic BMP and Notch signaling. FEBS J *285*, 1399-1402.
Pacheco-Leyva, I., Matias, A.C., Oliveira, D.V., Santos, J.M., Nascimento, R., Guerreiro, E., Michell, A.C., van De Vrugt, A.M., Machado-Oliveira, G., Ferreira, G., *et al.* (2016). CITED2 Cooperates with ISL1 and Promotes Cardiac Differentiation of Mouse Embryonic Stem Cells. Stem Cell Reports *7*, 1037-1049.
Paige, S.L., Plonowska, K., Xu, A., and Wu, S.M. (2015). Molecular Regulation of Cardiomyocyte Differentiation. Circulation Research *116*, 341-353.
Pan, G., and Thomson, J.A. (2007). Nanog and transcriptional networks in embryonic stem cell pluripotency. Cell Research *17*, 42-49.

Paneni, F., Diaz Cañestro, C., Libby, P., Lüscher, T.F., and Camici, G.G. (2017). The Aging Cardiovascular System: Understanding It at the Cellular and Clinical Levels. Journal of the American College of Cardiology *69*, 1952-1967.
Park, J., Cho, C.H., Parashurama, N., Li, Y., Berthiaume, F., Toner, M., Tilles, A.W., and Yarmush, M.L. (2007). Microfabrication-based modulation of embryonic stem cell differentiation. Lab Chip *7*, 1018-1028.
Pasini, D., Malatesta, M., Jung, H.R., Walfridsson, J., Willer, A., Olsson, L., Skotte, J., Wutz, A., Porse, B., Jensen, O.N., *et al.* (2010). Characterization of an antagonistic switch between histone H3 lysine 27 methylation and acetylation in the transcriptional regulation of Polycomb group target genes. Nucleic Acids Research *38*, 4958-4969.
Perin, E.C., Silva, G.V., Henry, T.D., Cabreira-Hansen, M.G., Moore, W.H., Coulter, S.A., Herlihy, J.P., Fernandes, M.R., Cheong, B.Y.C., Flamm, S.D., *et al.* (2011). A randomized study of transendocardial injection of autologous bone marrow mononuclear cells and cell function analysis in ischemic heart failure (FOCUS-HF). Am Heart J *161*, 1078-1087.e1073.
Pettinato, G., Wen, X., and Zhang, N. (2014). Formation of Well-defined Embryoid Bodies from Dissociated Human Induced Pluripotent Stem Cells using Microfabricated Cell-repellent Microwell Arrays. Scientific Reports *4*, 7402.
Pettitt, T.W. (2020). Quality Improvement in Congenital Heart Surgery. Neoreviews *21*, e179-e192.
Piunti, A., and Shilatifard, A. (2016). Epigenetic balance of gene expression by Polycomb and COMPASS families. Science *352*, aad9780.
Poon, K.L., Tan, K.T., Wei, Y.Y., Ng, C.P., Colman, A., Korzh, V., and Xu, X.Q. (2012). RNA-binding protein RBM24 is required for sarcomere assembly and heart contractility. Cardiovascular Research *94*, 418-427.
Potter, S.W., and Morris, J.E. (1985). Development of mouse embryos in hanging drop culture. Anat Rec *211*, 48-56.
Prentice, D.A. (2019). Adult Stem Cells. Circulation Research *124*, 837-839.
Pritsker, M., Ford, N.R., Jenq, H.T., and Lemischka, I.R. (2006). Genomewide gain-of-function genetic screen identifies functionally active genes in mouse embryonic stem cells. Proceedings of the National Academy of Sciences of the United States of America *103*, 6946-6951.
Pulkkinen, H.H., Kiema, M., Lappalainen, J.P., Toropainen, A., Beter, M., Tirronen, A., Holappa, L., Niskanen, H., Kaikkonen, M.U., Ylä-Herttuala, S., *et al.* (2021). BMP6/TAZ-Hippo signaling modulates angiogenesis and endothelial cell response to VEGF. Angiogenesis *24*, 129-144.
Raisner, R., Kharbanda, S., Jin, L., Jeng, E., Chan, E., Merchant, M., Haverty, P.M., Bainer, R., Cheung, T., Arnott, D., *et al.* (2018). Enhancer Activity Requires CBP/P300 Bromodomain-Dependent Histone H3K27 Acetylation. Cell Reports *24*, 1722-1729.
Ramalho-Santos, M., and Willenbring, H. (2007). On the origin of the term "stem cell". Cell Stem Cell *1*, 35-38.
Ravera, A., Carubelli, V., Sciatti, E., Bonadei, I., Gorga, E., Cani, D., Vizzardi, E., Metra, M., and Lombardi, C. (2016). Nutrition and Cardiovascular Disease: Finding the Perfect Recipe for Cardiovascular Health. Nutrients *8*, E363.
Rey, S., Lee, K., Wang, C.J., Gupta, K., Chen, S., McMillan, A., Bhise, N., Levchenko, A., and Semenza, G.L. (2009). Synergistic effect of HIF-1α gene therapy and HIF-1-activated bone marrow-derived angiogenic cells in a mouse model of limb ischemia. Proceedings of the National Academy of Sciences of the United States of America *106*, 20399-20404.
Rider, V., Talbott, A., Bhusri, A., Krumsick, Z., Foster, S., Wormington, J., and Kimler, B.F. (2016). WINGLESS (WNT) signaling is a progesterone target for rat uterine stromal cell proliferation. J Endocrinol *229*, 197-207.

Rikhtegar, R., Pezeshkian, M., Dolati, S., Safaie, N., Afrasiabi Rad, A., Mahdipour, M., Nouri, M., Jodati, A.R., and Yousefi, M. (2019). Stem cells as therapy for heart disease: iPSCs, ESCs, CSCs, and skeletal myoblasts. Biomed Pharmacother *109*, 304-313.
Risau, W., and Flamme, I. (1995). Vasculogenesis. Annu Rev Cell Dev Biol *11*, 73-91.
Ritchie, M.E., Phipson, B., Wu, D., Hu, Y., Law, C.W., Shi, W., and Smyth, G.K. (2015). limma powers differential expression analyses for RNA-sequencing and microarray studies. Nucleic Acids Research *43*, e47.
Rivera-Pérez, J.A., and Magnuson, T. (2005). Primitive streak formation in mice is preceded by localized activation of Brachyury and Wnt3. Developmental Biology *288*, 363-371.
Rivera-Torres, J., Calvo, C.J., Llach, A., Guzmán-Martínez, G., Caballero, R., González-Gómez, C., Jiménez-Borreguero, L.J., Guadix, J.A., Osorio, F.G., López-Otín, C., *et al.* (2016). Cardiac Electrical Defects in Progeroid Mice and Hutchinson-Gilford Progeria Syndrome Patients With Nuclear Lamina Alterations. Proceedings of the National Academy of Sciences of the United States of America *113*.
Rizzino, A., and Wuebben, E.L. (2016). Sox2/Oct4: A delicately balanced partnership in pluripotent stem cells and embryogenesis. Biochim Biophys Acta *1859*, 780-791.
Rochette, L., Dogon, G., Zeller, M., Cottin, Y., and Vergely, C. (2021). GDF15 and Cardiac Cells: Current Concepts and New Insights. International Journal of Molecular Sciences *22*, 8889.
Rodda, D.J., Chew, J.-L., Lim, L.-H., Loh, Y.-H., Wang, B., Ng, H.-H., and Robson, P. (2005). Transcriptional Regulation of Nanog by OCT4 and SOX2*. Journal of Biological Chemistry *280*, 24731-24737.
Rodgers, K., and McVey, M. (2016). Error-Prone Repair of DNA Double-Strand Breaks. Journal of Cellular Physiology *231*, 15-24.
Rogakou, E.P., Pilch, D.R., Orr, A.H., Ivanova, V.S., and Bonner, W.M. (1998). DNA double-stranded breaks induce histone H2AX phosphorylation on serine 139. The Journal of Biological Chemistry *273*, 5858-5868.
Rossi, D., Gamberucci, A., Pierantozzi, E., Amato, C., Migliore, L., and Sorrentino, V. (2021). Calsequestrin, a key protein in striated muscle health and disease. J Muscle Res Cell Motil *42*, 267-279.
Rowton, M., Guzzetta, A., Rydeen, A.B., and Moskowitz, I.P. (2021). Control of cardiomyocyte differentiation timing by intercellular signaling pathways. Semin Cell Dev Biol *118*, 94-106.
Ruiz-Ortiz, I., and De Sancho, D. (2020). Competitive binding of HIF-1alpha and CITED2 to the TAZ1 domain of CBP from molecular simulations. Phys Chem Chem Phys.
Salvador, J.M., Brown-Clay, J.D., and Fornace, A.J. (2013). Gadd45 in stress signaling, cell cycle control, and apoptosis. Adv Exp Med Biol *793*, 1-19.
Sampaio-Pinto, V., Rodrigues, S.C., Laundos, T.L., Silva, E.D., Vasques-Novoa, F., Silva, A.C., Cerqueira, R.J., Resende, T.P., Pianca, N., Leite-Moreira, A., *et al.* (2018). Neonatal Apex Resection Triggers Cardiomyocyte Proliferation, Neovascularization and Functional Recovery Despite Local Fibrosis. Stem Cell Reports *10*, 860-874.
Santander Ballestín, S., Giménez Campos, M.I., Ballestín Ballestín, J., and Luesma Bartolomé, M.J. (2021). Is Supplementation with Micronutrients Still Necessary during Pregnancy? A Review. Nutrients *13*, 3134.
Santos, J.M.A. (2019). Cited2 in cardiac development: an inside and outside job (Faro: Universidade do Algarve), pp. 184.
Santos, J.M.A., Mendes-Silva, L., Afonso, V., Martins, G., Machado, R.S.R., Lopes, J.A., Cancela, L., Futschik, M.E., Sachinidis, A., Gavaia, P., *et al.* (2019). Exogenous WNT5A and WNT11 proteins rescue CITED2 dysfunction in mouse embryonic stem cells and zebrafish morphants. Cell Death & Disease *10*, 582.

Saunders, A., Huang, X., Fidalgo, M., Reimer, M.H., Faiola, F., Ding, J., Sánchez-Priego, C., Guallar, D., Sáenz, C., Li, D., *et al.* (2017). The SIN3A/HDAC Corepressor Complex Functionally Cooperates with NANOG to Promote Pluripotency. Cell Reports *18*, 1713-1726.
Schindelin, J., Arganda-Carreras, I., Frise, E., Kaynig, V., Longair, M., Pietzsch, T., Preibisch, S., Rueden, C., Saalfeld, S., Schmid, B., *et al.* (2012). Fiji: an open-source platform for biological-image analysis. Nature Methods *9*, 676-682.
Schneider, V.A., and Mercola, M. (2001). Wnt antagonism initiates cardiogenesis in Xenopus laevis. Genes Dev *15*, 304-315.
Schulte-Merker, S., and Smith, J.C. (1995). Mesoderm formation in response to Brachyury requires FGF signalling. Curr Biol *5*, 62-67.
Sherman, M.H., Bassing, C.H., and Teitell, M.A. (2011). DNA damage response regulates cell differentiation. Trends in cell biology *21*, 312-319.
Shigeta, M., Ohtsuka, S., Nishikawa-Torikai, S., Yamane, M., Fujii, S., Murakami, K., and Niwa, H. (2013). Maintenance of pluripotency in mouse ES cells without Trp53. Scientific Reports *3*.
Shiloh, Y. (2001). ATM and ATR: networking cellular responses to DNA damage. Current Opinion in Genetics & Development *11*, 71-77.
Shroff, R., Arbel-Eden, A., Pilch, D., Ira, G., Bonner, W.M., Petrini, J.H., Haber, J.E., and Lichten, M. (2004). Distribution and dynamics of chromatin modification induced by a defined DNA double-strand break. Curr Biol *14*, 1703-1711.
Shuai, L., Feng, C.J., Zhang, H.J., Gu, Q., Jia, Y.D., Wang, L., Zhao, X.Y., Liu, Z.H., and Zhou, Q. (2013). Derivation of androgenetic embryonic stem cells from m-carboxycinnamic acid bishydroxamide (CBHA) treated androgenetic embryos. Chin Sci Bull *58*, 2862-2868.
Silva, J., Nichols, J., Theunissen, T.W., Guo, G., van Oosten, A.L., Barrandon, O., Wray, J., Yamanaka, S., Chambers, I., and Smith, A. (2009). Nanog is the gateway to the pluripotent ground state. Cell *138*, 722-737.
Somorjai, I.M.L., Lohmann, J.U., Holstein, T.W., and Zhao, Z. (2012). Stem cells: A view from the roots. Biotechnol J *7*, 704-722.
Songqing, T., Taoyong, C., Zhou, Y., Xuhui, Z., Mingjin, Y., Bin, X., Nan, L., Xuetao, C., and Jianli, W. (2014). RasGRP3 limits Toll-like receptor-triggered inflammatory response in macrophages by activating Rap1 small GTPase. Nature Communications *5*, 4657.
Spandidos, A., Wang, X., Wang, H., Dragnev, S., Thurber, T., and Seed, B. (2008). A comprehensive collection of experimentally validated primers for Polymerase Chain Reaction quantitation of murine transcript abundance. BMC Genomics *9*, 633.
Spandidos, A., Wang, X., Wang, H., and Seed, B. (2010). PrimerBank: a resource of human and mouse PCR primer pairs for gene expression detection and quantification. Nucleic Acids Research *38*, D792-D799.
Sperling, S., Grimm, C.H., Dunkel, I., Mebus, S., Sperling, H.-P., Ebner, A., Galli, R., Lehrach, H., Fusch, C., Berger, F., *et al.* (2005). Identification and functional analysis of CITED2 mutations in patients with congenital heart defects. Hum Mutat *26*, 575-582.
Stambrook, P.J., and Tichy, E.D. (2010). Preservation of genomic integrity in mouse embryonic stem cells. Adv Exp Med Biol *695*, 59-75.
Stennard, F., Ryan, K., and Gurdon, J.B. (1997). Markers of vertebrate mesoderm induction. Current Opinion in Genetics & Development *7*, 620-627.
Stirling, D.R., Swain-Bowden, M.J., Lucas, A.M., Carpenter, A.E., Cimini, B.A., and Goodman, A. (2021). CellProfiler 4: Improvements in Speed, Utility and Usability. bioRxiv, 2021.2006.2030.450416.
Sugimoto, M., Kondo, M., Koga, Y., Shiura, H., Ikeda, R., Hirose, M., Ogura, A., Murakami, A., Yoshiki, A., Chuva de Sousa Lopes, S.M., *et al.* (2015). A simple and robust method for

establishing homogeneous mouse epiblast stem cell lines by wnt inhibition. Stem Cell Reports *4*, 744-757.
Sullivan, M.R., and Bernstein, K.A. (2018). RAD-ical New Insights into RAD51 Regulation. Genes (Basel) *9*, E629.
Sultana, D.A., Tomita, S., Hamada, M., Iwanaga, Y., Kitahama, Y., Khang, N.V., Hirai, S., Ohigashi, I., Nitta, S., Amagai, T., *et al.* (2009). Gene expression profile of the third pharyngeal pouch reveals role of mesenchymal MafB in embryonic thymus development. Blood *113*, 2976-2987.
Suwaki, N., Klare, K., and Tarsounas, M. (2011). RAD51 paralogs: roles in DNA damage signalling, recombinational repair and tumorigenesis. Semin Cell Dev Biol *22*, 898-905.
Symington, L.S., and Gautier, J. (2011). Double-strand break end resection and repair pathway choice. Annu Rev Genet *45*, 247-271.
Takahashi, K., Tanabe, K., Ohnuki, M., Narita, M., Ichisaka, T., Tomoda, K., and Yamanaka, S. (2007). Induction of Pluripotent Stem Cells from Adult Human Fibroblasts by Defined Factors. Cell *131*, 861-872.
Takahashi, K., and Yamanaka, S. (2006). Induction of Pluripotent Stem Cells from Mouse Embryonic and Adult Fibroblast Cultures by Defined Factors. Cell *126*, 663-676.
Takashima, Y., Guo, G., Loos, R., Nichols, J., Ficz, G., Krueger, F., Oxley, D., Santos, F., Clarke, J., Mansfield, W., *et al.* (2014). Resetting Transcription Factor Control Circuitry toward Ground-State Pluripotency in Human. Cell *158*, 1254-1269.
Tanay, A., O'Donnell, A.H., Damelin, M., and Bestor, T.H. (2007). Hyperconserved CpG domains underlie Polycomb-binding sites. Proceedings of the National Academy of Sciences of the United States of America *104*, 5521-5526.
Taylor, S.C., Berkelman, T., Yadav, G., and Hammond, M. (2013). A Defined Methodology for Reliable Quantification of Western Blot Data. Mol Biotechnol *55*, 217-226.
Team, R.C. (2021). R: A language and environment for statistical computing (Vienna, Austria).
Thomson, J.A., Itskovitz-Eldor, J., Shapiro, S.S., Waknitz, M.A., Swiergiel, J.J., Marshall, V.S., and Jones, J.M. (1998). Embryonic stem cell lines derived from human blastocysts. Science *282*, 1145-1147.
Thomson, M., Liu, S.J., Zou, L.-N., Smith, Z., Meissner, A., and Ramanathan, S. (2011). Pluripotency factors in embryonic stem cells regulate differentiation into germ layers. Cell *145*, 875-889.
Tichy, E.D., Pillai, R., Deng, L., Liang, L., Tischfield, J., Schwemberger, S.J., Babcock, G.F., and Stambrook, P.J. (2010). Mouse Embryonic Stem Cells, but Not Somatic Cells, Predominantly Use Homologous Recombination to Repair Double-Strand DNA Breaks. Stem Cells and Development *19*, 1699-1711.
Tosic, J., Kim, G.J., Pavlovic, M., Schröder, C.M., Mersiowsky, S.L., Barg, M., Hofherr, A., Probst, S., Köttgen, M., Hein, L., *et al.* (2019). Eomes and Brachyury control pluripotency exit and germ-layer segregation by changing the chromatin state. Nature Cell Biology *21*, 1518-1531.
Towbin, H., and Gordon, J. (1984). Immunoblotting and dot immunobinding--current status and outlook. Journal of Immunological Methods *72*, 313-340.
Townley-Tilson, W.H.D., Wu, Y., Ferguson, J.E., and Patterson, C. (2014). The ubiquitin ligase ASB4 promotes trophoblast differentiation through the degradation of ID2. PLOS ONE *9*, e89451.
Turinetto, V., Orlando, L., Sanchez-Ripoll, Y., Kumpfmueller, B., Storm, M.P., Porcedda, P., Minieri, V., Saviozzi, S., Accomasso, L., Cibrario Rocchietti, E., *et al.* (2012). High Basal γH2AX Levels Sustain Self-Renewal of Mouse Embryonic and Induced Pluripotent Stem Cells. Stem Cells *30*, 1414-1423.

Uphoff, C.C., and Drexler, H.G. (2002). Comparative PCR analysis for detection of mycoplasma infections in continuous cell lines. In Vitro Cell Dev Biol Anim *38*, 79-85.
Varadi, M., Anyango, S., Deshpande, M., Nair, S., Natassia, C., Yordanova, G., Yuan, D., Stroe, O., Wood, G., Laydon, A., *et al.* (2022). AlphaFold Protein Structure Database: massively expanding the structural coverage of protein-sequence space with high-accuracy models. Nucleic Acids Res *50*, D439-D444.
Vida, V.L., Zanotto, L., Torlai Triglia, L., Zanotto, L., Maruszewski, B., Tobota, Z., Bertelli, F., Cattapan, C., Ebels, T., Bottigliengo, D., *et al.* (2020). Surgery for Adult Patients with Congenital Heart Disease: Results from the European Database. J Clin Med *9*, 2493.
Viebahn, C., Stortz C Fau - Mitchell, S.A., Mitchell Sa Fau - Blum, M., and Blum, M. Low proliferative and high migratory activity in the area of Brachyury expressing mesoderm progenitor cells in the gastrulating rabbit embryo.
Vitale, I., Manic, G., De Maria, R., Kroemer, G., and Galluzzi, L. (2017). DNA Damage in Stem Cells. Molecular Cell *66*, 306-319.
Voigt, P., Tee, W.-W., and Reinberg, D. (2013). A double take on bivalent promoters. Genes Dev *27*, 1318-1338.
Walsh, J.C., Lebedev, A., Aten, E., Madsen, K., Marciano, L., and Kolb, H.C. (2014). The Clinical Importance of Assessing Tumor Hypoxia: Relationship of Tumor Hypoxia to Prognosis and Therapeutic Opportunities. Antioxid Redox Signal *21*, 1516-1554.
Wang, J., Huang, M., Torre, E., Dueck, H., Shaffer, S., Murray, J., Raj, A., Li, M., and Zhang, N.R. (2018). Gene expression distribution deconvolution in single-cell RNA sequencing. Proceedings of the National Academy of Sciences of the United States of America *115*, E6437-E6446.
Wang, J.Y.J. (2001). DNA damage and apoptosis. Cell Death Differ *8*, 1047-1048.
Wang, K., Sengupta, S., Magnani, L., Wilson, C.A., Henry, R.W., and Knott, J.G. (2010). Brg1 Is Required for Cdx2-Mediated Repression of Oct4 Expression in Mouse Blastocysts. PLOS ONE *5*, e10622.
Wang, L., Xu, X., Cao, Y., Li, Z., Cheng, H., Zhu, G., Duan, F., Na, J., Han, J.J., and Chen, Y.G. (2017). Activin/Smad2-induced Histone H3 Lys-27 Trimethylation (H3K27me3) Reduction Is Crucial to Initiate Mesendoderm Differentiation of Human Embryonic Stem Cells. Journal of Biological Chemistry *292*, 1339-1350.
Wang, T., Chen, L., Yang, T., Huang, P., Wang, L., Zhao, L., Zhang, S., Ye, Z., Chen, L., Zheng, Z., *et al.* (2019). Congenital Heart Disease and Risk of Cardiovascular Disease: A Meta-Analysis of Cohort Studies. J Am Heart Assoc *8*, e012030.
Ward, J.F., Evans, J.W., Limoli, C.L., and Calabro-Jones, P.M. (1987). Radiation and hydrogen peroxide induced free radical damage to DNA. Br J Cancer Suppl *8*, 105-112.
Wei, Z., Lei, X., Seldin, M.M., and Wong, G.W. (2012). Endopeptidase Cleavage Generates a Functionally Distinct Isoform of C1q/Tumor Necrosis Factor-related Protein-12 (CTRP12) with an Altered Oligomeric State and Signaling Specificity. The Journal of Biological Chemistry *287*, 35804-35814.
Weidgang, C.E., Seufferlein, T., Kleger, A., and Mueller, M. (2016). Pluripotency Factors on Their Lineage Move. Stem Cells Int *2016*, 6838253.
Who (2021). Cardiovascular diseases (CVDs). https://wwwwhoint/news-room/fact-sheets/detail/cardiovascular-diseases-(cvds).
Wickham, H. (2016). ggplot2: Elegant graphics for data analysis (Springer-Verlag New York).
Williams, M., Burdsal, C., Periasamy, A., Lewandoski, M., and Sutherland, A. (2012). Mouse primitive streak forms in situ by initiation of epithelial to mesenchymal transition without migration of a cell population. Dev Dyn *241*, 270-283.

Wilson, V., Manson, L., Skarnes, W.C., and Beddington, R.S. (1995). The T gene is necessary for normal mesodermal morphogenetic cell movements during gastrulation. Development *121*, 877-886.
Wolfgang, J.W., Kylie Lopes, F., Michael, B.B., Sarah, L.W., Jost, I.P., Juan Pedro Martinez, B., Timothy, J.M., and Sally, L.D. (2005). Cited2 is required both for heart morphogenesis andestablishment of the left-right axis in mouse development. Development, 1337-1348.
Wray, J., Kalkan, T., and Smith, A.G. (2010). The ground state of pluripotency. Biochem Soc Trans *38*, 1027-1032.
Xie, A., Puget, N., Shim, I., Odate, S., Jarzyna, I., Bassing, C.H., Alt, F.W., and Scully, R. (2004). Control of sister chromatid recombination by histone H2AX. Molecular Cell *16*, 1017-1025.
Xie, W.R., Jen, H.I., Seymour, M.L., Yeh, S.Y., Pereira, F.A., Groves, A.K., Klisch, T.J., and Zoghbi, H.Y. (2017). An Atoh1-S193A Phospho-Mutant Allele Causes Hearing Deficits and Motor Impairment. In J Neurosci, pp. 8583-8594.
Xu, X., Duan, S., Yi, F., Ocampo, A., Liu, G.-H., and Izpisua Belmonte, J.C. (2013). Mitochondrial regulation in pluripotent stem cells. Cell Metab *18*, 325-332.
Yadav, M.L., Jain, D., Neelabh, n., Agrawal, D., Kumar, A., and Mohapatra, B. (2021). A gain-of-function mutation in CITED2 is associated with congenital heart disease. Mutat Res *822*, 111741.
Yamakawa, M., Liu, L.X., Date, T., Belanger, A.J., Vincent, K.A., Akita, G.Y., Kuriyama, T., Cheng, S.H., Gregory, R.J., and Jiang, C. (2003). Hypoxia-inducible factor-1 mediates activation of cultured vascular endothelial cells by inducing multiple angiogenic factors. Circulation Research *93*, 664-673.
Yan, Y., Su-Yun, W., Zhe-Fu, H., Hong-Mei, Z., Bing-Ru, Y., Wei-Wei, L., and Yan-Yi, W. (2016). The RNA-binding protein Mex3B is a coreceptor of Toll-like receptor 3 in innate antiviral response. Cell Research *26*, 288.
Yang, H., Shao, N., Holmström, A., Zhao, X., Chour, T., Chen, H., Itzhaki, I., Wu, H., Ameen, M., Cunningham, N.J., *et al.* (2021). Transcriptome analysis of non human primate-induced pluripotent stem cell-derived cardiomyocytes in 2D monolayer culture vs. 3D engineered heart tissue. Cardiovascular Research *117*, 2125-2136.
Yang, X.-f., Wu, X.-y., Li, M., Li, Y.-g., Dai, J.-t., Bai, Y.-h., and Tian, J. (2010). Mutation analysis of Cited2 in patients with congenital heart disease. Chinese Journal of Pediatrics *48*, 293-296.
Ye, S., Zhang, D., Cheng, F., Wilson, D., Mackay, J., He, K., Ban, Q., Lv, F., Huang, S., Liu, D., *et al.* (2016). Wnt/β-catenin and LIF-Stat3 signaling pathways converge on Sp5 to promote mouse embryonic stem cell self-renewal. Journal of Cell Science *129*, 269-276.
Yin, Z., Haynie, J., Yang, X., Han, B., Kiatchoosakun, S., Restivo, J., Yuan, S., Prabhakar, N.R., Herrup, K., Conlon, R.A., *et al.* (2002). The essential role of Cited2, a negative regulator for HIF-1alpha, in heart development and neurulation. Proceedings of the National Academy of Sciences of the United States of America *99*, 10488-10493.
Ying, Q.-L., Wray, J., Nichols, J., Batlle-Morera, L., Doble, B., Woodgett, J., Cohen, P., and Smith, A. (2008). The ground state of embryonic stem cell self-renewal. Nature *453*, 519-523.
Yu-Shik, H., Bong Geun, C., Daniel, O., Nobuaki, H., Hannes-Christian, M., and Ali, K. (2009). Microwell-mediated control of embryoid body size regulates embryonic stem cell fate via differential expression of WNT5a and WNT11.
Yu, Z., Kong, J., Pan, B., Sun, H., Lv, T., Zhu, J., Huang, G., and Tian, J. (2013). Islet-1 may function as an assistant factor for histone acetylation and regulation of cardiac development-related transcription factor Mef2c expression. PLOS ONE *8*, e77690.
Zakrzewski, W., Dobrzyński, M., Szymonowicz, M., and Rybak, Z. (2019). Stem cells: past, present, and future. Stem Cell Research & Therapy *10*, 68.

Zandstra, P.W., Bauwens, C., Yin, T., Liu, Q., Schiller, H., Zweigerdt, R., Pasumarthi, K.B.S., and Field, L.J. (2003). Scalable production of embryonic stem cell-derived cardiomyocytes. Tissue Eng *9*, 767-778.
Zeineddine, D., Papadimou, E., Chebli, K., Gineste, M., Liu, J., Grey, C., Thurig, S., Behfar, A., Wallace, V.A., Skerjanc, I.S., *et al.* (2006). Oct-3/4 dose dependently regulates specification of embryonic stem cells toward a cardiac lineage and early heart development. Developmental Cell *11*, 535-546.
Zentner, G.E., Tesar, P.J., and Scacheri, P.C. (2011). Epigenetic signatures distinguish multiple classes of enhancers with distinct cellular functions. Genome Research *21*, 1273-1283.
Zhang, E., Li, X., Zhang, S., Chen, L., and Zheng, X. (2005). Cell cycle synchronization of embryonic stem cells: Effect of serum deprivation on the differentiation of embryonic bodies in vitro. Biochemical and Biophysical Research Communications *333*, 1171-1177.
Zhang, H., Xing, Z., Mani, S.K.K., Bancel, B., Durantel, D., Zoulim, F., Tran, E.J., Merle, P., and Andrisani, O. (2016a). RNA helicase DEAD box protein 5 regulates Polycomb repressive complex 2/Hox transcript antisense intergenic RNA function in hepatitis B virus infection and hepatocarcinogenesis. Hepatology *64*, 1033-1048.
Zhang, J., Ratanasirintrawoot, S., Chandrasekaran, S., Wu, Z., Ficarro, S.B., Yu, C., Ross, C.A., Cacchiarelli, D., Xia, Q., Seligson, M., *et al.* (2016b). LIN28 Regulates Stem Cell Metabolism and Conversion to Primed Pluripotency. Cell Stem Cell *19*, 66-80.
Zhang, M., Zhang, Y., Xu, E., Mohibi, S., de Anda, D.M., Jiang, Y., Zhang, J., and Chen, X. (2018). Rbm24, a target of p53, is necessary for proper expression of p53 and heart development. Cell Death Differ *25*, 1118-1130.
Zhang, Q., Carlin, D., Zhu, F., Cattaneo, P., Ideker, T., Evans, S.M., Bloomekatz, J., and Chi, N.C. (2021). Unveiling Complexity and Multipotentiality of Early Heart Fields. Circulation Research *129*, 474-487.
Zhang, X., and Branciamore, S. (2021). The convergent CTCF loop formed by DNA extrusion is the basis of promoter enhancer interactions. bioRxiv, 2021.2006.2028.450073.
Zhao, M.-T., Shao, N.-Y., and Garg, V. (2020). Subtype-specific cardiomyocytes for precision medicine: Where are we now? STEM CELLS *38*, 822-833.
Zhong, X., and Jin, Y. (2009). Critical roles of coactivator p300 in mouse embryonic stem cell differentiation and Nanog expression. The Journal of Biological Chemistry *284*, 9168-9175.
Zhou, S., Wang, J., Wang, Q., Meng, Z., Peng, J., Song, W., Zhou, Y., Chen, S., Chen, F., and Sun, K. (2020). Essential Role of the ELABELA-APJ Signaling Pathway in Cardiovascular System Development and Diseases. J Cardiovasc Pharmacol *75*, 284-291.
Zhu, H., Li, J., Li, Y., Zheng, Z., Guan, H., Wang, H., Tao, K., Liu, J., Wang, Y., Zhang, W., *et al.* (2021). Glucocorticoid counteracts cellular mechanoresponses by LINC01569-dependent glucocorticoid receptor-mediated mRNA decay. Science Advances *7*.
Ziegler-Birling, C., Helmrich, A., Tora, L., and Torres-Padilla, M.-E. (2009). Distribution of p53 binding protein 1 (53BP1) and phosphorylated H2A.X during mouse preimplantation development in the absence of DNA damage. Int J Dev Biol *53*, 1003-1011.